

VELOCITY OF PARTICULATE IN
LAMINAR AND TURBULENT GAS FLOW
BY HOLOGRAPHIC TECHNIQUES

October 1971

J. B. Allen	R. F. Tanner
D. M. Meadows	L. M. Boggs

Contract EHSD 71-34

Lockheed-Georgia Company
Marietta, Georgia

**VELOCITY OF PARTICULATE IN
LAMINAR AND TURBULENT GAS FLOW
BY HOLOGRAPHIC TECHNIQUES**

October 1971

J. B. Allen

R. F. Tanner

D. M. Meadows

L. M. Boggs

Contract EHSD 71-34

**Lockheed-Georgia Company
Marietta, Georgia**

OFFICIAL USE ONLY

Final, interim, and monthly reports submitted under this contract contain information and statements which are preliminary and represent only the state of the information developed as of the reporting date. This information is also subject to review and critique by NAPCA personnel before release outside of NAPCA. To prevent inappropriate dissemination of information which could be misinterpreted and/or misleading, you are asked to regard these reports strictly as internal working documents and treat them accordingly. You are requested to observe the following guidelines:

- (1) Use the reports for information and coordination purposes only.**
- (2) Do not discuss the reports or the information contained in them with persons outside of NAPCA.**
- (3) Refer all inquiries relating to the reports to the Project Officer.**
- (4) Provide comments to the Project Officer for his use in managing the contract.**

FOREWORD

This is the final report of the contract "Velocimetry of Particulate in Laminar and Turbulent Gas Flow by Holographic Techniques," Contract EHSD 71-34, sponsored by the Office of Air Programs of the Environmental Protection Agency (EPA) and carried out by the Lockheed-Georgia Company.

The research done under this contract was carried out by members of the Lockheed-Georgia Research Laboratory. Project Directors for this contract were D. M. Meadows and L. M. Boggs. J. B. Allen directed the technical effort and was responsible for the design of the holographic systems. R. F. Tanner designed and instrumented the duct used in the experiments. D. M. Meadows and L. M. Boggs were responsible for the electronic instrumentation and electrical systems used in the experiments. J. R. Williams, Consultant, designed the particulate dispenser to seed the air flow in the duct. C. R. Huie constructed the duct and particulate dispenser and provided invaluable assistance in all aspects of the experimental work.

ABSTRACT

A technique for measuring the velocity and behavior of particulate suspended in potential and turbulent air flows by means of double-pulsed holography is presented.

Descriptions of the air duct facility, particulate dispenser, and holographic systems are provided as well as discussions of experimental results and theoretical considerations. Double-pulsed holography was proved to be an excellent technique for measuring the characteristics of suspended particulate of sizes greater than 6 microns. The measurable characteristics include velocity, three-dimensional coordinates of the particle, size and shape. Specific experiments were performed to determine the feasibility of the double-pulsed holographic technique. These experiments included studies of particulate behavior in electrostatic fields, in potential and turbulent flow, and around a sampling probe for various sampling conditions.

TABLE OF CONTENTS

<u>Section</u>	<u>Title</u>	<u>Page</u>
	FOREWORD	ii
	ABSTRACT	iii
	LIST OF ILLUSTRATIONS	vi
I	INTRODUCTION	1
II	TEST FACILITY	
	A. General Description	3
	B. Air Duct Facility	
	1. General Design Considerations	3
	2. Turbulent Flow Test Section	6
	3. Potential Flow Test Section	6
	4. Fan Motor Sizing	8
	C. Velocity/Density Surveys	
	1. Survey Stations	11
	2. Probe Drive Mechanism	14
	3. Profiles	18
	D. Particulate Dispenser	30
	E. Holographic Systems	
	1. Systems for Making and Reconstructing Holograms	37
	2. Systems to Obtain Data from Holograms	49
	3. Holographic Systems Selected for Experimental Programs	59
III	EXPERIMENTAL PROGRAM	
	A. Potential Flow Holograms	80
	B. Turbulent Flow Holograms	87

<u>Section</u>	<u>Title</u>	<u>Page</u>
	C. Holograms of APCO Train Probe	87
	D. Holograms of Charged Plates	101
IV	CONCLUSIONS AND RECOMMENDATIONS	113

LIST OF ILLUSTRATIONS

<u>Figure</u>	<u>Title</u>	<u>Page</u>
1	Air Duct Facility and Particulate Dispenser	4
2	Holographic Reconstruction System	5
3	Pulsed Laser System	5
4	Turbulent Test Section	7
5	Side View of Air Duct Intake	9
6	Front View of Air Duct Intake	9
7	Potential Test Section and Transition Section	10
8	Potential Flow Test Section Windows	10
9	Nozzle, Fan, and Exit Ducting	12
10	Potential Flow Test Section	13
11	Turbulent Flow Test Section	15
12	Probe Drive Mechanism Mounted at Potential Test Section	16
13	Probe Drive Mechanism	16
14	Probe Drive Power Supply, Position Readout (DVM), Airspeed Indicator, and Control Box	17
15	Particulate Sampling Probe (APCO Train Probe) and Velocity Profile Probes	17
16	Velocity Profile Potential Flow Test Section Position C-1 (Upper)	20
17	Velocity Profile Potential Flow Test Section Position C-2	21
18	Velocity Profile Potential Flow Test Section Position C-3	22
19	Velocity Profile Potential Flow Test Section Position C-4 (Lower)	23

LIST OF ILLUSTRATIONS

<u>Figure</u>	<u>Title</u>	<u>Page</u>
20	Velocity Profile Potential Flow Test Section Position C-1 (Upper)	24
21	Velocity Profile Potential Flow Test Section Position C-2 (Upper)	25
22	Velocity Profile Potential Flow Test Section Position C-3	26
23	Velocity Profile Potential Flow Test Section Position C-4 (Lower)	27
24	Velocity Profile Turbulent Flow Test Section	28
25	Velocity Profile Turbulent Flow Test Section	29
26	Blender Type Particulate Dispenser	31
27	Particulate Dispenser Assembly	32
28	Dispenser Hopper, Mixing Blades, and Mixing Chamber	32
29	Internal Construction of Mixing Chamber	33
30	Dispenser Hopper and Auger Feed	33
31	Particulate Dispenser Drum and Preserve System	34
32	Slotted Tube (Rake) Used to Dispense Flyash into Duct Facility	36
33	Screens and Slotted Tube	36
34	Single Beam Holographic System	38
35	Reconstruction System for Single Beam Hologram	39
36	System to Magnify and Spatially Filter the Reconstructed Image	41
37	Schematic of Two-Beam Hologram	42
38	Reconstruction of a Two-Beam Hologram	43
39	Reconstruction of a Hologram of Small Glass Balls Made with Forward Scattered Light	45

LIST OF ILLUSTRATIONS

<u>Figure</u>	<u>Title</u>	<u>Page</u>
40	Reconstruction of a Hologram of Small Glass Balls Made with Side Scattered Light	46
41	Test Tube Dispenser for Small Glass Balls	48
42	Example of a Reconstruction from a Double Pulsed Hologram Showing Reconstruction Pairs	51
43	Schematic of Fourier Transform Method of Estimating Velocity	52
44	Plot of the Correlation Function of $r(x, y)$ Showing the Central Peak and Two Smaller Peaks at $(-x_0, 0)$ and $(x_0, 0)$	55
45	Schematic of the System to Make a Two-Beam Hologram of Light from the Reconstruction in the Focal Plane of a Lens	56
46	Schematic of Correlation Method for Measuring the Velocity from Particle Holograms	57
47	Schematic of Potential Flow Test Section Holographic System	60
48	Schematic of Turbulent Flow Test Section Holographic System	60
49	Pulsed Ruby Laser Used in the Experimental Work and the Pulse Monitoring System Consisting of a Glass Plate Which Reflects a Small Portion of the Beam, a Photoelectric Cell, and a Storage Scope	61
50	Holographic System for the Potential Flow Test Section Showing Aperture, Negative Lens, Mirror, and Collimating Lens, and the Test Section	63
51	The Holographic System Around the Potential Flow Test Section Showing the Optical System, Test Section, and Film Holder	64
52	The Holographic System for the Turbulent Flow Test Section Showing the Laser Beam, Negative Lens, Collimating Lens, Mirror, Test Section, and Film Holder	65

LIST OF ILLUSTRATIONS

<u>Figure</u>	<u>Title</u>	<u>Page</u>
53	Schematic of the System to View and Make Measurements of the Particle Holograms	66
54	The System Used to Reconstruct the Particle Holograms Showing the One-Watt, Argon Laser, Lens Pinhole Combination, Collimating Lens, Hologram, Microscope Objective, Spatial Filter, and Ground Glass Viewing Screen	68
55	Close-up of the Reconstruction System Showing the Hologram, Microscope Objective, and Spatial Filter	69
56	Sketch of the Potential Flow Section Showing the Cylindrical Portion of the Test Section Which is Holographed	71
57	Micrometer Positioned Hologram Holder Used in Particle Reconstruction Experiments	72
58	Example No. 1 - Distinctively Shaped Particle Pair	76
59	Example No. 2 - Distinctively Shaped Particle Pair	76
60	Two Particle Pair Reconstruction	77
61	Four Double Pulsed Particle Pairs in Potential Flow	78
62	Particle Reconstruction of Flow About the APCO Train Probe (.5 Isokinetic)	79
63	Personnel Programming Facility for Tests	81
64	Scanning Electron Microscope Photograph of Flyash 1250 x	81
65	Potential Flow Hologram No. 110	83
66	Turbulent Flow Hologram No. 175	93
67	APCO Hologram No. 142	95
68	Particle Position Diagram for Sampling Probe	96
69	Particle Sampling System Using the APCO Train	99
70	Sampling Probe Located in Potential Flow Section	99

LIST OF ILLUSTRATIONS

<u>Figure</u>	<u>Title</u>	<u>Page</u>
71	System for Calibrating APCO Train Assembly	100
72	Air Sampling System	100
73	Schematic of Calibration System and Sampling System	102
74	Precipitator Plates Hologram No. 196	104
75	Charged Plates Device	111
76	Time Exposure Showing Corona Discharge Patterns Between Plates and Screen	111

LIST OF TABLES

<u>Number</u>	<u>Title</u>	<u>Page</u>
I	Potential Flow Holograms	82
Ia	Potential Flow Hologram No. 110	84
Ib	Potential Flow Hologram No. 110	85
Ic	Potential Flow Hologram No. 110	86
II	Turbulent Flow Holograms	88
IIa	Turbulent Flow Hologram No. 175	89
IIb	Turbulent Flow Hologram No. 175	90
IIc	Turbulent Flow Hologram No. 175	91
IId	Turbulent Flow Hologram No. 175	92
III	APCO Train	94
IIIa	APCO Train Hologram No. 142	97
IV	Charged Plates	103
IVa	Precipitator Plate Hologram No. 196	105
IVb	Precipitator Plate Hologram No. 196	106
IVc	Precipitator Plate Hologram No. 196	107
IVd	Precipitator Plate Hologram No. 196	108
IVe	Precipitator Plate Hologram No. 196	109
IVf	Precipitator Plate Hologram No. 196	110

I. INTRODUCTION

The primary object of this contract was to develop a technique based on double-pulsed holography to measure the velocity and behavior of particulate in potential and turbulent duct flows. The development of this technique provides an important method for investigating particle behavior on a microscopic level. Potential applications of this technique include the validation of present particle sampling techniques and setting of tolerances on probe sampling parameters. Additionally, the technique provides an excellent method for observing and studying particle behavior under various flow conditions such as in electrostatic precipitators and in other air control systems. A better understanding of particulate behavior in these areas should contribute to improved system efficiencies and lower system costs.

Major sub-objectives for the contract included the following:

- o Design, construct and test an air duct facility capable of producing both potential and turbulent flow.
- o Design, construct, and test a particulate dispenser for injecting selected particulate into the air duct facility.
- o Design, construct, and test a double-pulsed holographic system for recording 3-dimensional images of particulate in both the potential and turbulent test sections.
- o Design, construct, and test an image reconstruction system for accurately reproducing the particle pairs for determination of particle characteristics (velocity vectors, particle size, particle shape).

The following major experiments were conducted under the contract to evaluate the capability of the holographic systems to meet the primary objective.

- o Holograms were made of particles suspended in potential flows to provide base-line data and to provide a method of validating system calibration.
- o Holograms were made of particles suspended in turbulent flow to determine the ability of the system to capture the particles and to resolve double-pulse pairs.
- o Holograms were made of a sampling probe connected to the APCO Train to evaluate particle behavior at 1.0 isokinetic, 1.5 isokinetic, and .5 isokinetic sampling conditions.

- o Holograms were made of particles passing between charged plates to determine the feasibility of applying double-pulsed holography to this type of problem.

The official start date of the contract was December 9, 1970. The end date is December 9, 1971. All technical objectives have been met, on schedule and within budget.

II. TEST FACILITY

II. A. - GENERAL DESCRIPTION

The test facility was set up in two adjacent rooms, each measuring approximately 20 x 25 feet. The air duct facility, the particulate dispenser, and all items relating to these major items were located in one room (See Figure 1). The holographic reconstruction system and the pulsed laser were located in the other room (See Figures 2 and 3). A small hole was bored in the wall separating the two rooms to allow the pulsed laser beam to pass through. A major reason for separating the majority of the optical components from the rest of the facility was to prevent damage to the optical systems due to particulate present in the air around the duct facility.

II. B. - AIR DUCT FACILITY

II. B.1 - General Design Considerations

The constraints placed on the design of the air duct facility included the following:

- a. The facility must include two test sections -- a potential flow section and a turbulent flow section.
- b. The facility must accept various types and amounts of particulate.
- c. The effects of gravity and ambient air fluctuations upon particle velocity measurements must be negligible.
- d. The range of velocities was contractually set at 10 - 120 feet per second.
- e. Wall effects upon the flow must be negligible.
- f. Means must be provided to measure velocity profiles in both the turbulent and potential flow sections.

The initial design of the system resulted in a horizontal, non-return type, tandem test section duct (consisting of the potential and turbulent test sections). A vertical tunnel was eliminated as a possibility due to the potential difficulty of injecting the particulate smoothly into the air duct against gravity in a low velocity inlet. Space was another consideration

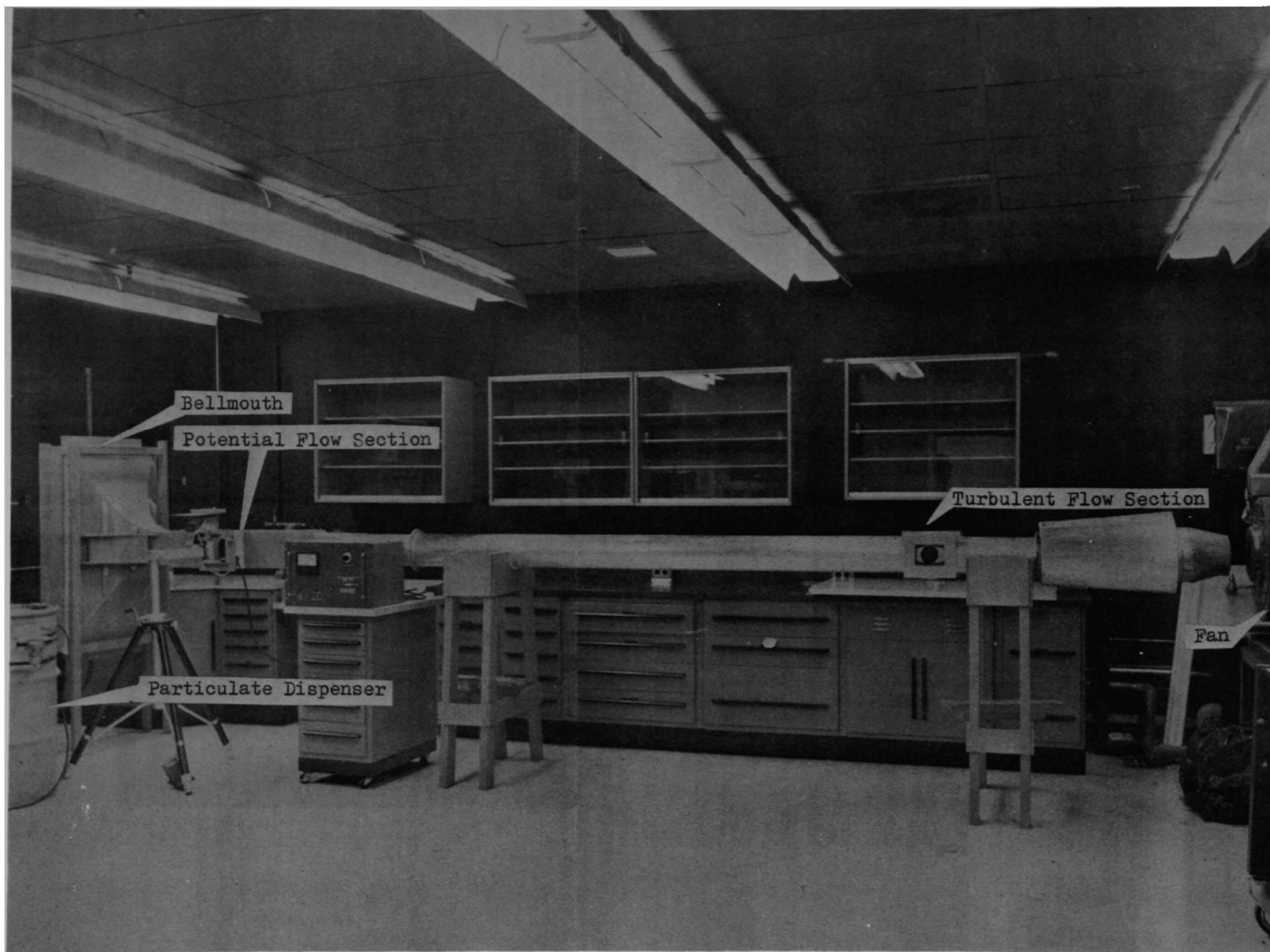


FIGURE 1
AIR DUCT FACILITY AND PARTICULATE DISPENSER

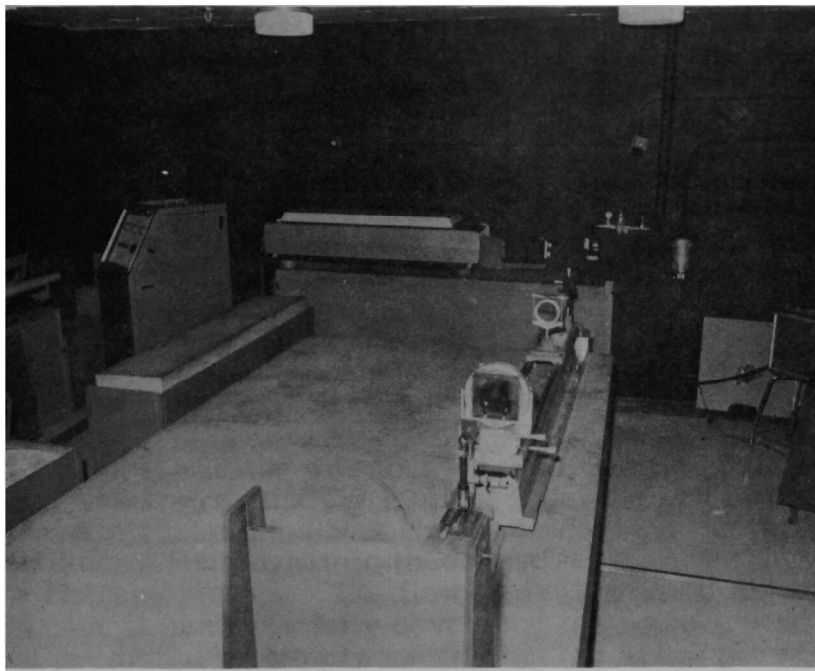


FIGURE 2
HOLOGRAPHIC RECONSTRUCTION SYSTEM

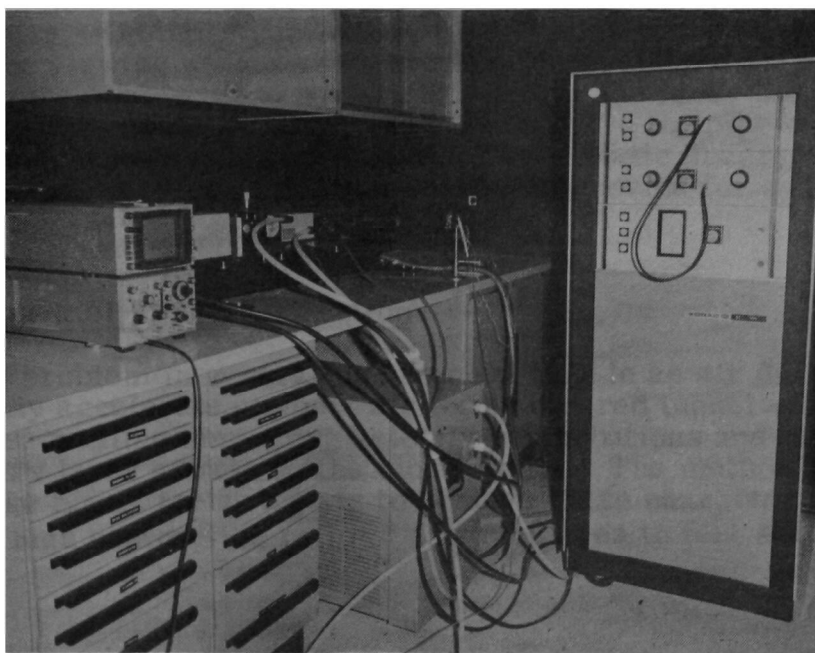


FIGURE 3
PULSED LASER SYSTEM

in eliminating the vertical tunnel since such an installation would have to extend through the roof. Also, in the analysis of particulate velocities, it could have been extremely difficult to separate the effects of gravity and fluid dynamic forces acting on the particles since the two forces would act along the same line.

A closed circuit facility was eliminated from consideration since varying amounts of particulate had to be injected into the tunnel. If used, this type system would require a number of undesirable features such as filtering systems and special particulate injection systems to maintain proper loading conditions.

II. B. 2 - Turbulent Flow Test Section

The turbulent flow test section was located downstream of the potential flow section and was approximately 1.5 feet from the end of the tunnel (See Figure 4). A circular pipe was chosen to develop the turbulent flow since well-known fluid dynamic theory exists for precisely calculating air flow characteristics. The flow is symmetrical about the centerline and once it becomes fully developed the boundary layer profiles can be predicted by simply measuring the static pressure drop.

Initial plans called for a 60-foot long section to permit the flow to become fully developed. However, due to space limitations, the length was restricted to 10 feet which provided partially developed turbulent flow.

The turbulent flow section was designed first since it contained the only component constrained by commercial specifications. An aluminum pipe was selected having a 6.3 inch inside diameter and 0.16 inch wall. At the test section, sections of pipe were contoured and welded normal to the main pipe. On these sections of pipe, metal frames were mounted for holding the viewing windows (Figure 4). Three-inch diameter holes were cut into the pipe to allow a viewing area for the laser beam. Provision was also made for mounting a plate above the pipe on which the probe drive mechanism could be placed. Three static pressure ports were installed on one side of the test section to provide for system calibration.

II. B. 3 - Potential Flow Test Section

The primary problem in generating potential flow in an air duct facility is to uniformly accelerate ambient air to the desired tunnel velocity while at the same time smoothing velocity perturbations and preventing rapid boundary layer growth on the tunnel walls. The method normally used by smoke tunnel technologists to achieve these characteristics is to provide a high contraction ratio of entrance area to test section area.

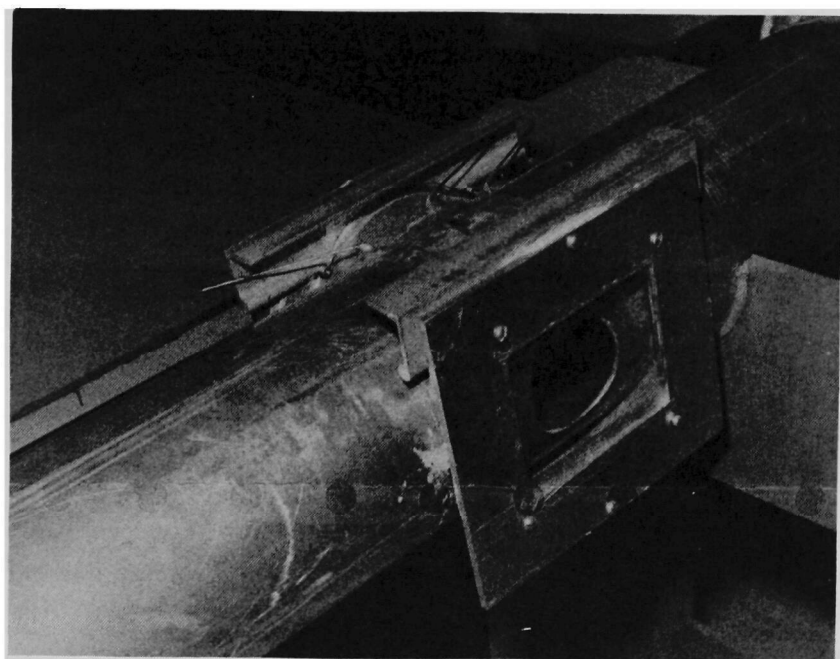


FIGURE 4
TURBULENT TEST SECTION

Figures 5 and 6 illustrate the "bellmouth" selected for the duct facility to assure good potential flow. A rectangular entrance section was chosen which has the same ratio of side lengths as the potential test section. A contraction ratio of 37.5 to 1 was used, and the surfaces joining the entrance area to the test section area were defined by modified exponential curves.

The bellmouth was constructed using sheet aluminum, cut to the proper contours and heliarc welded. A wooden frame was used to maintain the shape during assembly. Discontinuities were removed by contouring with putty and sanding smooth.

The potential flow test section was designed to be 7.0 inches high and 4.5 inches wide (See Figure 7). The cross sectional area of the potential flow section was set to be the same as the area of the turbulent section to minimize transition problems between the two test sections. Figure 7 shows the transition section on the right hand side of the photograph. The rectangular shape of the potential flow section was selected primarily from considerations of the optical system. A rectangular shape allowed the use of inexpensive, optically flat windows to be used with a minimum of perturbations introduced into the flow by the windows. Seven inches of height assured that the hologram viewing area would be well above any boundary layer problems or perturbations that might arise from the tunnel walls.

Mounting of the windows was accomplished by using aluminum plates with 4" x 5" cutouts. Figure 8 shows front and back views of the window holders. On the back side of the holder, thin strips of metal were attached to the holder to prevent the 1/4" thick optical windows from moving inward. Interference of the strips with the flow was minimized by keeping the strips small, 0.20" thick and .375" wide and by fairing the strips in with the holder. At the top of one of the window holders, as shown in Figure 8, static pressure ports were implaced to provide a reference for the air speed indicator and to provide data for calculating air density.

The test section was constructed of 1/2" plywood to facilitate changes that were anticipated during the test phases of the program. The internal faces of the plywood were smoothed and coated with automotive primer paint.

II. B. 4 - Fan Motor Sizing

High priority was given to the choice of the fan in terms of air flow capacity and ability to withstand the abrasive effects of particulate for long periods of time. The type fan which appeared to be most suitable was a radial flow materials handling fan which could deliver a large quantity of flow while working against a moderate pressure.

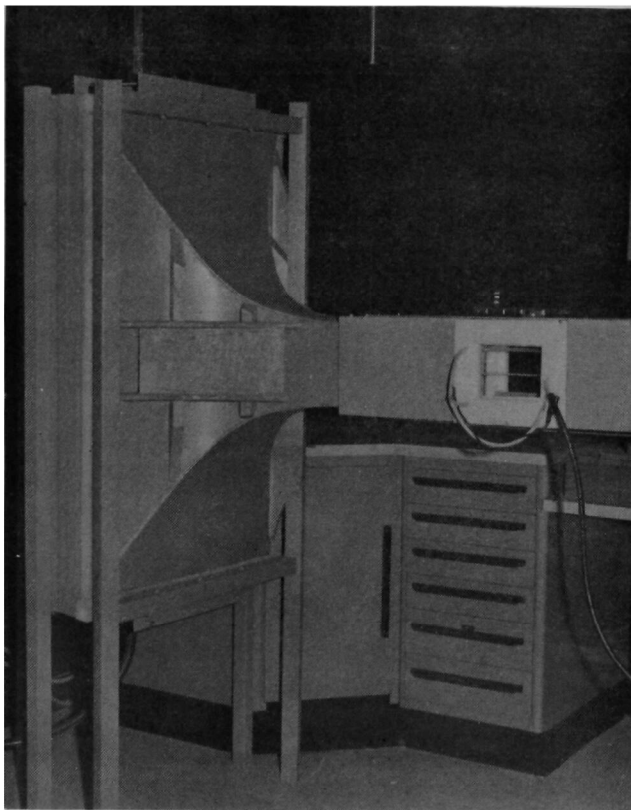


FIGURE 5
SIDE VIEW OF AIR DUCT INTAKE

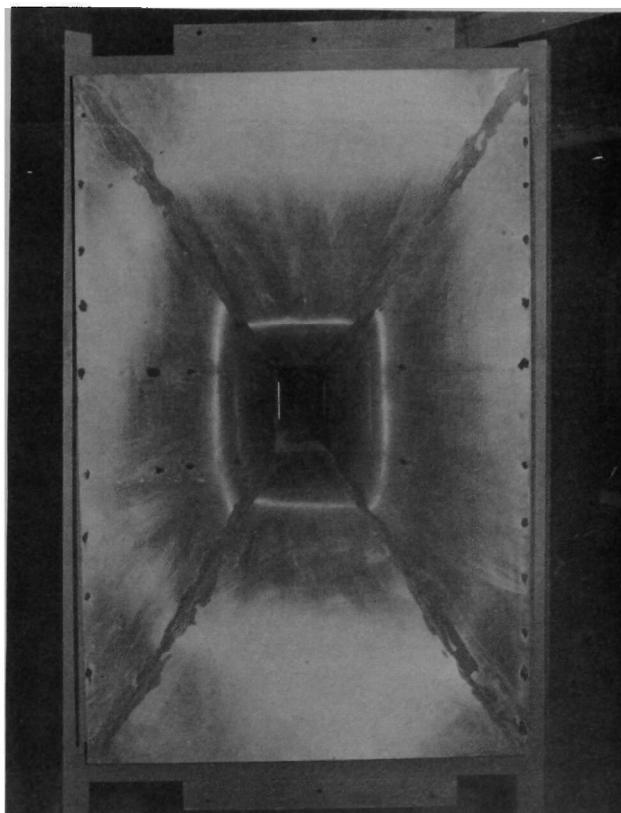


FIGURE 6
FRONT VIEW OF AIR DUCT INTAKE

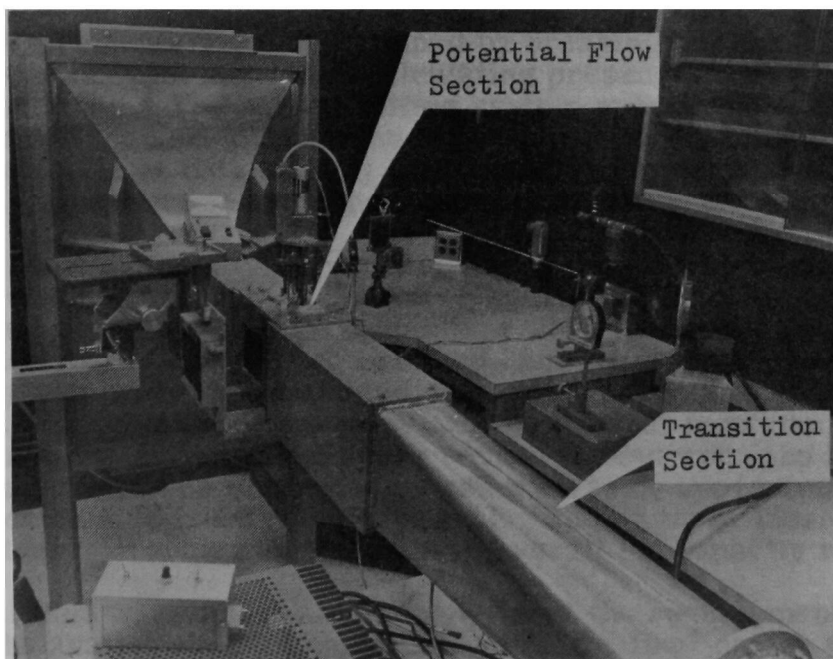


FIGURE 7
POTENTIAL TEST SECTION AND TRANSITION SECTION

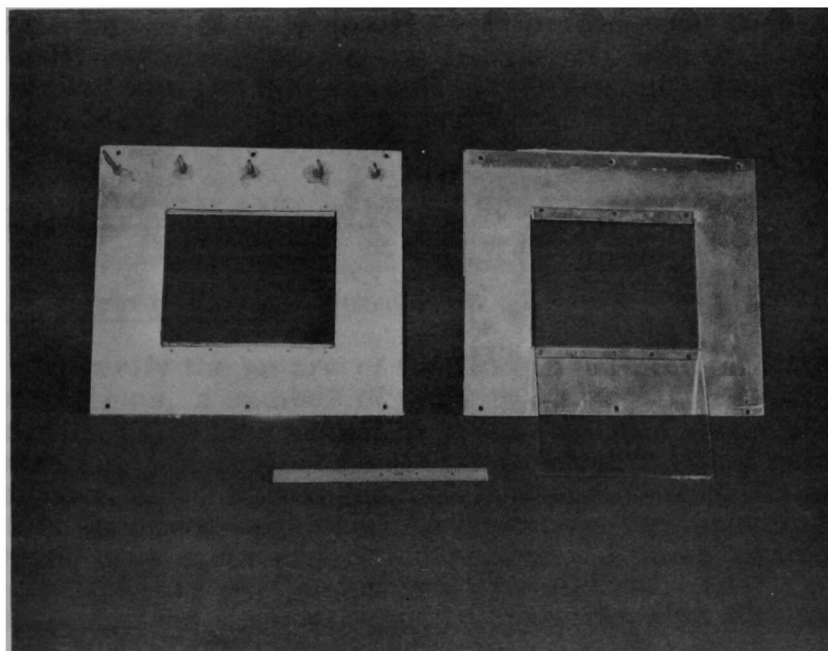


FIGURE 8
POTENTIAL FLOW TEST SECTION WINDOWS

Fan requirements were determined by breaking the air duct facility into its component parts and calculating pressure losses in each of these sections. The basic limiting system specification which determined the assumptions made in computing the losses was the requirement that the potential flow section have at least a 120 ft/sec. velocity capability at standard temperature and pressure.

For each of the sections -- bellmouth, potential flow section, transition section and turbulent section -- equivalent circular cross-sectional areas and Reynolds numbers were calculated from which pressure losses could be determined, and the pressure losses for the total system were approximated as a summation of the individual losses. Since at this time plans were somewhat indeterminate as to what form the ducting would have beyond the fan exit, the losses associated with this ducting were assumed to be approximately equal to the calculated losses for the tunnel. Adding these losses to those of the tunnel provided an estimate of overall fan capacity requirements.

Several fans were found which could fulfill the requirements; however, from the availability and cost standpoint, the final choice was a blower made by the New York Blower Company. The model chosen was the GI fan size 142 with LS wheel and unitary base, powered by a 3, 500 RPM, 7-1/2 HP, 3 phase, 208 volt motor. The blower had a counterclockwise up blast configuration which was selected to facilitate installation of the exit ducting. The blower and exit ducting are shown in Figure 9.

Since the range of air velocities required were quite large and the particular velocities used would be dependent on holographic considerations, it was decided to provide a continuous velocity adjustment on the duct facility. This consisted of a conical diffuser section with a conical exit nozzle immediately in front of the fan but separated from it by an air gap. By adjusting the air gap and thereby changing the amount of room air bled into the fan, the velocity in the tunnel could be adjusted to within $\pm 1/4$ MPH of a desired velocity.

II. C. - VELOCITY AND DENSITY SURVEYS

II. C. 1 - Survey Stations

In order to verify the nature of the flow in both the potential and turbulent test sections, a number of velocity surveys were made using a mechanically positioned pressure probe. It was anticipated that if there were any non-symmetrical flow present it would occur in the potential section. For this reason, it was considered important to completely survey the potential flow whereas the turbulent flow could be surveyed over more restricted regions. Fifteen stations were chosen in the potential flow section and are schematically illustrated in Figure 10. These stations were selected to cover the area that would be visible

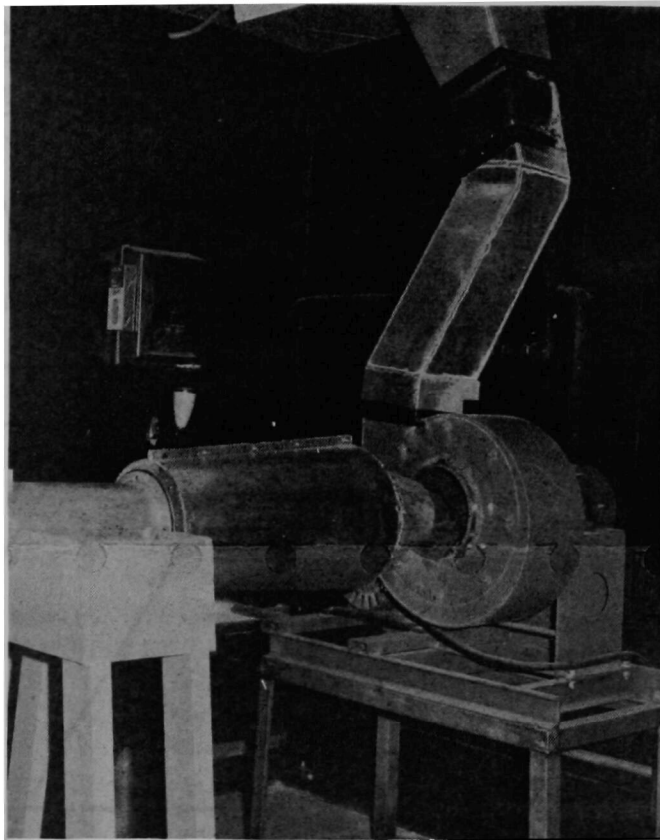


FIGURE 9
NOZZLE, FAN AND EXIT DUCTING

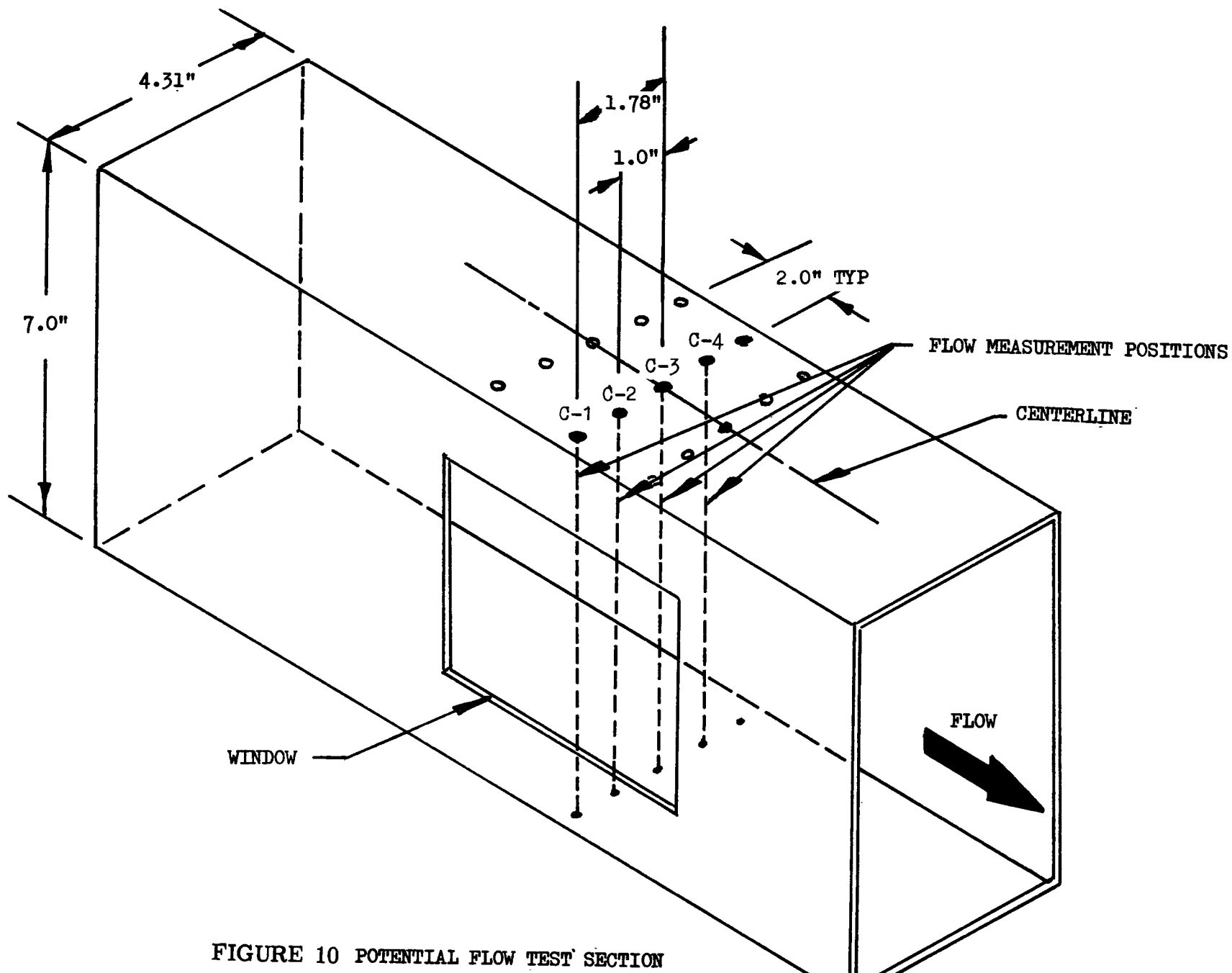


FIGURE 10 POTENTIAL FLOW TEST SECTION

in the holograms. Three axial locations, at the front, middle, and rear of the test section, were used so that any longitudinal velocity gradients could be measured. The five stations across the test section could determine the extent of velocity variation in this direction.

Because of the symmetrical nature of the flow in the turbulent test section, only profiles in one plane were measured (Figure 11). It was decided that the slight distortion of the flow caused by the window holes in the cylindrical section would not be extreme. The probe drive mechanism had a limited travel, and it was necessary to make two separate traverses to span the duct. Each traverse began at the upper or lower surface and continued across the centerline of the duct. The data was reduced and the velocity profiles matched at the appropriate point on the centerline. In order to adequately measure the profile, a large number of points were recorded near the tunnel surfaces. Areas away from the wall needed less definition to adequately describe the flow.

II. C. 2 - Probe Drive Mechanism

Figure 12 shows the probe drive mechanism mounted on top of the potential flow test section. Figure 13 is a close up of the mechanism with a probe attached. The mechanism consists of a steel plate free to move linearly on guide rails, driven by an electric lead screw. Attached to the plate is a total pressure probe and the movable end of a 0 to 10K ohms linear potentiometer. The potentiometer is used as a position indicator for the probe. Microswitches are used to limit the travel and prevent damage to the mechanism. Total travel of the probe is 3.6 inches which is slightly more than half the distance from floor to ceiling of the tunnel.

Figure 14 shows the digital voltmeter (DVM) used to measure displacement of the probe, the airspeed indicator used for air velocity measurements, the control box, and two power supplies. The regulated power supply provides 10 volts across the linear potentiometer in the probe drive mechanism. Therefore, the voltage output to the DVM is proportional to probe displacement. This system was calibrated using a depth micrometer, accurate to 0.001 inch. The overall accuracy of the readout system was ± 0.010 inch; i. e., the tolerance between actual probe position versus DVM readout. The mechanical parts of the probe drive assembly contributed little to the overall error. Over a 3.6" up and down traverse the probe return was within 0.001" of the starting point.

The power supply used with the probe drive motor was set at 12 volts. In Figure 14, the control box shown on top of the potentiometer power supply was used to control direction of travel and provided incremental motion (center button) as well as continuous motion. Velocity data was read out on the airspeed indicator which was connected to the probe and a static

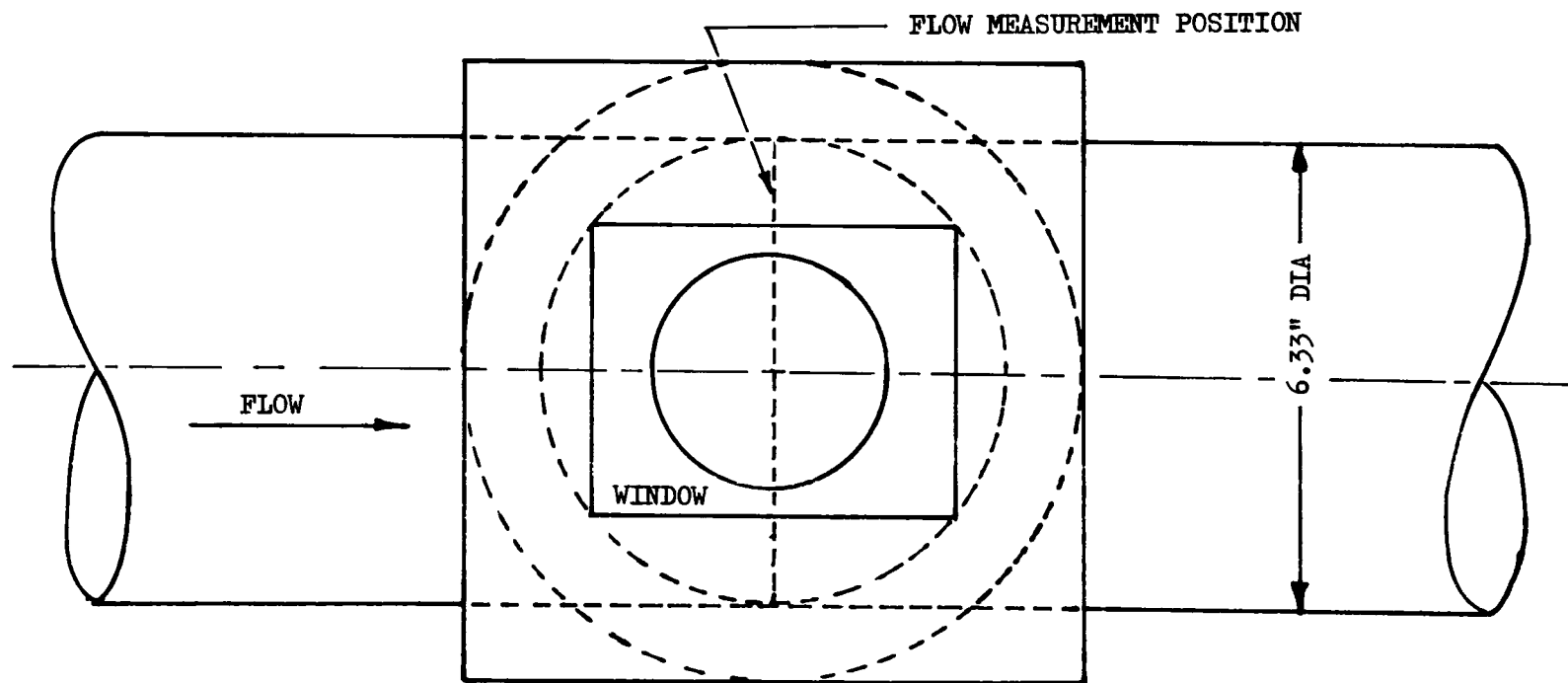


FIGURE 11 TURBULENT FLOW TEST SECTION

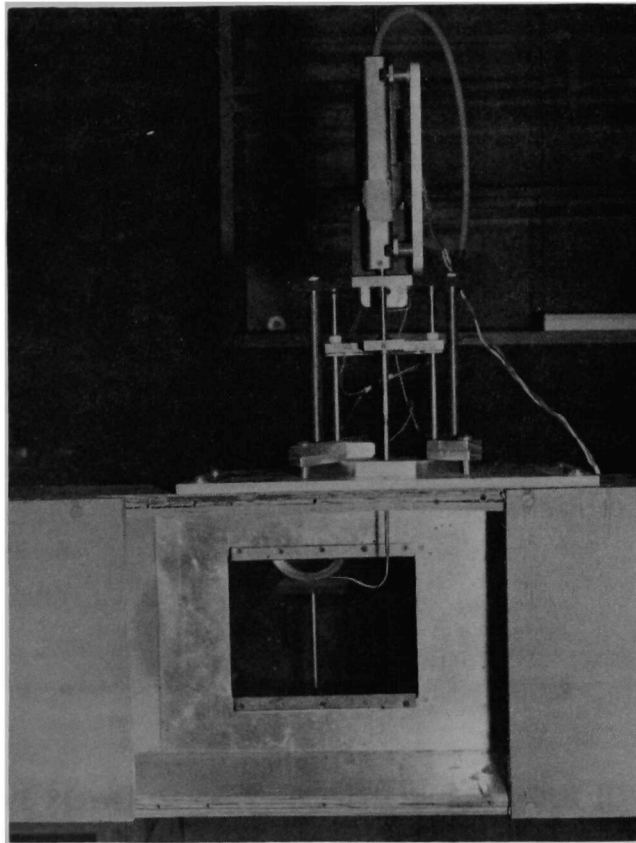


FIGURE 12
PROBE DRIVE MECHANISM
MOUNTED AT POTENTIAL TEST SECTION

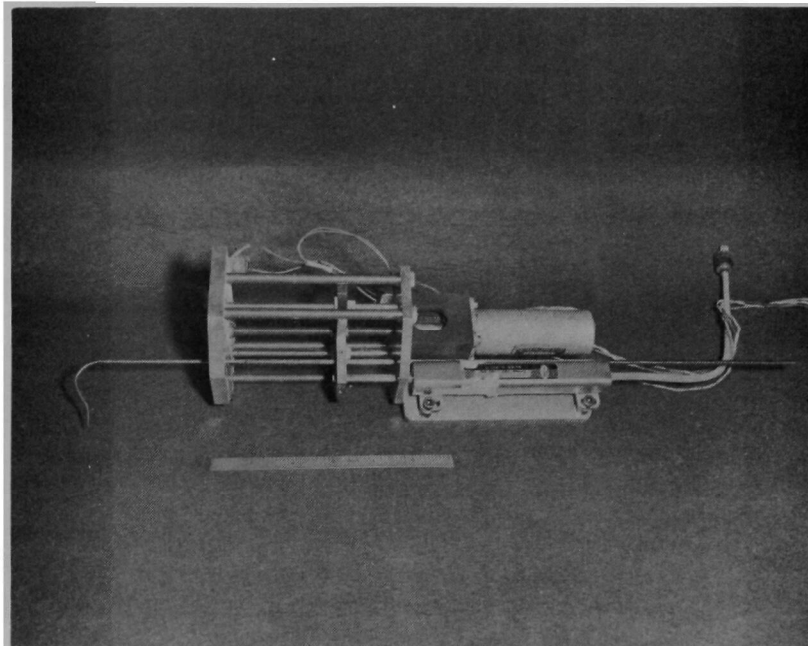


FIGURE 13
PROBE DRIVE MECHANISM



FIGURE 14
 PROBE DRIVE POWER SUPPLY, POSITION READOUT (DVM)
 AIRSPEED INDICATOR, AND CONTROL BOX

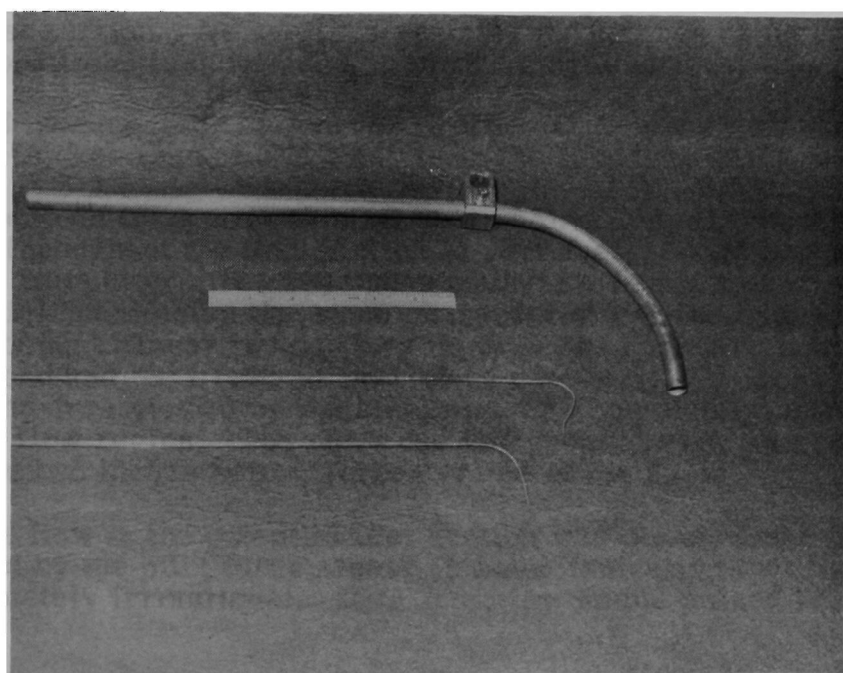


FIGURE 15
 PARTICULATE SAMPLING PROBE (APCO TRAIN PROBE) AND
 VELOCITY PROFILE PROBES

pressure port. The airspeed indicator was accurate to better than 1/4 MPH.

In Figure 15, three probes are shown. The large probe at the top was used in the air sampling experiments described later in the report. The other two probes were used in measuring the velocity profiles. The middle pitot probe was used to survey from the ceiling of the test section to the centerline; the bottom probe was used to survey from the floor up to the centerline. Both of the small probes had the same size and orifice shape. They were made from soft stainless steel tubing flattened at the end to form a rectangular tube with inside measurements of 0.004 inch high and approximately 0.09 inches wide, and a wall thickness of approximately 0.0015 inches.

II. C. 3 - Profiles

Velocity profiles were recorded in both the potential flow test section (Figures 16 - 23) and the turbulent flow test section (Figures 24 and 25) at 25.0 feet/second and 58.7 feet/second. The stations at which the profiles were recorded are shown in Figures 10 and 11.

Since a complete profile may require up to 200 data points, only position C-3 was used to run the complete set of profile measurements (at 25 feet/second and 58.7 feet/second). Half profiles were made at positions C-1, C-2, and C-4 with only spot checks made in the other half of the profile. All fifteen positions were spot checked to assure that the flow reflected the characteristics shown in C-1, C-2, C-3, and C-4. Position C-4 is the mirror image of C-2. The design of the duct facility was such that these two positions should accentuate any asymmetric flow conditions in the test section. As can be seen from the figures, agreement between the two positions is quite good, indicating symmetrical flow.

As would be expected, the corner profile, C-1, shows a boundary layer which is thicker than at other points in the tunnel.

As can be seen from the potential section profiles, the flow was quite uniform throughout the test section at 25.0 feet/second and 58.7 feet/second. Sample profiles were also made at a number of other velocities, all of which manifested the same characteristics, the only major difference being changes in boundary layer. The boundary layers at 25.0 feet/second and 58.7 feet/second were nominally 3/8 inch thick. In all cases, the area viewed by the hologram was completely in the steady or potential flow region. The recorded holographic view was two inches above and two inches below the centerline of the duct.

While the flow in the potential test section was steady and uniform as measured by the pitot tubes, there is some indication that the flow was not completely irrotational. Data from the double pulsed holograms

indicate that rotational forces were present. This was evident from observing particles which were distinctly shaped and noting the slight change in shape that occurred from the first light pulse recording to the second. It appeared that the particles in certain cases had rotated, indicating that small rotational forces had been introduced into the system somewhere upstream. The suspected point of rotational force introduction was at the point where the flow passes through the screens.

To assure the best potential flow, it was necessary to keep the screens clean and sealed against the bellmouth. Leaks at this point could cause small perturbations in the flow in the form of asymmetric flow. This effect is noted in the small differences in boundary layer growth at the top and bottom of the test section as shown in the profile plots.

The partially developed turbulent flow was as predicted at 58.7 feet/second. However, at 27.9 feet/second the flow was somewhat irregular. The difference is attributed to the short transition section and the lower Reynolds number associated with the lower velocity. These combined effects would cause the turbulent flow to develop slower and be more susceptible to perturbations from upstream sources. It is also suspected that at the lower Reynolds number, separation may have occurred in the transition section.

Values for static pressure were obtained using the wall pressure taps and an inclined manometer. Because of the indraft nature of the duct facility, the pressures were slightly below the atmospheric value. Pressures ranged from 14.16 PSIA in the potential section at 25 feet/second to 14.12 PSIA in the turbulent flow section at 58.7 feet/second. The densities corresponding to these values were 0.00228 and 0.00227 slugs/feet³. Density is constant over the cross section of the tunnel at a particular point along the tunnel. The very small longitudinal pressure gradients, or those along the tunnel, result in only minute variation in density.

Since there was no density variation across the test section, no density profiles were made. For all the experimental tests conducted, the nominal density was 0.00228 slugs/feet³. The conversion formula is shown below:

$$\rho = \frac{P}{RTg}$$

where ρ is density in slugs/feet³

P is pressure in lbs/ft².

R is a constant (53.3 ft/degrees Rankine).

T is temperature in degrees Rankine .

g is gravitational acceleration (32.2 ft/sec²).

FIGURE 16
Velocity Profile
Potential Flow Test Section
Position C-1 (Upper)

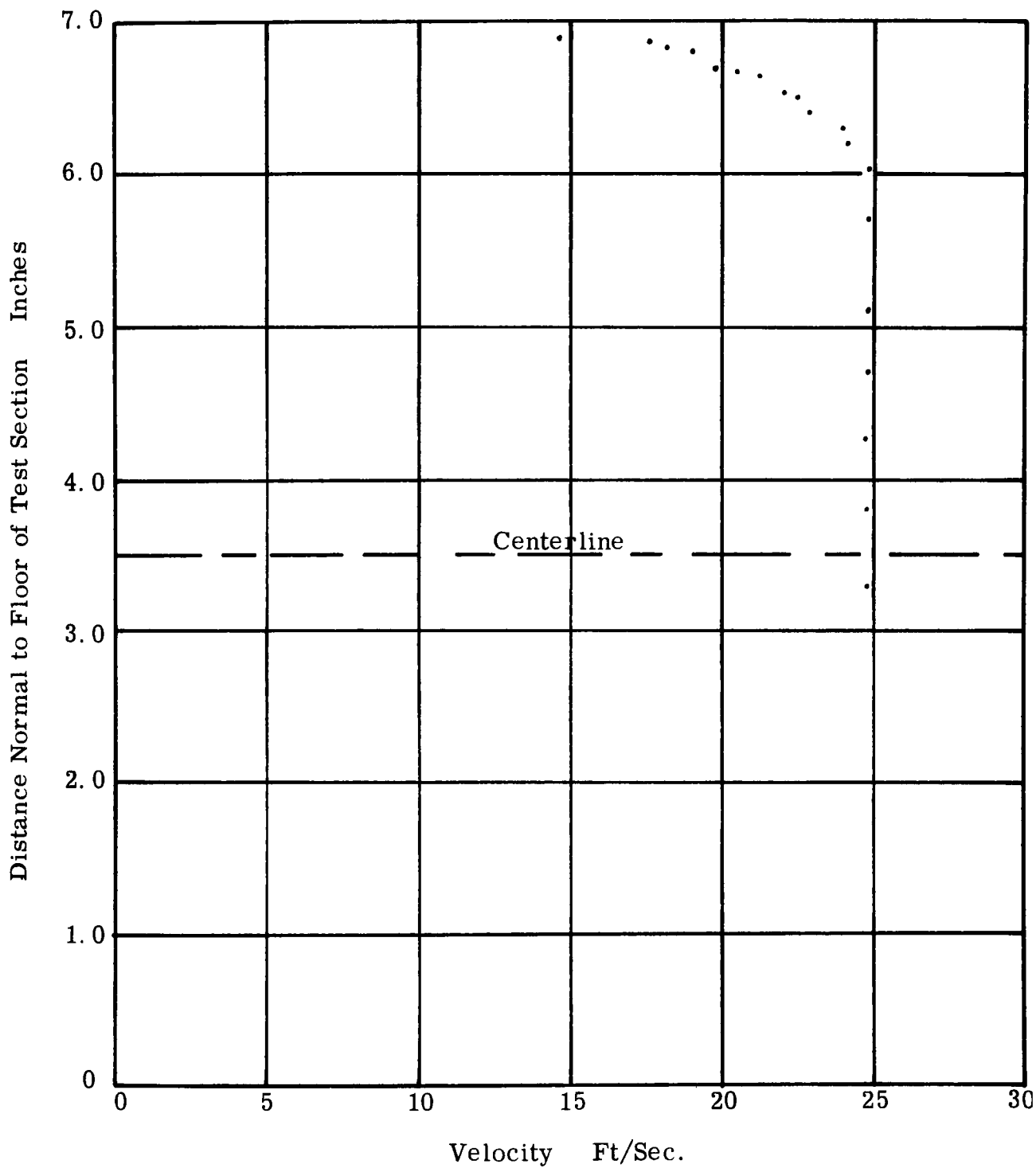


FIGURE 17
Velocity Profile
Potential Flow Test Section
Position C-2

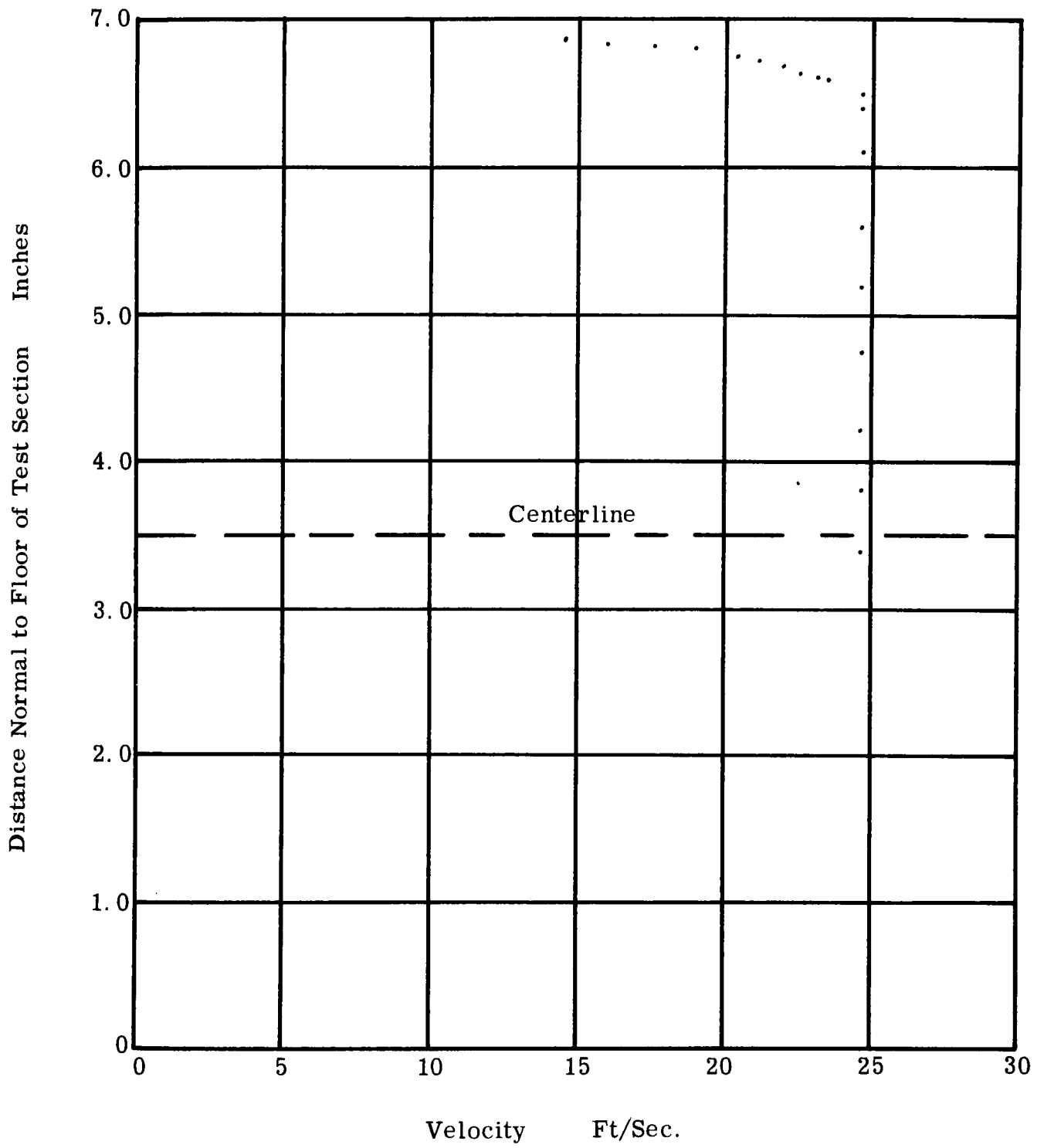


FIGURE 18
Velocity Profile
Potential Flow Test Section
Position C-3

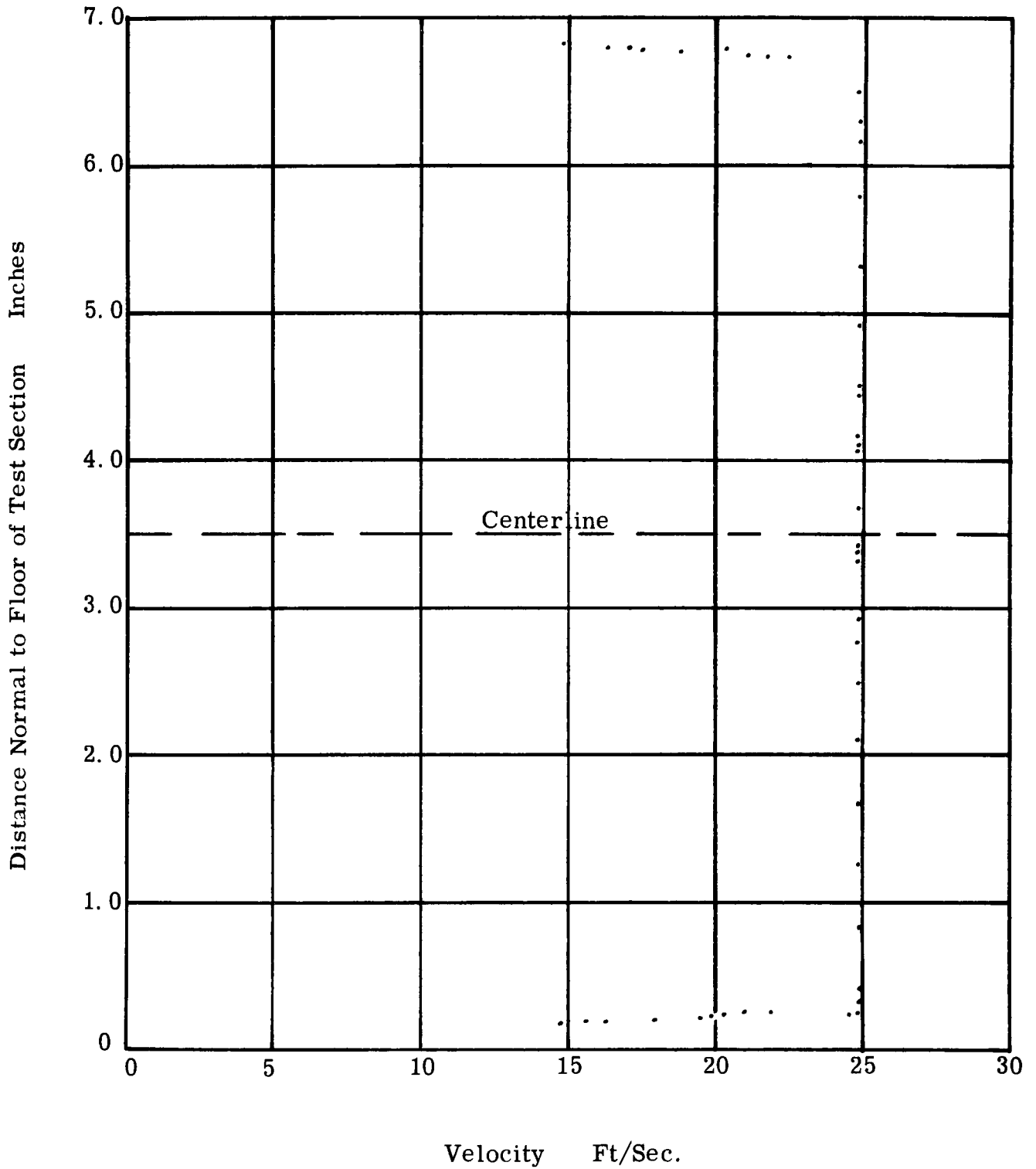


FIGURE 19
Velocity Profile
Potential Flow Test Section
Position C-4 (Lower)

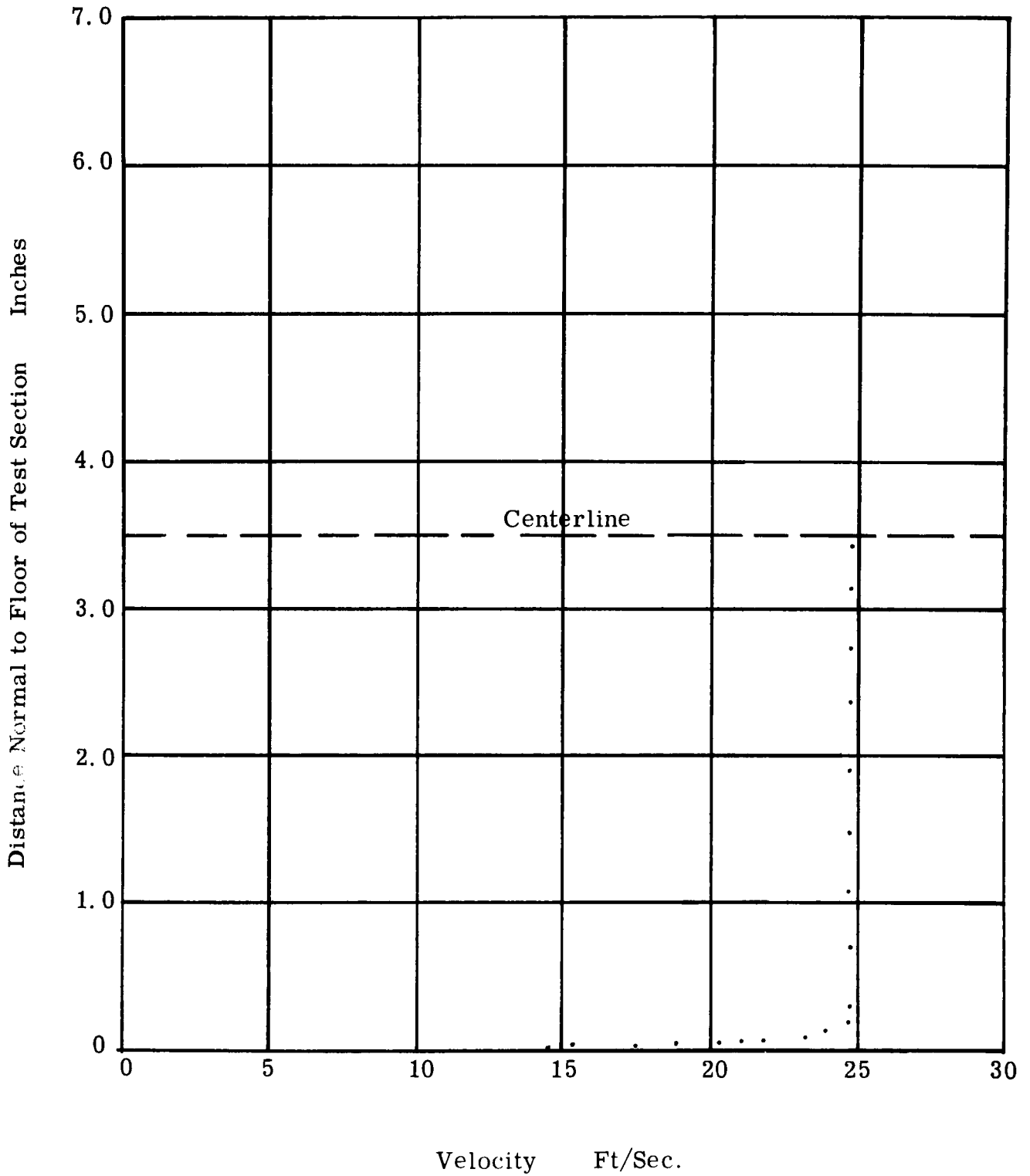


FIGURE 20
Velocity Profile
Potential Flow Test Section
Position C-1 (Upper)

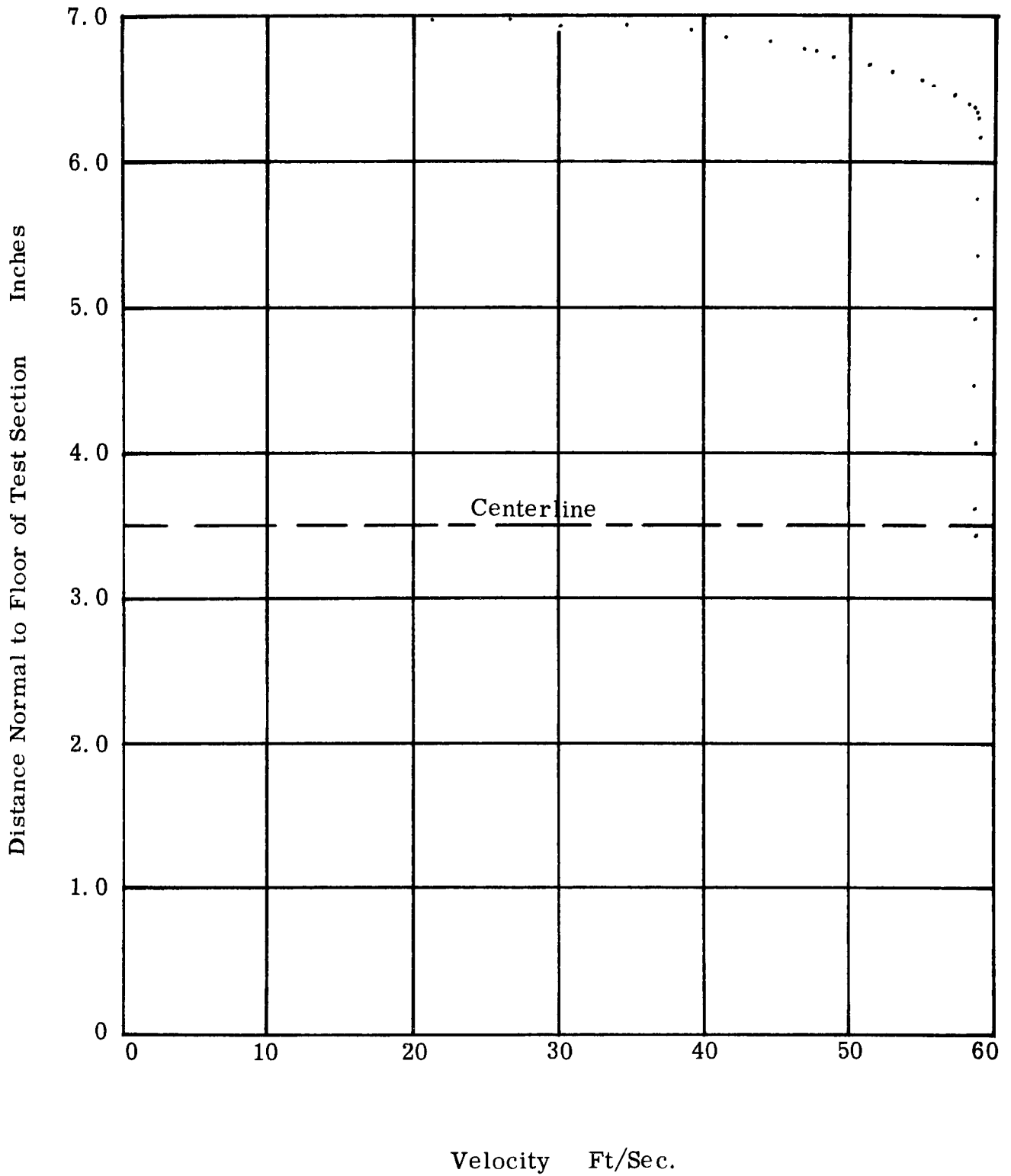


FIGURE 21
Velocity Profile
Potential Flow Test Section
Position C-2 (Upper)

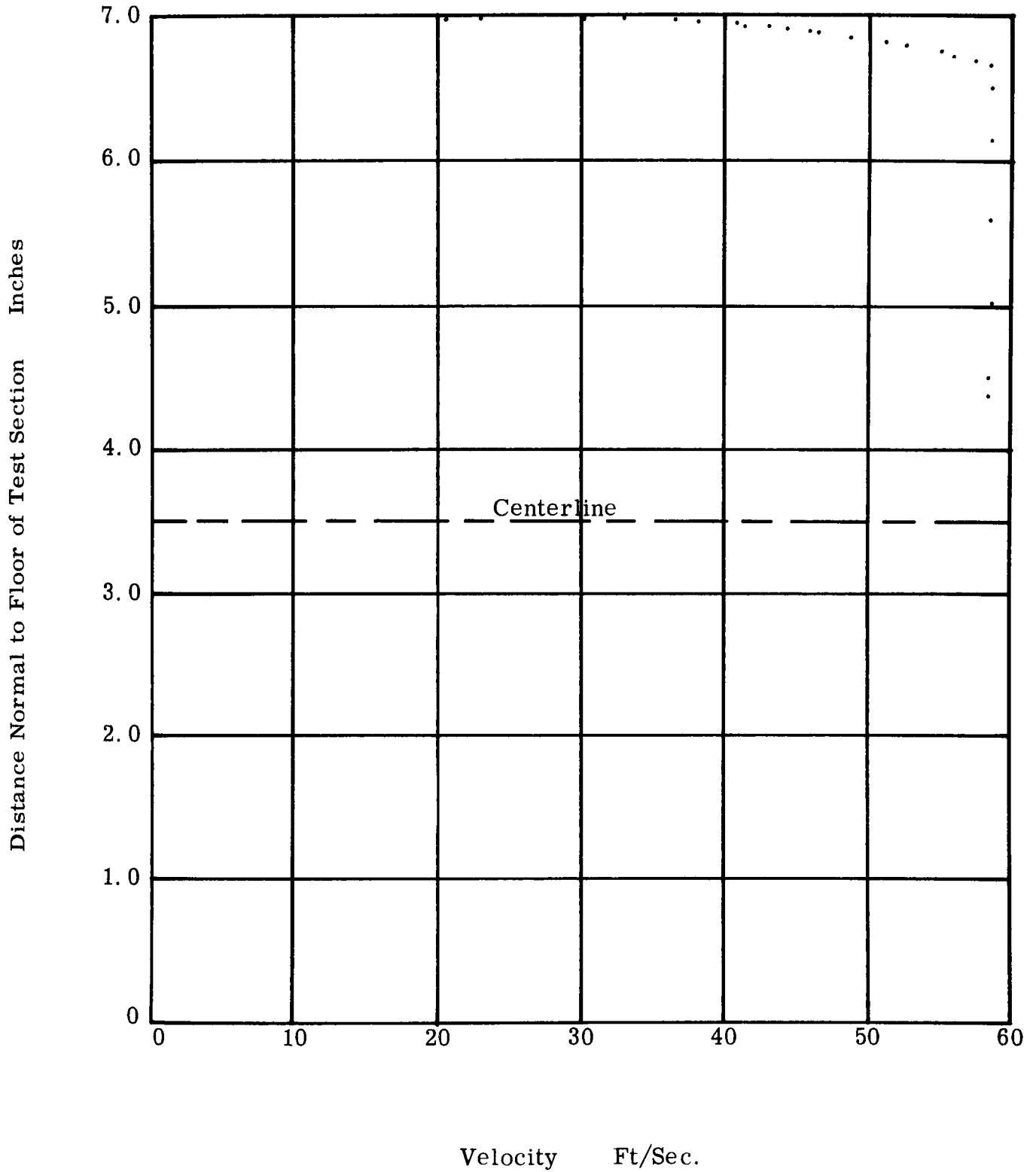


FIGURE 22
Velocity Profile
Potential Flow Test Section
Position C-3

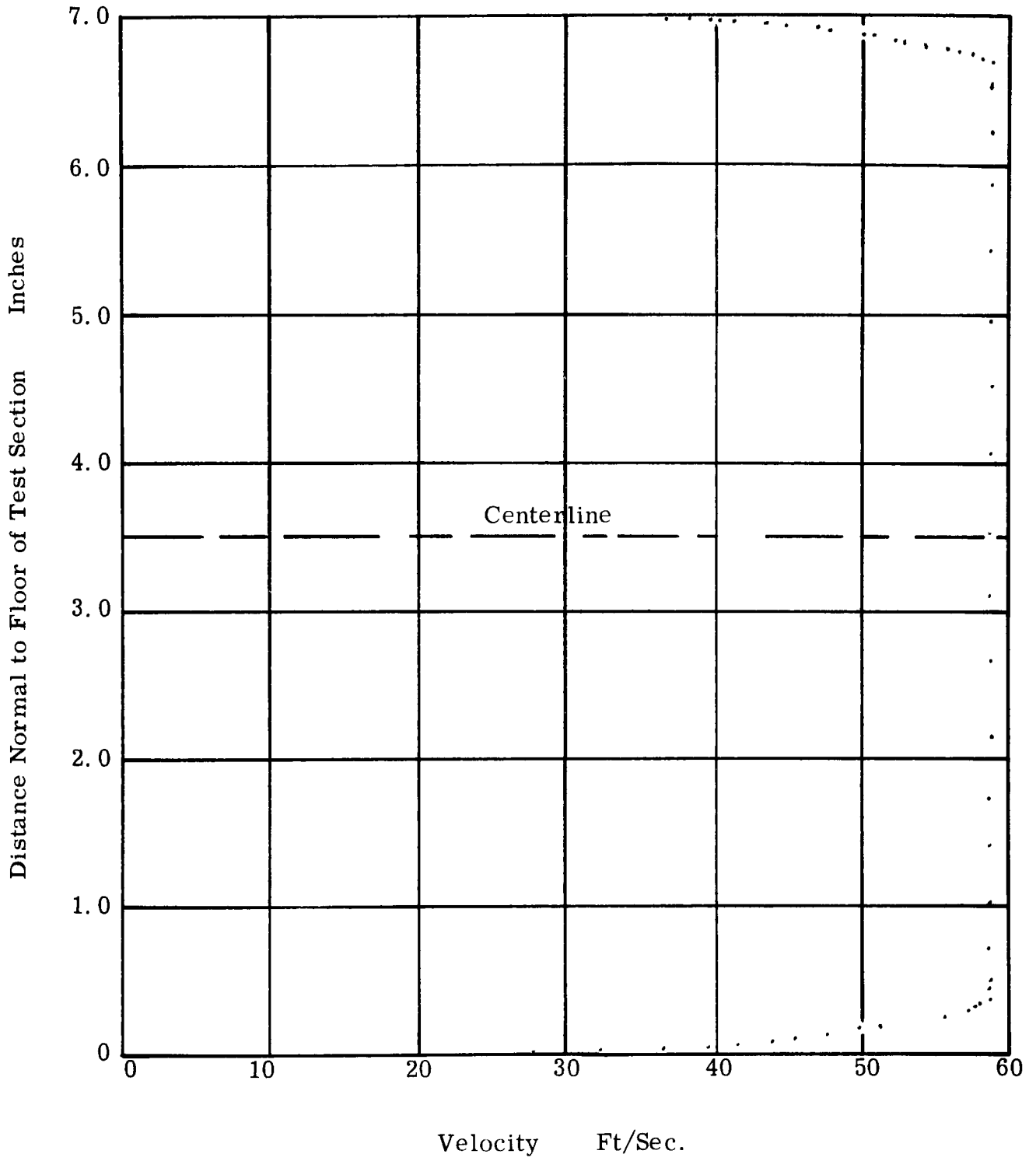


FIGURE 23
Velocity Profile
Potential Flow Test Section
Position C-4 (Lower)

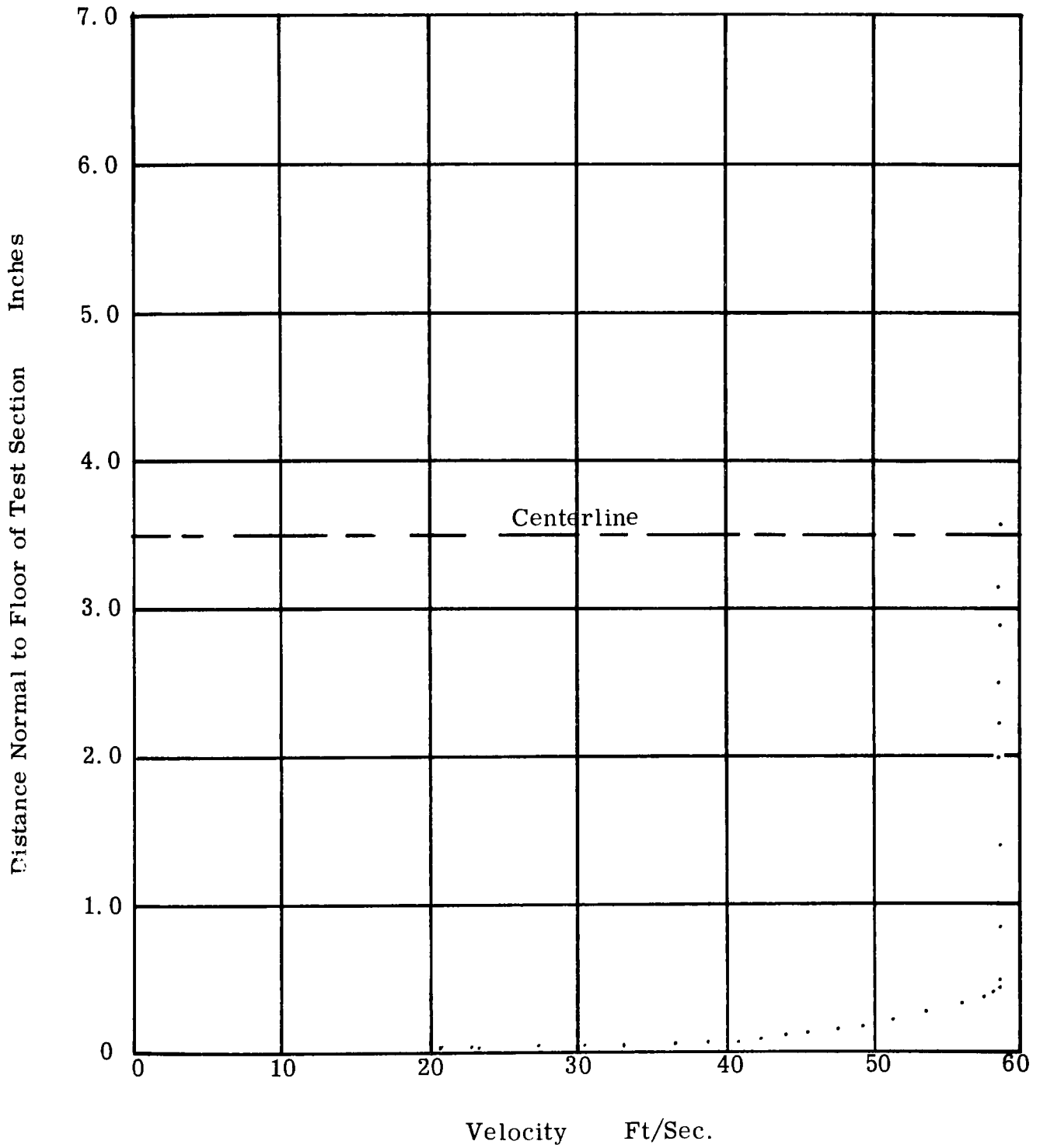


FIGURE 24
Velocity Profile
Turbulent Flow Test Section

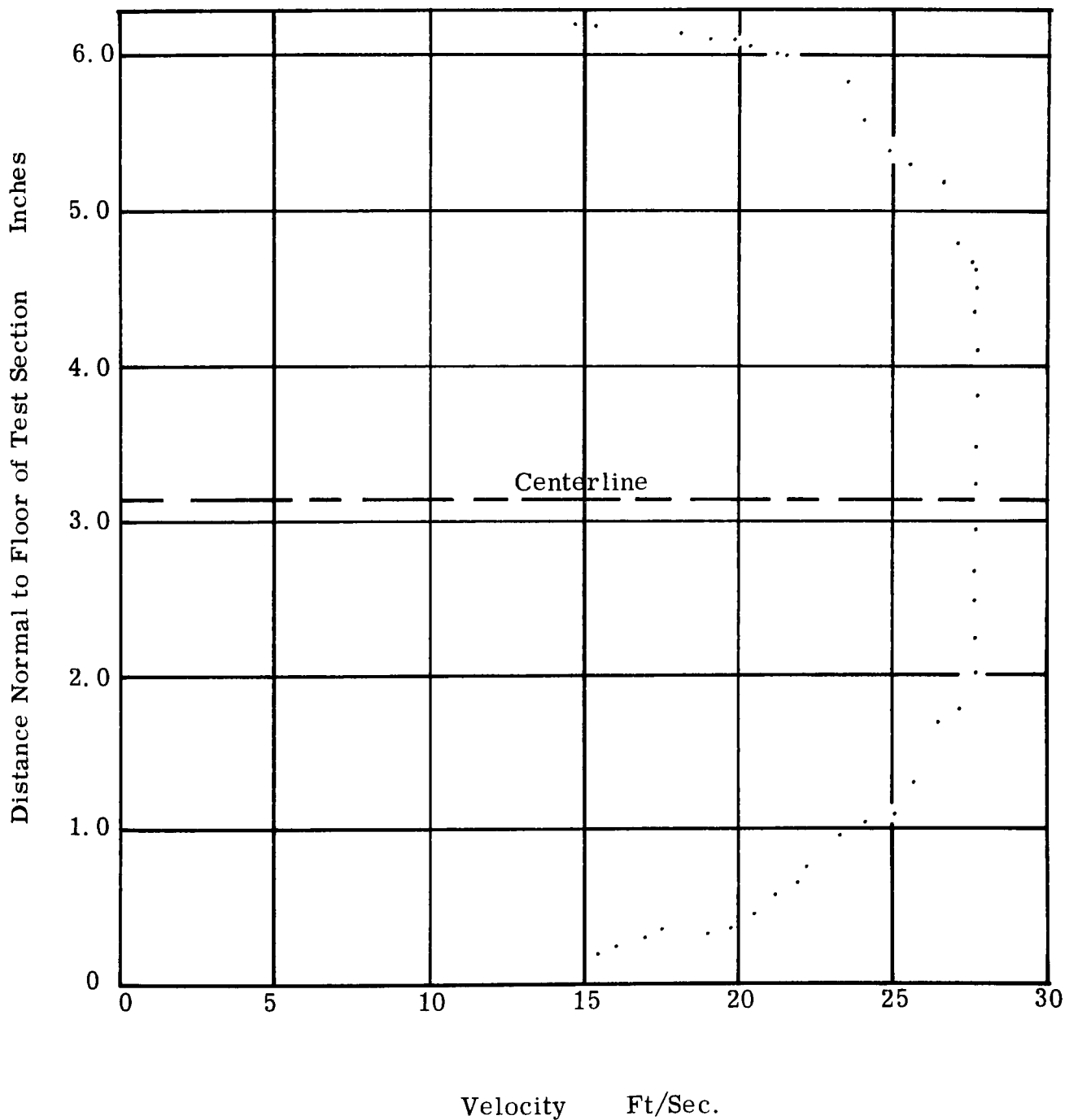
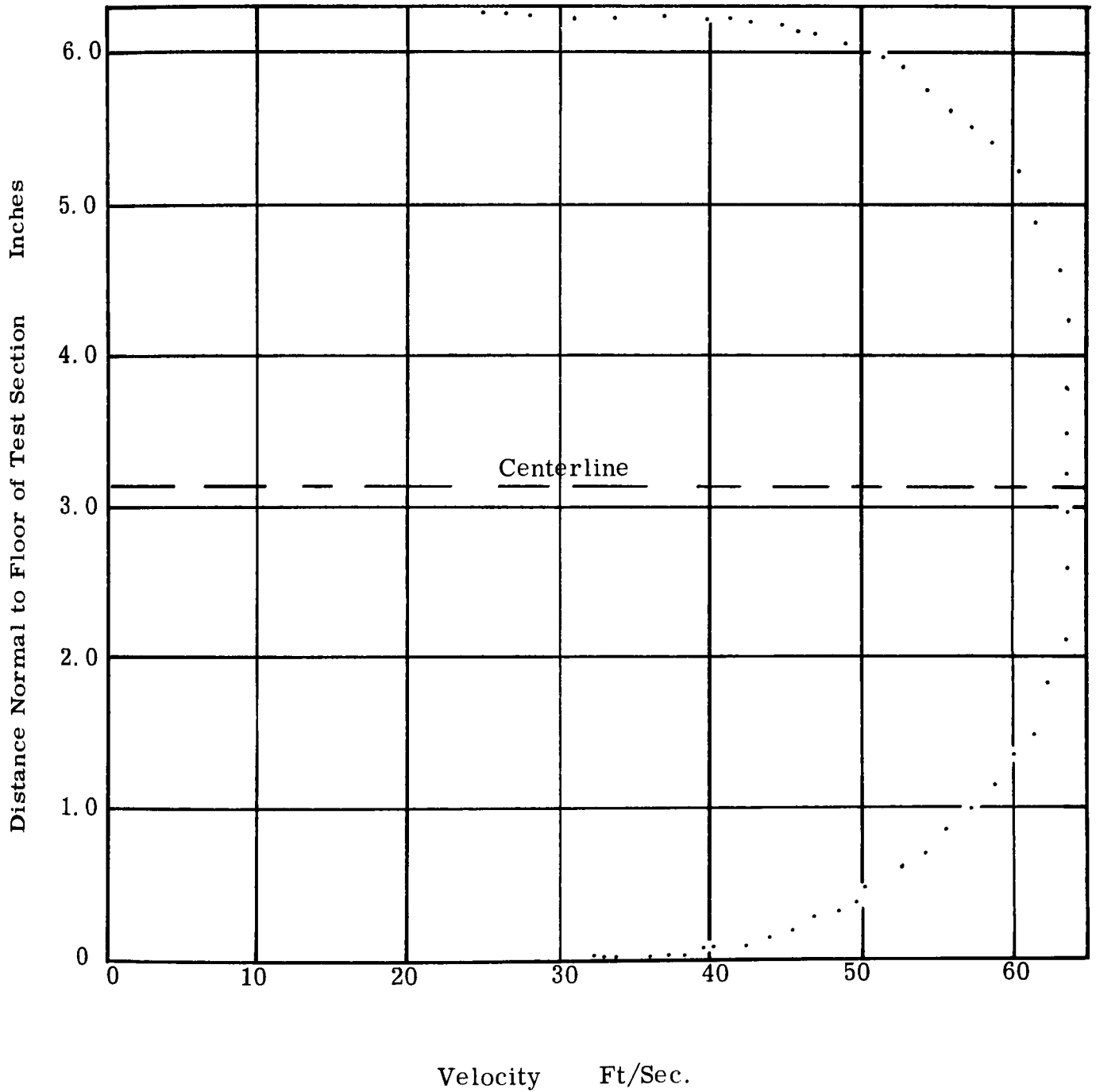


FIGURE 25
Velocity Profile
Turbulent Flow Test Section



II. D. - PARTICULATE DISPENSER

The particulate of interest in this contract included limestone, iron oxide, and in particular flyash. Dry powders, including those mentioned above, generally fall into two categories: Those that can be packed into a somewhat solid cake, and those that remain free flowing regardless of all attempts to pack them into a container. It was found that powders that can be packed are dispersed easily by a generator similar to the Wright dust feed generator, but such a generator was not useful for dispersing powders such as flyash that remain free-flowing. The Wright dust feed generator scrapes a thin layer of powder from a solid packed cake and disperses the powder scraped off, and works well with powders such as iron oxide that pack easily. On the other hand, powders which remain free flowing are dispersed well by a dispenser employing high speed mixing blades in a chamber which mix the particulate with air much like a food blender that uniformly mixes food particles with a liquid. This type of generator has worked well with free flowing powders such as carbon and flyash, but does not perform satisfactorily with powders that pack, such as tungsten or iron oxide, because of the tendency for such powders to cake around the sides of the mixing chamber.

In the initial stages of the program, all three types of particulate were tried in a Wright dust feed generator. A pellet was made of each material by compressing it in a hydraulic press to a pressure of 8,000 psi. The pellets were placed in the Wright generator, and it was found, as anticipated that only the iron oxide yielded a consistent stream of particulate. Both the flyash and limestone tended to crumble under the scraper blade and gave inconsistent results.

Since the major portion of the contract work concentrated on flyash, the particulate generator selected for use was one which would work well with free flowing materials. The design selected was a modified version of a generator which had previously been developed on a NASA sponsored study at the Georgia Institute of Technology by Dr. Richard Williams.

The selected design is shown in Figure 26. The actual device used is shown in Figure 27. Figure 28 shows the hopper, mixing blades and mixing chamber as an exploded view. The internal construction of the mixing chamber is shown in Figure 29. The hopper and auger feed arrangement is illustrated in Figure 30. The complete assembly (Figure 27) fits inside a pressurized, 55 gallon drum (Figure 31).

The operation of the particulate dispenser is described below: An external air line (100 psi) was connected to a filter and regulator with the regulator normally set at approximately 10 psi. The regulated 10 psi air supply was connected to a tee fitting; one side of the tee fed air into the drum and the other led to a by-pass valve. The air entering the drum was forced to pass through a matrix of fine holes in the bottom of the mixing chamber (Figure 29). Particulate was constantly fed into the top of the mixing

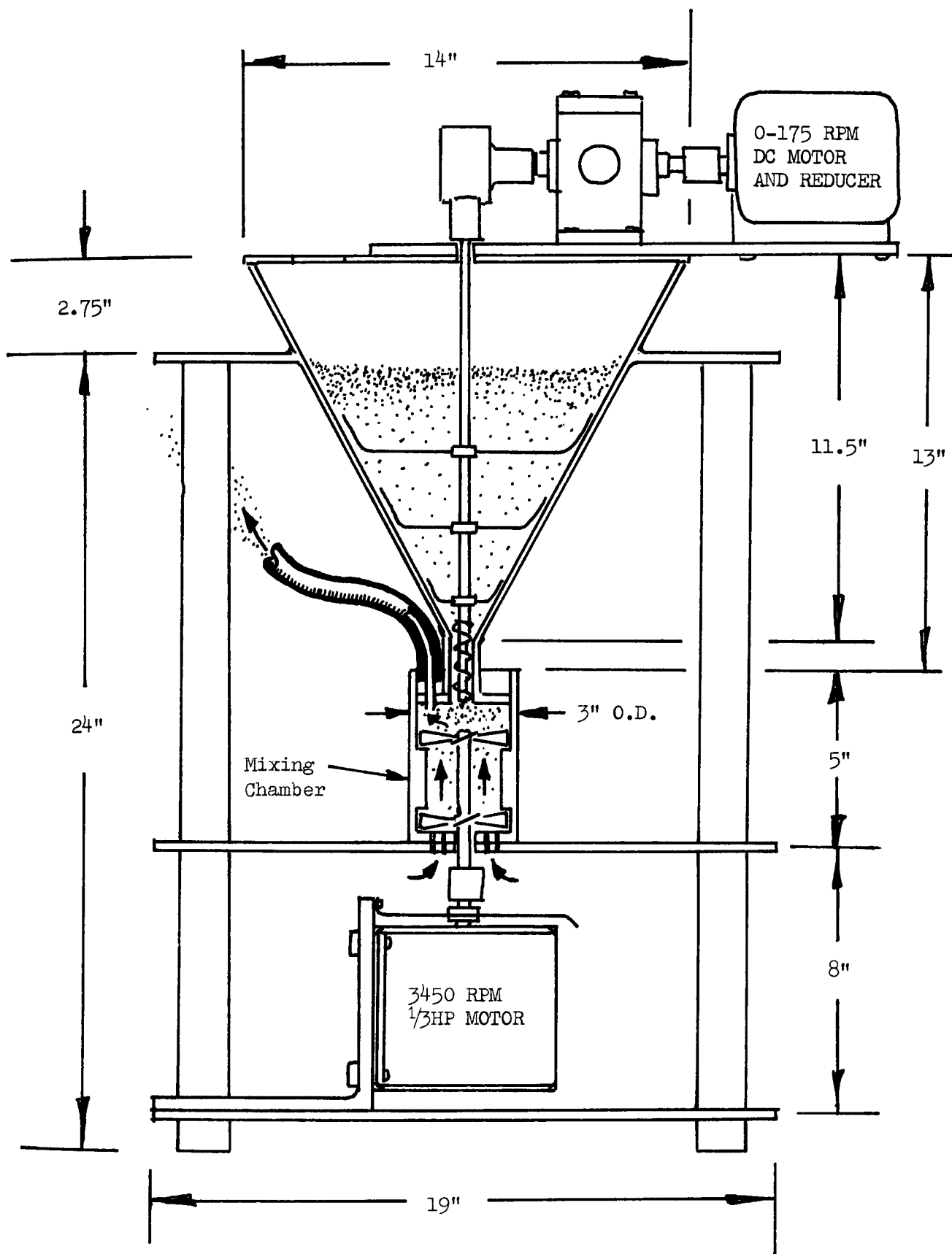


FIGURE 26. BLENDER TYPE PARTICULATE DISPENSER

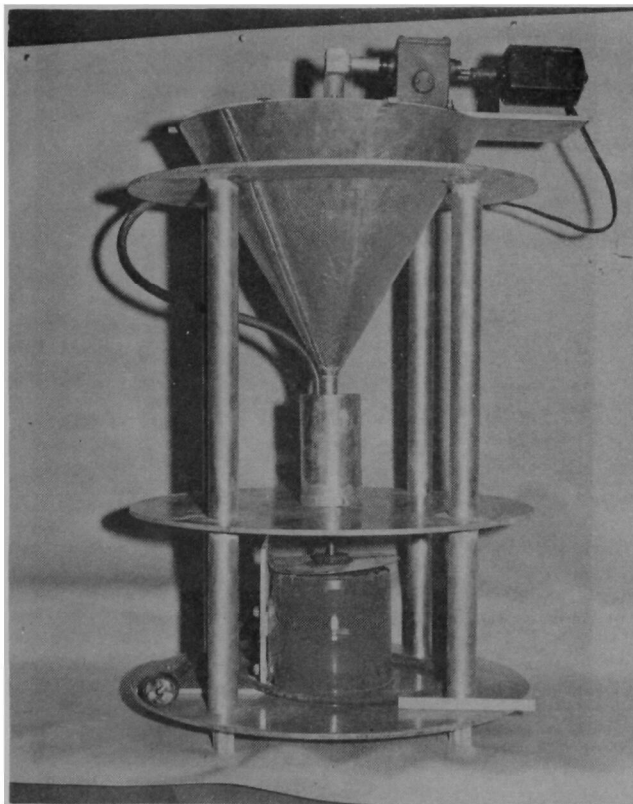


FIGURE 27
PARTICULATE DISPENSER ASSEMBLY

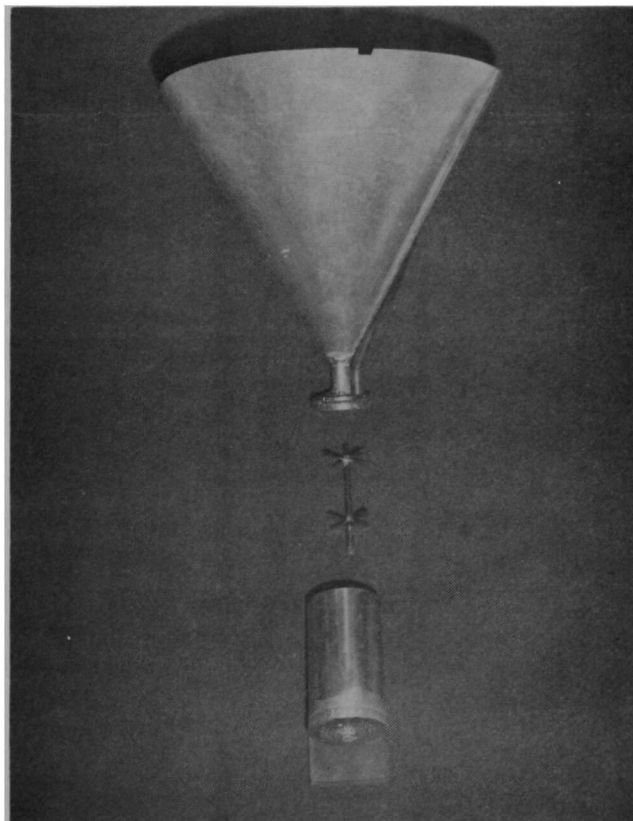


FIGURE 28
DISPENSER HOPPER, MIXING BLADES, AND MIXING CHAMBER

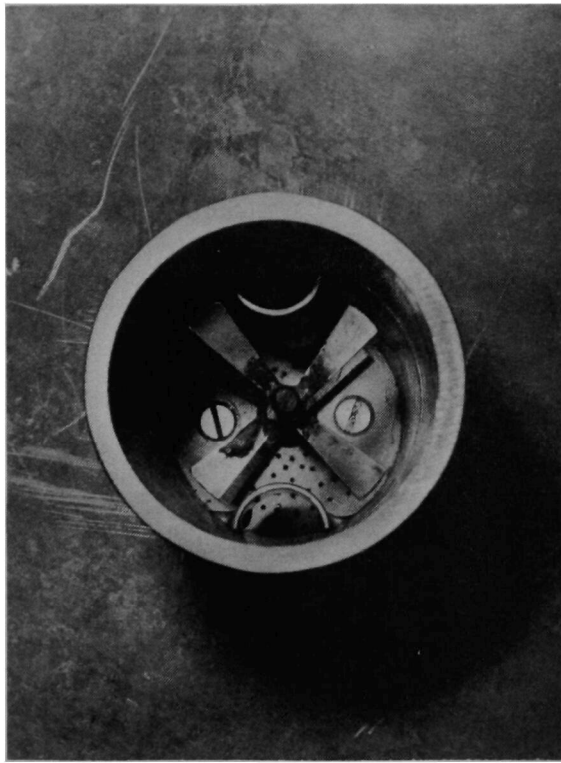


FIGURE 29
INTERNAL CONSTRUCTION OF MIXING CHAMBER

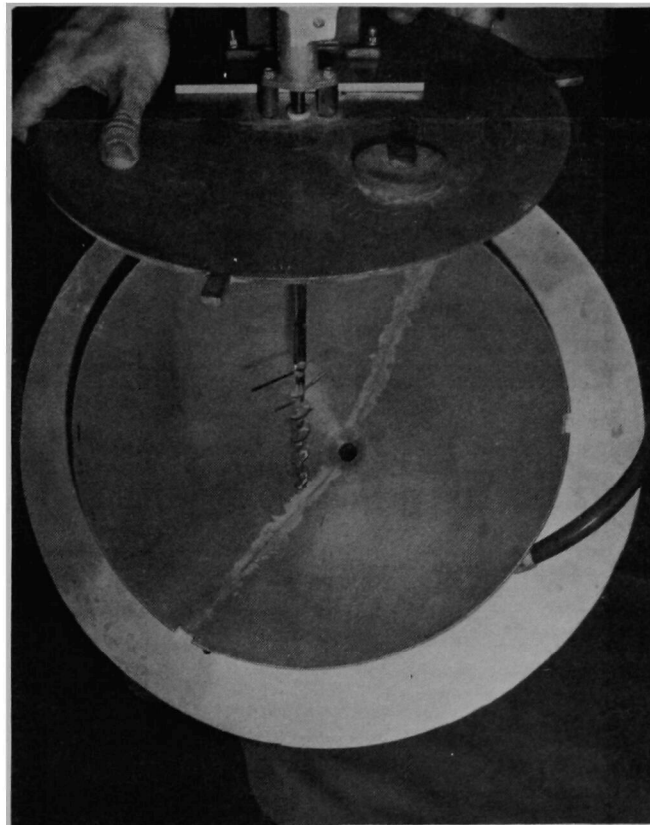


FIGURE 30
DISPENSER HOPPER AND AUGER FEED

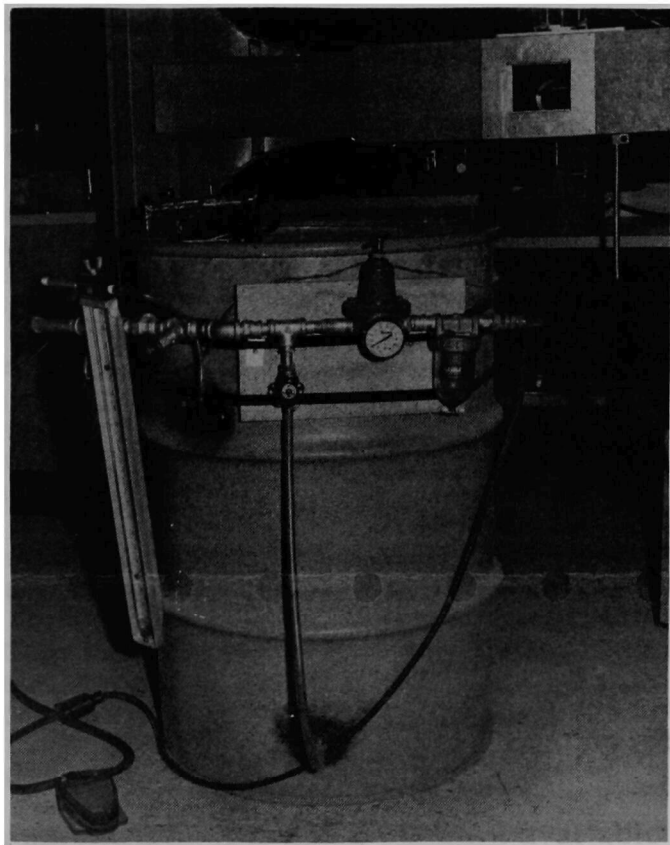


FIGURE 31
PARTICULATE DISPENSER DRUM AND PRESSURE SYSTEM

chamber from the conical hopper by a modified 3/8 inch wood auger. The rate of feed from the hopper was controlled by a variable speed d. c. motor connected through reduction gears to the auger. In the mixing chamber, two sets of blades, one above the other, were used to continuously stir the mixture of air and particulate. Two protrusions were placed in the chamber to prevent the particulate from concentrating along the walls of the chamber due to centrifugal forces generated by the blades. The mixture of air and particulate passed through a 3/8 inch tube connected to the mixing chamber and extended out through the wall of the drum. The line carrying the air entrained particulate joined the bypass air line at a tee outside the drum.

The bypass control valve allowed the concentration of particulate emerging from the dispenser to be diluted by mixing it with controlled amounts of bleed air. The resulting mixture was sent via a 3/4" flexible tube to a rake positioned in front of the duct facility bellmouth. The rake consisted of a vertical 3/4" diameter aluminum tube, slotted on the side facing the bellmouth intake (Figure 32). Figure 33 shows the set of screens positioned in front of the bellmouth which were used to damp out ambient pressure fluctuations. Since particulate would eventually build up on these screens, it was necessary to periodically clean them with an air gun.

Pressure inside the dispenser drum was monitored by a "U" type manometer which was normally set at 15" of water. The manometer also served as a pressure relief valve in that if the pressure exceeded 20" of water in the drum, the water was blown out and air was allowed to bleed out of the drum.

The concentration of particulate emitted into the duct facility was controlled by the internal pressure of the drum, the auger speed, and the bypass control valve. For major changes in particulate loadings, the air holes in the bottom of the mixing chamber could be opened or closed with a sealing material; the auger could also be changed such that more or fewer threads per unit length were available to feed particulate into the mixing chamber, or the gear reduction ratio could be changed between the D. C. motor and auger.

Using flyash as particulate, the grain loadings available in the duct facility ranged from .11 grains per standard cubic foot at 57 feet/second to 8 grains/scf at 24 feet/second. Normal operating ranges were between .15 and 5.0 grains/scf at 24 feet/second.

The dispenser proved to be quite versatile, inexpensive, and capable of operating for extended periods of time over a wide range of flow rates and particulate loadings. For reliable operation of the dispenser, it was necessary to use flyash with a low moisture content and to periodically inspect and clean out any clogged holes in the mixing chamber. The dispenser also worked well with powdered limestone, but with a material such as iron oxide, the system did not perform as satisfactorily due to the tendency of the material to cake in the mixing chamber.

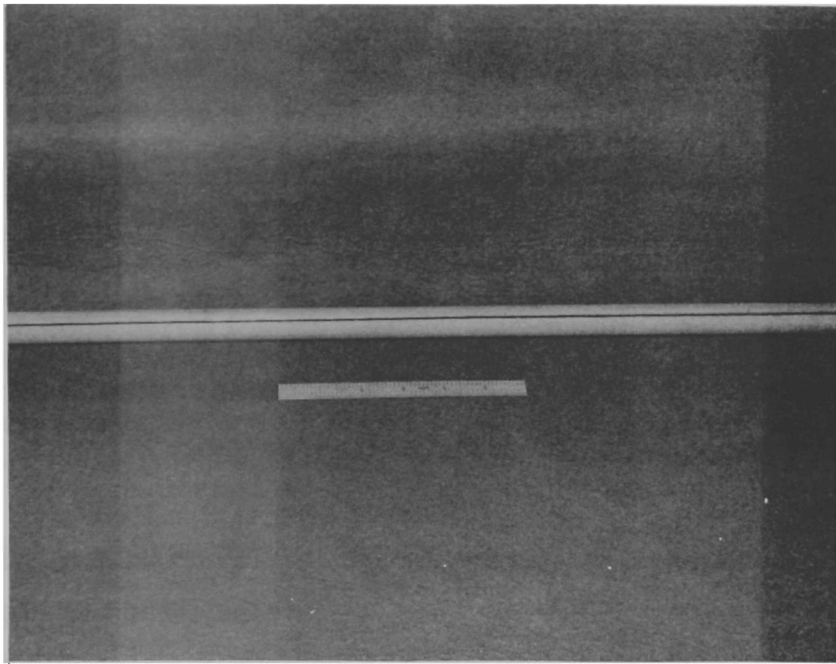


FIGURE 32
SLOTTED TUBE (RAKE) USED TO DISPENSE
FLYASH INTO DUCT FACILITY

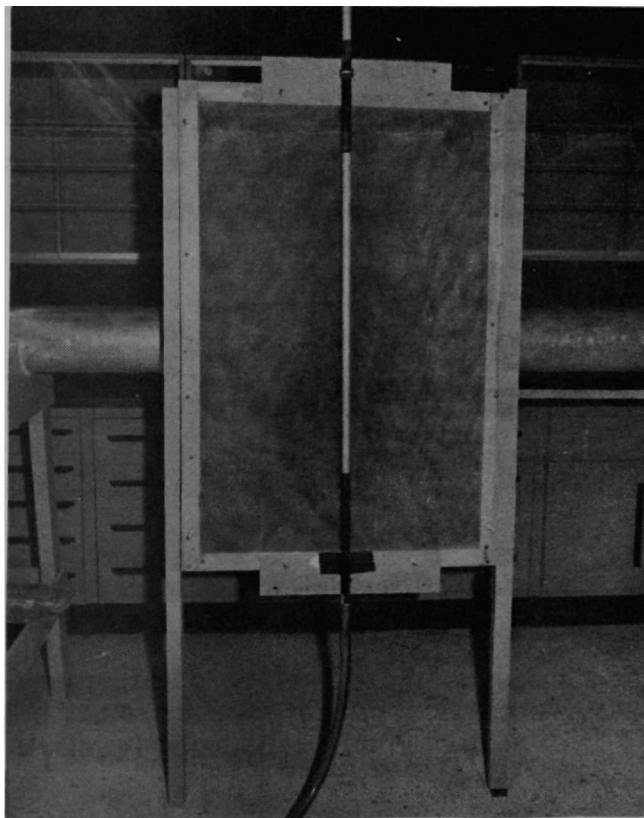


FIGURE 33
SCREENS AND SLOTTED TUBE

II. E. - HOLOGRAPHIC SYSTEMS

The design of the holographic system consisted of two phases, namely the system to make the holograms and the system to view and obtain data from the holograms. One-beam and two-beam holographic systems were considered for making the holograms. Several systems, including automatic data reduction techniques, were considered as means to obtain data from the holograms. The various systems which were studied to make and to obtain holographic data are discussed below followed by a detailed description of the systems chosen.

II. E. 1 - Systems for Making and Reconstructing Holograms

Single Beam Hologram:

The single beam hologram (sometimes referred to as the Gabor hologram) is the simplest to implement of the various holographic systems and has been used on other particle holography experiments. The beam leaving the laser is expanded and collimated as illustrated in Figure 34. The particle scene is illuminated by the collimated beam and then the light is recorded on a photographic plate that becomes the hologram.

The operation of the single beam hologram can be best understood by considering the beam striking the photographic plate as consisting of two components, one, the light scattered by the particles, and two, the light that passed by or missed the particles. Denoting the light scattered by the particles as $A_s(x, y) e^{j\phi_s(x, y)}$ and the unscattered light by A_o , the complex wavefront in the plane of the hologram is $A_o + A_s(x, y) e^{j\phi_s(x, y)}$; the amplitude transmission $T_1(x, y)$ of the resulting hologram is then given by

$$\begin{aligned} T_1(x, y) &= K |A_o + A_s(x, y) e^{j\phi_s(x, y)}|^2 \\ &= K A_o^2 + K A_s(x, y)^2 + K A_o A_s(x, y) e^{j\phi_s(x, y)} \\ &\quad + K A_o A_s(x, y) e^{-j\phi_s(x, y)} \end{aligned}$$

The unscattered light A_o is generally called the reference beam and $A_s(x, y)$ is called the signal beam.

Figure 35 illustrates a system to reconstruct a single beam hologram. A collimated wavefront of amplitude B strikes the hologram and the wavefront $U_1(x, y)$ leaving the hologram is

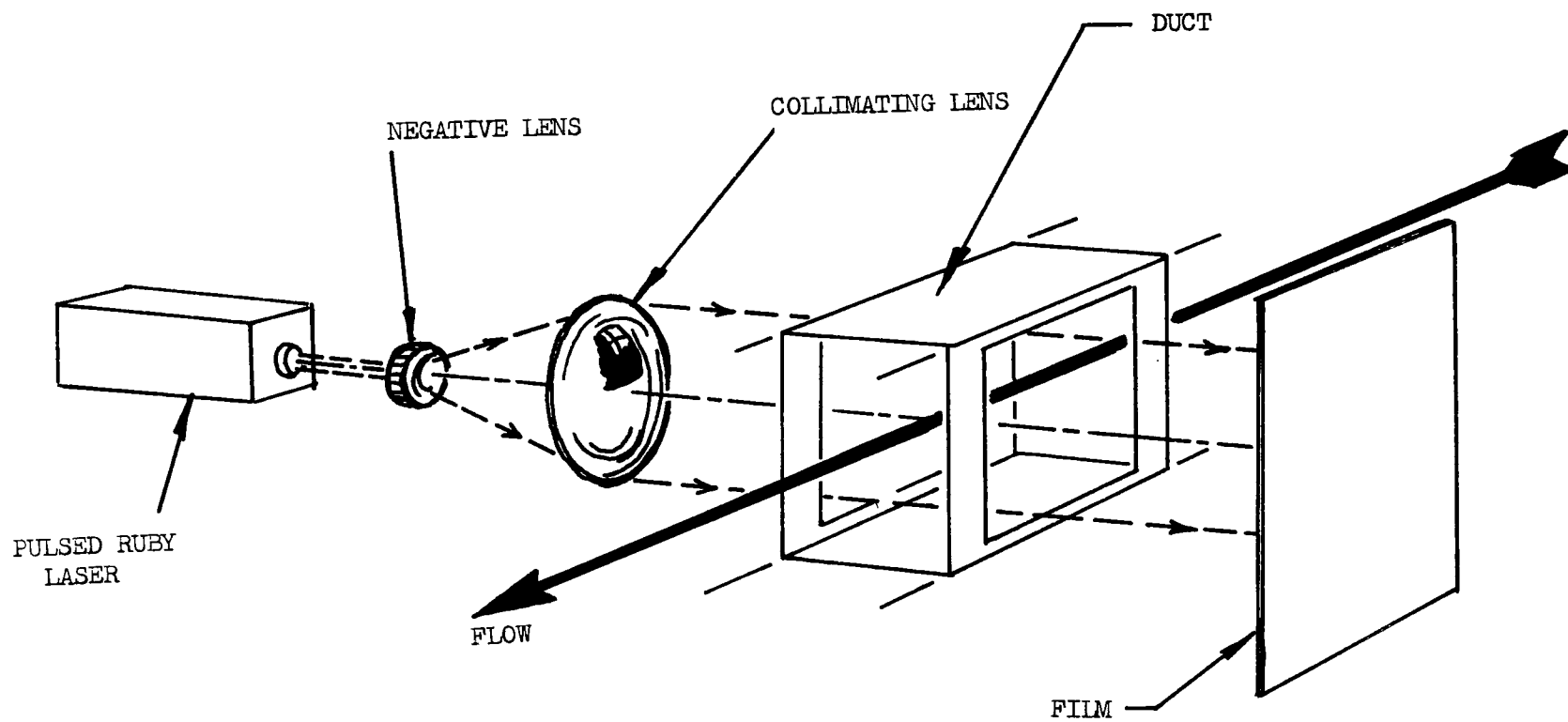


FIGURE 34. SINGLE BEAM HOLOGRAPHIC SYSTEM

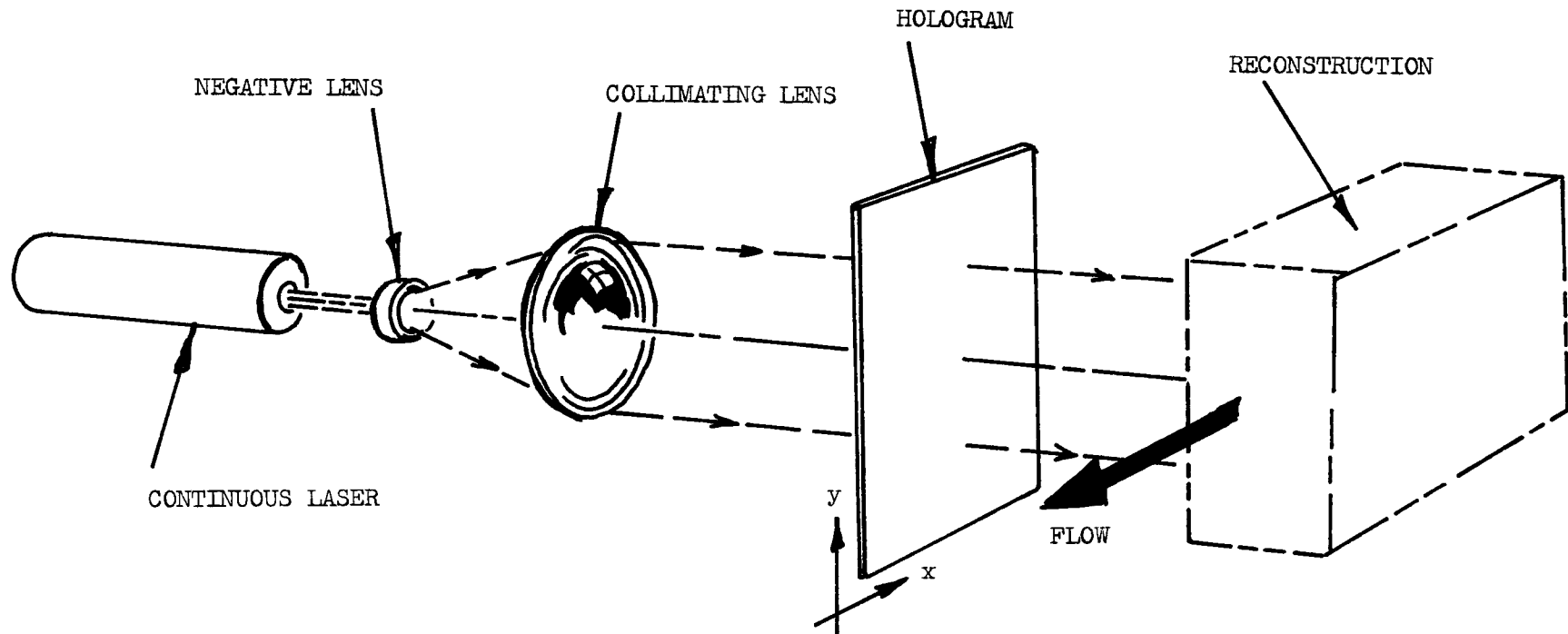


FIGURE 35. RECONSTRUCTION SYSTEM FOR SINGLE BEAM HOLOGRAM

$$U_1(x, y) = B K A_o^2 + B K A_s^2(x, y) + B K A_o A_s(x, y) e^{j\phi_s(x, y)} \\ + B K A_o A_s(x, y) e^{-j\phi_s(x, y)}$$

The wavefront leaving the hologram is composed of four components as indicated by the above equation. The first two components are of low spatial frequency and contain no useful information. The

$B K A_o A_s(x, y) e^{-j\phi_s(x, y)}$ component forms a real image of the particles and the $B K A_o A_s(x, y) e^{j\phi_s(x, y)}$ forms a virtual image of the particles

which appears behind the hologram. Since the low frequency components are generally bright enough to obscure or "wash out" the particle images and the particles are often too small to see, the real image is magnified by a lens as shown in Figure 36. The low frequency terms are brought to focus near the focal point of the lens and can be removed by placing a small opaque spot there. The lens, therefore, performs the dual function of magnifying the particle reconstructions and focussing the low frequency terms so that the spot can remove them.

Two-Beam Holograms:

The two-beam hologram (sometimes referred to as the Leith-Upatnieks hologram) differs from the single beam hologram in that the reference beam, rather than being the unscattered light is a separate beam introduced at an angle with the beam illuminating the particles as illustrated in Figure 37. Denoting the beam from the particle scene striking the

hologram by $D(x, y) e^{j\beta(x, y)}$ and the reference beam by $C e^{jk_0 x}$, the amplitude transmission of the film exposed as illustrated is given by

$$T_2(x, y) = K |D(x, y) e^{j\beta(x, y)} + C e^{jk_0 x}|^2 \\ = K C^2 + K D^2(x, y) + K C D(x, y) e^{j[k_0 x - \beta(x, y)]} \\ + K C D(x, y) e^{-j[k_0 x - \beta(x, y)]}$$

The method of reconstructing the hologram is shown in Figure 38. The hologram is illuminated by a collimated laser beam and the wavefronts leaving the holograms are indicated. Note that the real and virtual images are now separated from each other by an angle 2α and separated from the low frequency light components $K C^2$ and $K D^2(x, y)$ by an angle of α . The real image from the hologram has the same amplitude as the wavefront recorded by the Gabor hologram and is given by

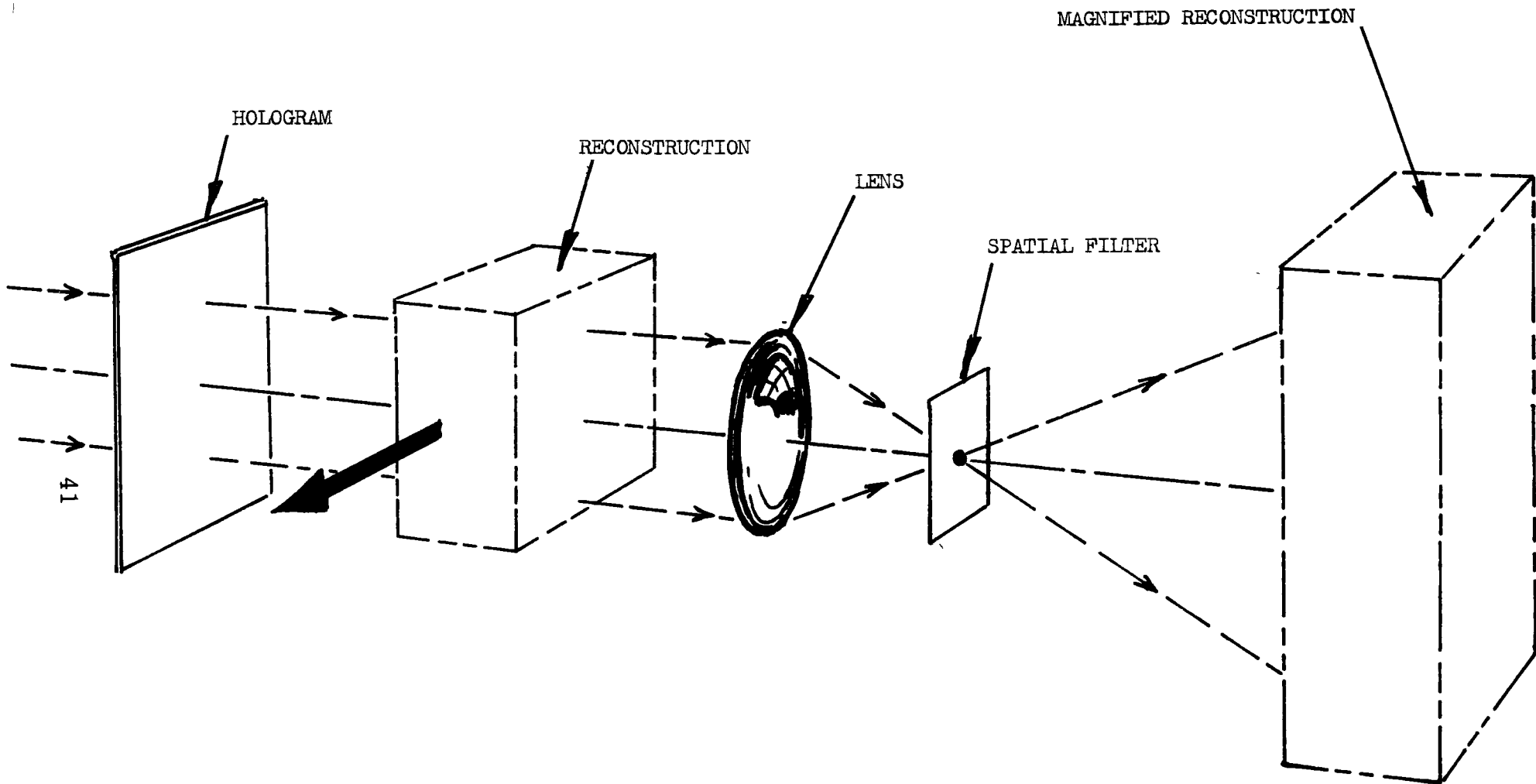


FIGURE 36. SYSTEM TO MAGNIFY AND SPATIALLY FILTER THE RECONSTRUCTED IMAGE

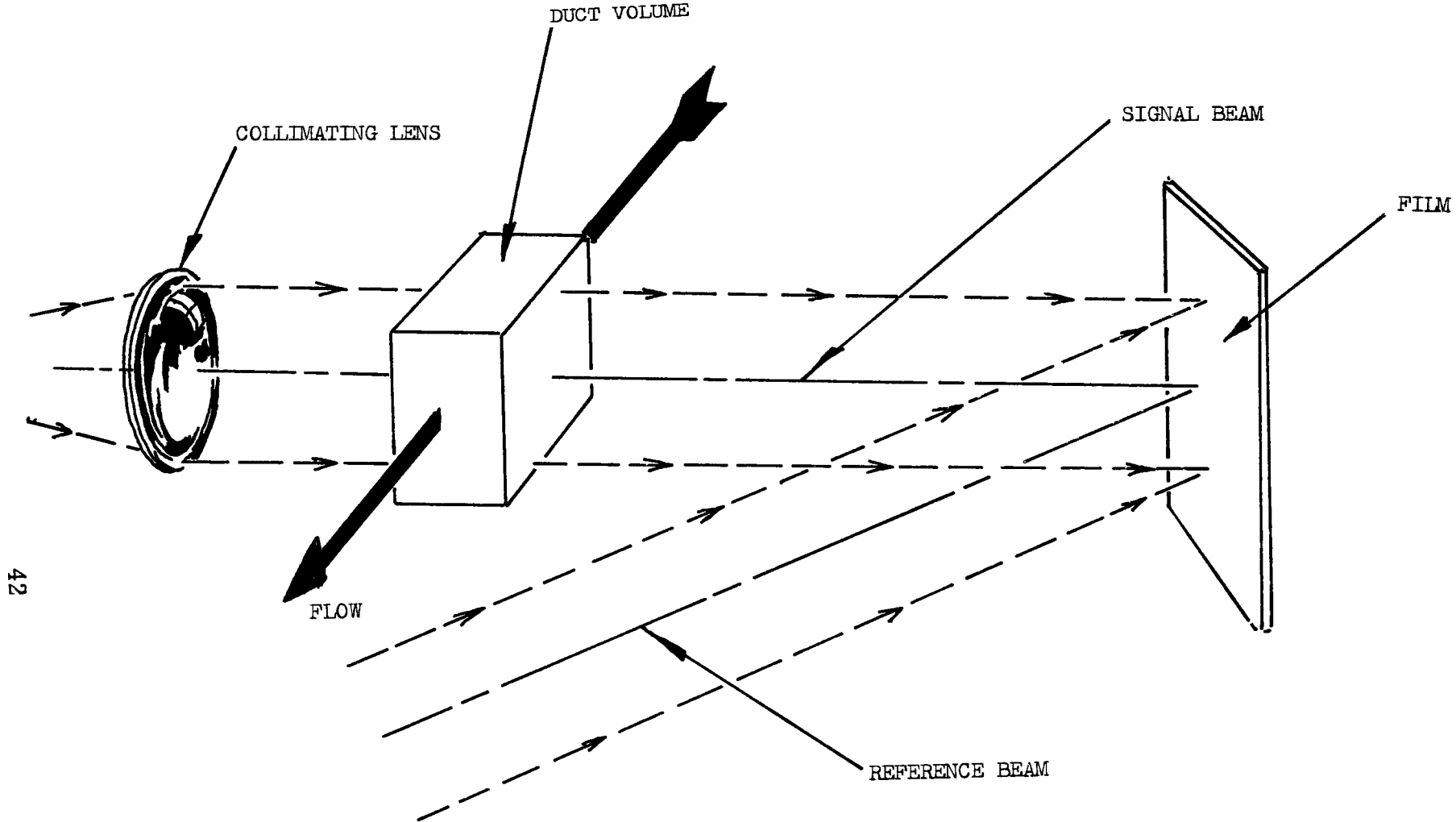


FIGURE 37. SCHEMATIC OF TWO-BEAM HOLOGRAM

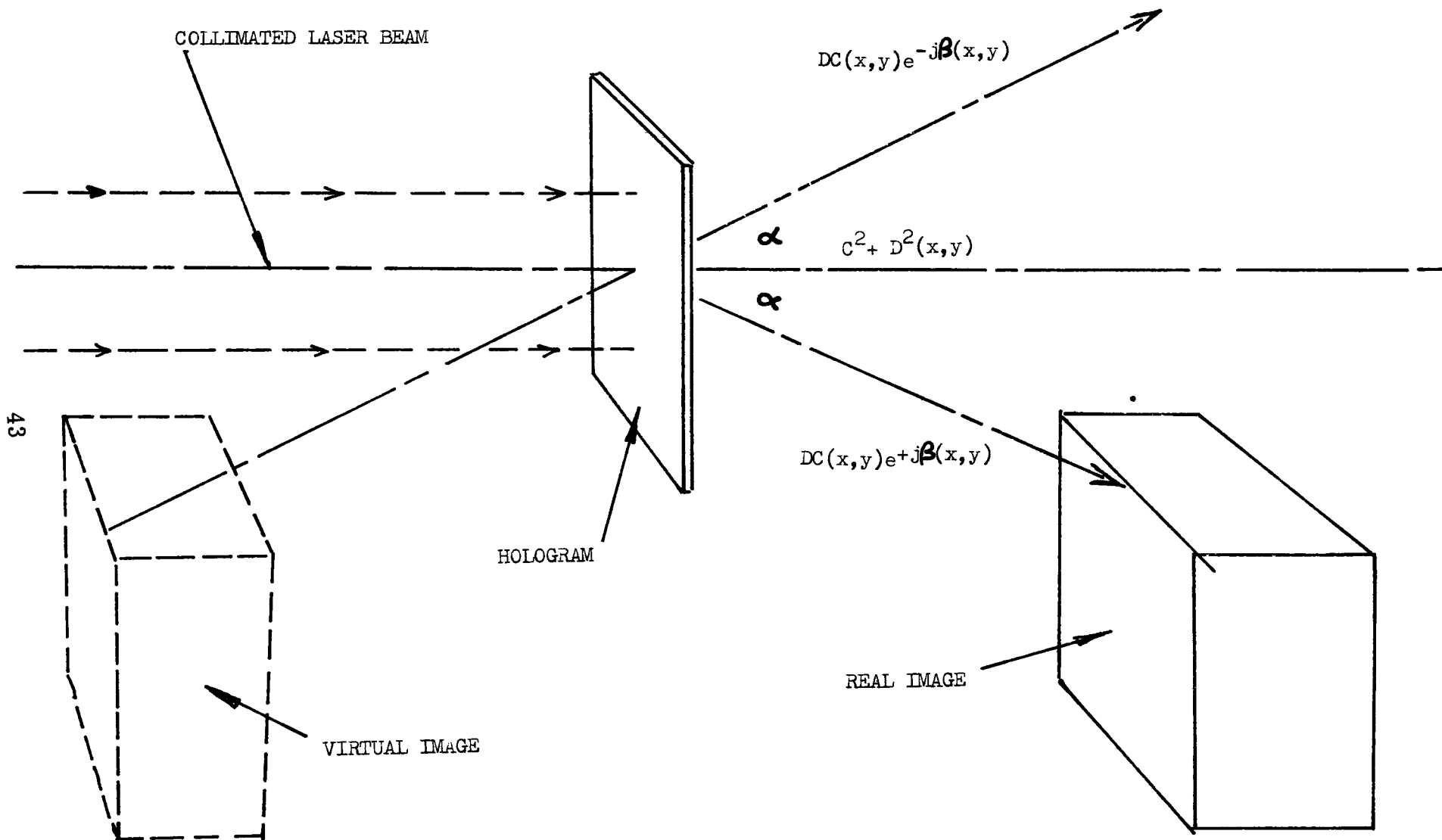


FIGURE 38. RECONSTRUCTION OF A TWO-BEAM HOLOGRAM

$$CD(x, y) e^{j\beta(x, y)} = B + A(x, y) e^{j\phi(x, y)}$$

The particles can be made a little easier to view by spatially filtering the B term out by an opaque spot as was done with single beam holograms.

Comparison of One- and Two-Beam Systems Applied to Particle Holography:

The most obvious difference between one- and two-beam systems applied to the particle holography problem is that one-beam systems can only make holograms of light scattered in the forward direction while two-beam systems can make holograms of light scattered in any direction. Since the light recorded by a hologram must coincide with the reference beam and since the reference beam of a single beam hologram is in the forward direction, it follows that only forward-scattered light can be recorded by a single beam hologram. The two-beam hologram is more flexible in that the direction of the reference beam is independent of the direction of the beam scattered by the particle. Therefore, the two-beam system can be used to holographically record light scattered to the side or scattered backwards by the particles.

However, one of the goals of this effort was to precisely determine the size and shape of the particulate and forward-scattered light is better suited for this purpose than light scattered in other directions. First of all, the particles considered in this experiment are 5 microns or larger and light scattered by particles in this size range are governed by the laws of Fraunhofer and Mie scattering. In the Fraunhofer and Mie regimes, the light scattered in the forward direction is much stronger than light scattered in the side or back directions giving the hologram a stronger beam to record. Since such a small amount of light is scattered by the particles, it is important that the hologram records the strongest components of the scattered light. Hence, one would expect that holograms of forward-scattered light would record smaller particles than holograms of light scattered in other directions. Also, forward-scattered light contains more information about particle shape than light scattered in other directions. The light scattered in the forward direction is related to the particle shape by a Fresnel transform relation. The reconstruction of the hologram performs essentially an inverse Fresnel transform yielding an accurate replica of the shape of the particle. However, light scattered to the side and backwards will depend on the reflectivity of the particle, and, therefore, portions of the particle with high reflectivity will produce a good reconstruction while portions with poor reflectivity will provide a poor reconstruction. The net result is a poor reconstruction of the particle. Figure 39 is a photograph of the reconstruction from a particle hologram made with forward-scattered light while Figure 40 is a photograph of a reconstruction made with side-scattered light. Note how much more clearly the shape of the particles are shown in Figure 39 as compared with Figure 40. The experiments carried out to obtain these photographs are described toward the end of this section.

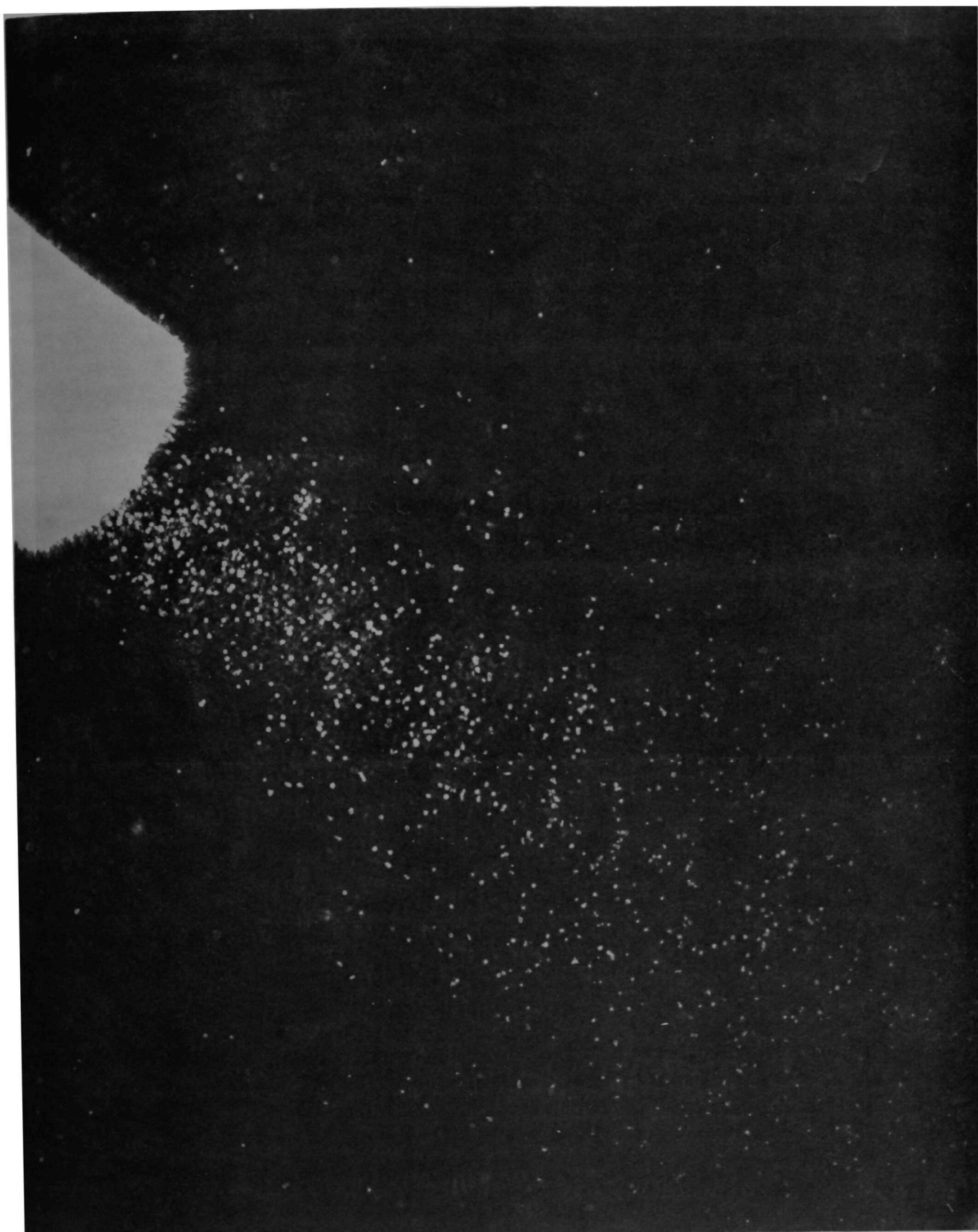


FIGURE 39
RECONSTRUCTION OF A HOLOGRAM OF SMALL GLASS BALLS
MADE WITH FORWARD SCATTERED LIGHT

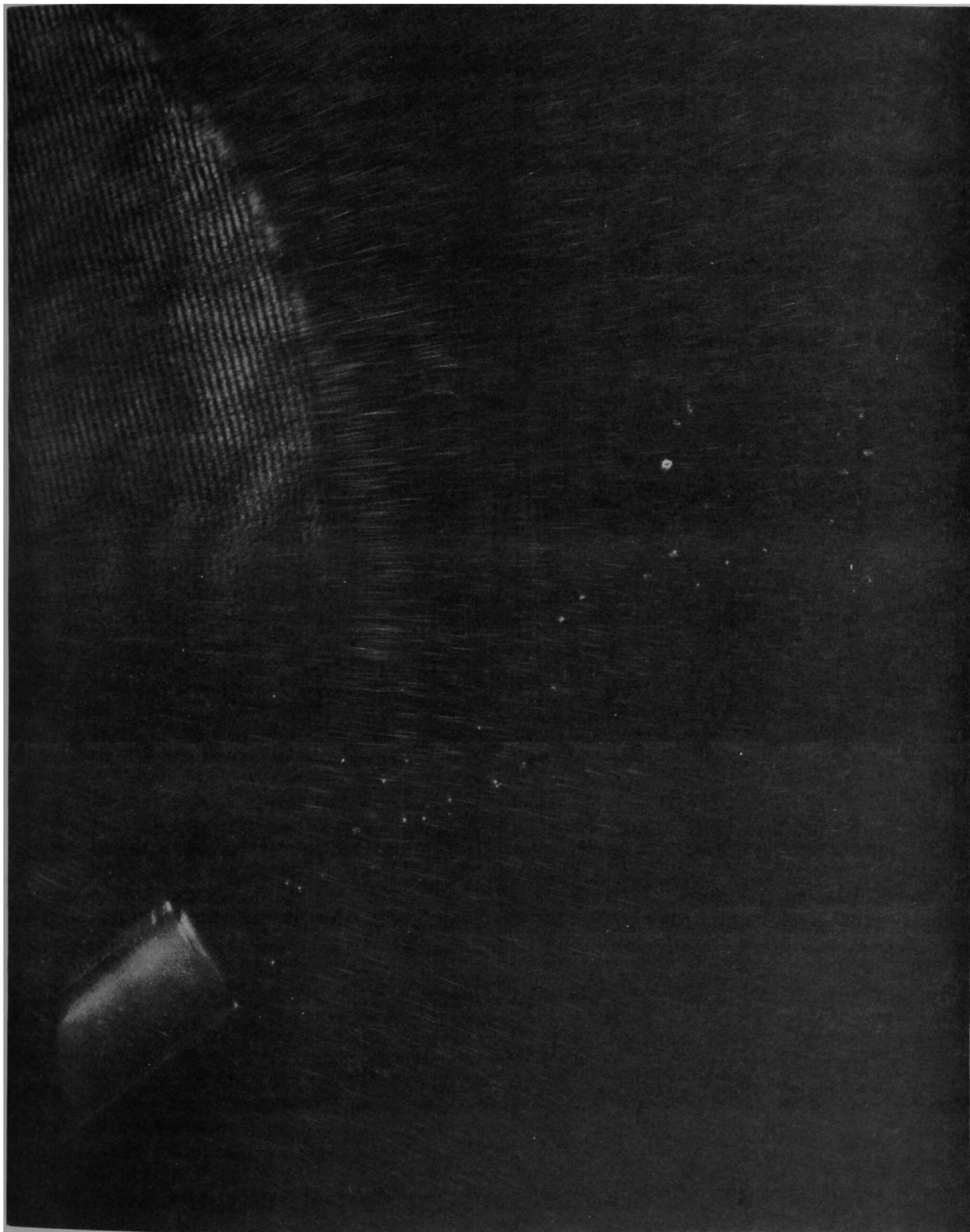


FIGURE 40
RECONSTRUCTION OF A HOLOGRAM OF SMALL GLASS BALLS
MADE WITH SIDE SCATTERED LIGHT

The light scattered in the forward direction needed to reconstruct the particle is confined to a relatively small cone whereas the light required to reconstruct the complete particle is scattered over large angles on the side or backward directions.

The single beam hologram depends very heavily on a large portion of the beam not being scattered at all by the particles. The unscattered portion of the beam acts as the reference beam and is necessary in order for a hologram to be made. If the particle concentration is so large that virtually all of the light is scattered by the particles, effectively there is no reference beam. A very poor hologram, if any at all, is formed. In addition, if the particle concentration is that high, it is unlikely that double pulsed pairs could be identified for velocity measurements.

If the particle concentration is very large, a two-beam holographic system would likely give better results since the reference beam in the two-beam system is independent of the beam illuminating the particles and, therefore, is unaffected by particle concentration. The two-beam system no doubt would reconstruct the light scattered by large concentrations of particles, but it might be difficult reconstructing individual particles in the central portions of a particle cloud. Light from particles in the center of the cloud of particles might well be scattered a second time by other particles making reconstruction difficult. Also, light from out of focus particles will act as noise making it difficult to see individual particles. In any event, when the particle concentrations become very large, it becomes very difficult to make holograms of any kind which can resolve the individual particles. A two-beam system can make a good hologram of the scattered light which can be used to measure the intensity of the scattered light. However, because of secondary scattering and light from out of focus particles, it may be difficult to see individual particles clearly enough for velocity measurements.

Based on the above considerations, the single beam system was selected for the experimental work in this contract. The prime advantage of two-beam systems is for holography in dense particle clouds where the reference beam in single beam holograms would be destroyed. However, single beam holography worked well in all of the experiments and hence the particle concentrations must have been low enough that a large portion of the light was unscattered. The single beam hologram is also much easier to set up and align which was an important factor since the system had to be moved frequently from one test section to the other.

Since the duct and particulate dispenser were not available early in the effort, the initial experimental work on the holographic systems was performed with a test tube particle dispenser using small glass spheres rather than flyash. The glass balls ranged in diameter from 35 to 200 microns which is, on the average, larger than flyash which occur in sizes as small as one micron or less. The test tube dispenser used is shown in Figure 41. The balls are placed in the test tube as shown and shop air is forced into the test tube through a small glass tube. Air

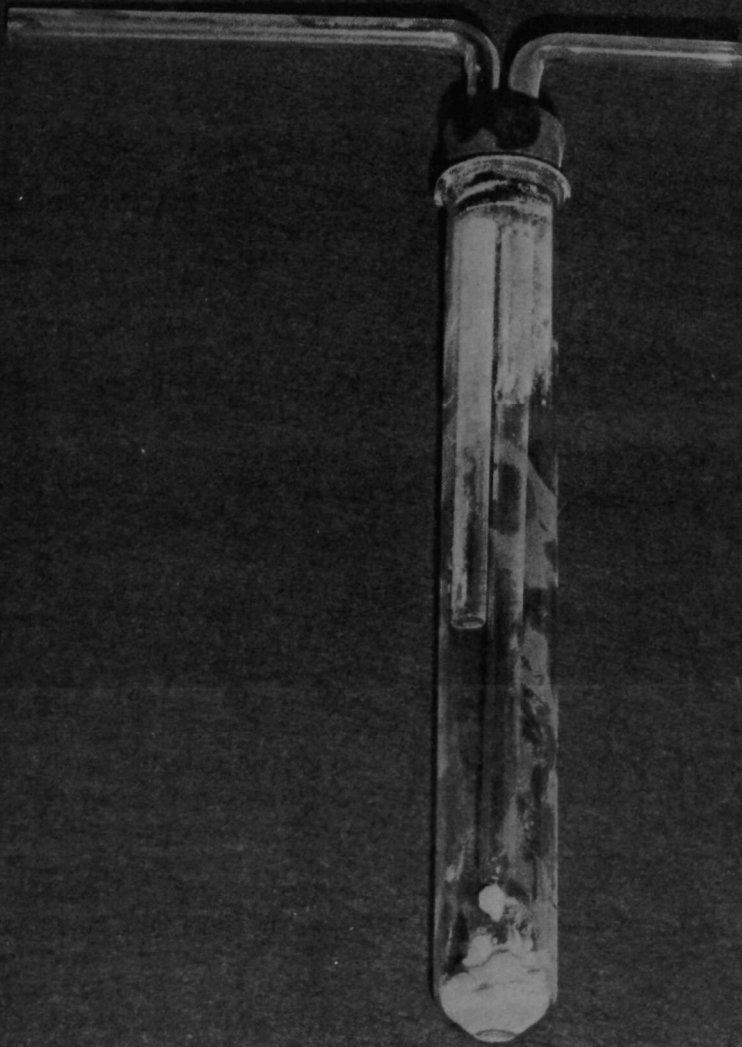


FIGURE 41
TEST TUBE DISPENSER FOR SMALL GLASS SPHERES

going into the tube stirs up the particles and forces them out through a second glass tube. Figure 39 is a photograph of the reconstruction of a single beam hologram of the glass balls being ejected from the test tube. Since the hologram is a single beam hologram, the test light recorded is forward-scattered light. Figure 40 is a photograph of a reconstruction from a two-beam hologram of balls ejected from the test tube. The light recorded in this instance is side-scattered rather than forward-scattered light. Since side-scattered light is primarily reflected light as discussed earlier, the reconstructions of the balls are not as clear as Figure 39.

II. E. 2 - Systems to Obtain Data from the Holograms

The approaches considered to obtain data from the holograms were direct measurement and optical data reduction. It was necessary to measure the size and shape of each particle, the distance between the two reconstructions of a particle pair, and the location of the particle pair in the test section.

The most straightforward means of obtaining the necessary data from the hologram is by direct measurement on the reconstruction of the particle. The reconstruction is either photographed or viewed on a ground glass viewing screen in the plane of the magnified reconstruction of Figure 36. The image on the screen or film can be viewed with a comparator and the size and shape of the particles and the distance between particle pairs can be measured. By having a reference object recorded on the hologram and hence appearing in the reconstruction, the location of the particle pair in the test section can be determined. This method of measurement is time consuming, but can yield very accurate results if done carefully.

Rather than using a ground glass viewing screen or film, a TV camera can be used to scan a reconstruction of the hologram and the image viewed on a television monitor. If the lenses on the camera are removed, and if the real image from the hologram falls directly on the vidicon, the particles will be magnified on the TV screen by the ratio of the cross-sectional area of the real image to the area of the vidicon. With the TV camera and monitor used in some of the experimental work in this contract, the magnification was about 30. The magnification can be varied by imaging and magnifying the reconstructed volume in relation to the TV camera using a lens system.

The problem of obtaining data from particle holograms is a good candidate for optical data processing techniques. Optical data processing techniques are a general class of computational techniques which make use of the mathematical properties of coherent light. Such methods have been successfully used in reducing large quantities of data which must be processed by linear transformations. These techniques in the past have

been applied to the aircraft flight test data reduction problem, side-looking radar data reduction, and particle size analysis. Optical data processing works well when the data to be processed is large in quantity and is available on photographic film. For the problem of reducing the data from particle holograms, the optical data processor, conceptually, would be a device into which the hologram is placed and which would then give the size, shape, location, and velocity of each particle on the hologram.

There are several optical data reduction techniques which may be applicable to the particle holography problem. One technique makes use of the assumption that all of the particles in a sufficiently small region of the test section will be travelling at the same speed and in the same direction. This situation is illustrated in Figure 42 in which the reconstructed pairs of a group of particles are depicted. The light amplitudes (x, y) distribution in this plane can be described by the expression

$$s(x, y) = s(x - x_0/2, y) + s(x + x_0/2, y) \quad (1)$$

where $s(x + x_0/2, y)$ is the first reconstruction of the particles in the double pulsed hologram and $s(x - x_0/2, y)$ is the second reconstruction. It is assumed here that the velocity \bar{v} of the particles is in the x direction and that $x_0 = vT$ where T is the pulse separation. The two dimensional optical Fourier transform of $s(x, y)$ denoted by $R(w_x, w_y)$ is given by

$$R(w_x, w_y) = 2s(w_x, w_y) \cos(w_x x_0/2) \quad (2)$$

where $s(w_x, w_y)$ is the Fourier transform of $s(x, y)$. The optical Fourier transform of $s(x, y)$ can be performed with the system illustrated in Figure 43. An aperture is placed in the region of the real image in which the velocity is to be measured. The aperture serves primarily to allow only the light from the particles reconstructed in the aperture to pass through the lens. In the focal plane of the lens, the light amplitude distribution is given by Eq. (2) which is a cosine wave with an envelope of $2s(w_x, w_y)$. By measuring the frequency w_0 of the cosine wave, the velocity is given by

$$|\bar{v}| = \frac{2w_0}{T} \quad (3)$$

The aperture can be scanned in the volume occupied by the real image of the test section in order to measure other velocities. The above discussion was specialized to the entire velocity being in the x direction. If the velocity is in other directions, the same discussion applies through rotation of the (x, y) coordinate systems.

$$s(x + x_0/2, y)$$

$$s(x - x_0/2, y)$$

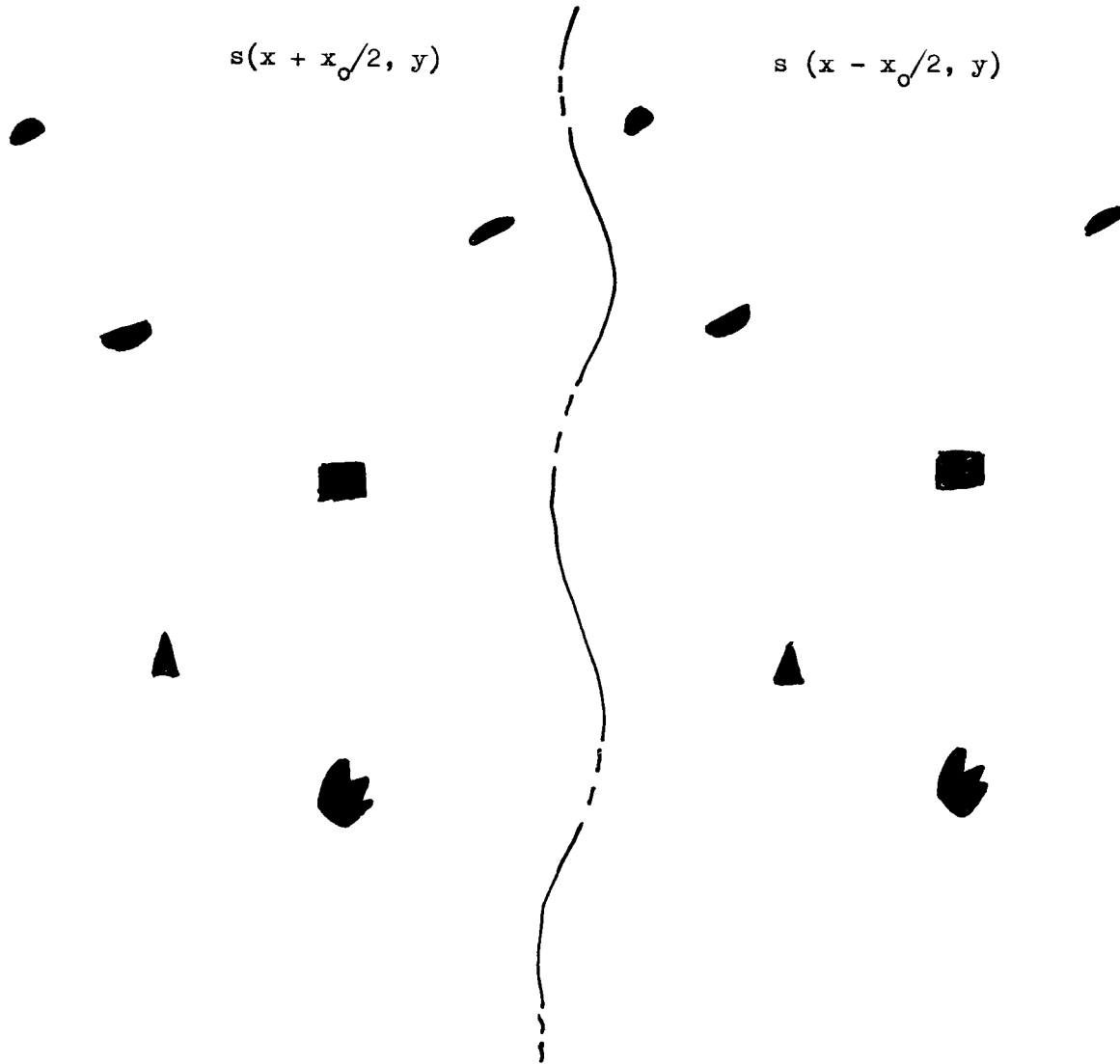


FIGURE 42
EXAMPLE OF A RECONSTRUCTION
FROM A DOUBLE PULSED HOLOGRAM
SHOWING RECONSTRUCTED PAIRS

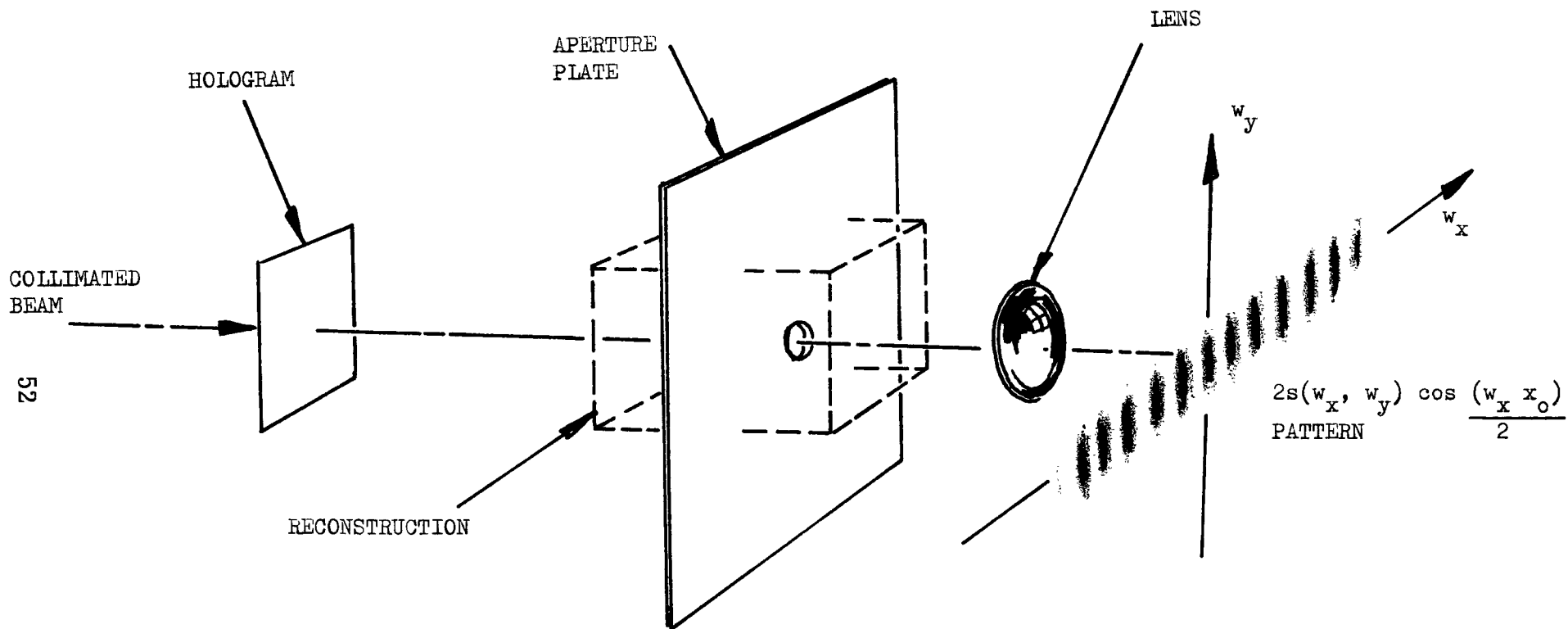


FIGURE 43
SCHEMATIC OF FOURIER TRANSFORM
METHOD OF ESTIMATING VELOCITY

The problem of measuring velocity in the z direction is very difficult and not considered in this discussion. Since the depth of focus of the particles is in the z direction, it is difficult to tell exactly where the particle comes to focus in that dimension. Therefore, it is difficult to determine the z coordinate of each particle and hence the z velocity component. This problem is also complicated by the fact that the z component is transverse to the free stream of the test section and for that reason is likely to be very small. This problem of the z component is discussed in more detail in the section describing the holographic system used in the experimental work.

Effectively, the optical data reduction technique described which can be called the "Fourier transform method" changes the problem of measuring distances between many individual particles to the problem of measuring the frequency of a cosine wave. The frequency of the cosine wave determines the magnitude of the velocity and the direction across the cosine wave determines the direction of the velocity. This technique would be advantageous when there are so many particles in the incremental volume in which the velocity is being measured that it is difficult to locate the particle pairs.

Another optical data processing technique which will be called the "correlation method" correlates the particle reconstruction with itself. The double pulsed reconstruction in a portion of the test section is essentially one particle pattern in two different positions. The two positions are separated from each other by a distance equal to the distance the particles travelled between the two pulses from the laser as stated in Eq. (1). The correlation function of this pattern produces two large peaks as illustrated in Figure 44, the distance between which can be related to the velocity by

$$V = \frac{d}{2T} \quad (4)$$

To mathematically demonstrate this method, the correlation function $V(x, y)$ is by definition

$$\begin{aligned} V(x, y) &= \iint_{-\infty}^{\infty} r(x', y') r(x' + x, y' + y) dx' dy' \\ &= \iint_{-\infty}^{\infty} [s(x' - x_0/2 + x, y' + y) + s(x' + x_0/2 + x, y' + y)] \\ &\quad [s(x' - x_0/2, y') + s(x' + x_0/2, y')] dx' dy' \\ &= \iint_{-\infty}^{\infty} s(x' - x_0/2 + x, y' + y) s(x' - x_0/2, y') dx' dy' \\ &\quad + \iint_{-\infty}^{\infty} s(x' + x_0/2 + x, y' + y) s(x' + x_0/2, y') dx' dy' \end{aligned}$$

$$\begin{aligned}
& + \int \int_{-\infty}^{\infty} s(x' - x_0/2 + x, y' + y) s(x' + x_0/2, y') dx' dy' \\
& + \int \int_{-\infty}^{\infty} s(x' + x_0/2 + x, y' + y) s(x' - x_0/2, y') dx' dy'
\end{aligned} \tag{5}$$

The correlation $v(x, y)$ consists of four terms as shown above. Since the amplitude pattern $s(x, y)$ of Eq. (1) consists of point-like particle reconstructions, each of the four components of the correlation $v(x, y)$ has its maximum value I when (x, y) is such that the component reduces to

$$I = \int \int_{-\infty}^{\infty} s^2(x', y') dx' dy' \tag{6}$$

Hence, at $v(0, 0)$, the first two integrals reduce to the form of Eq. (6). At $v(x_0, 0)$ the third integral has its maximum value and at $v(-x_0, 0)$ the fourth integral is maximum. Hence, the plot of $v(x, y)$ has a large central peak at $(0, 0)$ and two smaller peaks at $(-x_0, 0)$ and $(x_0, 0)$ as shown in Figure 44. By measuring the distance between the two smaller peaks, x_0 and $-x_0$, the velocity can be determined.

The correlation method can be implemented by an optical data processing system shown in Figures 45 and 46. The light from the real image of the particle hologram is passed through a lens and a new two-beam hologram is made of the light distribution in the focal plane of the lens. The wavefront recorded on the second hologram is related to the Fourier transform of the wavefront of the real image $r(x, y, z)$ on the first hologram and is given by

$$R[w_x, w_y, z] e^{j \left[\frac{2\pi}{\lambda F} \left(1 - \frac{f-z}{f} \right) (w_x^2 + w_y^2) \right]} \tag{7}$$

where $R(w_x, w_y, z)$ is the two-dimensional Fourier transform of the wavefront $r(x, y, z)$. The Fourier transform is with respect to x and y for a given value of z . For simplicity, the case in which $z = 0$ is now considered so that the phase factor of Eq. (7) can be ignored. For planes other than $z = 0$, the phase factor must be considered. The net result of considering the phase factor is a predictable adjustment of magnification. The second hologram, after being developed, is placed back where it was made as shown in Figure 46. First of all, a collimated laser beam illuminates the particle hologram producing a real image of the particles in front of the hologram. An aperture is placed in the region of the reconstruction where the velocity is to be measured in this case the $z = 0$ plane called P1. The light from this region passes to the focal plane P2 of the lens L1 in which the hologram is located. If the wavefront in the aperture is given by $r(x, y, 0)$, the wavefront in the plane of the

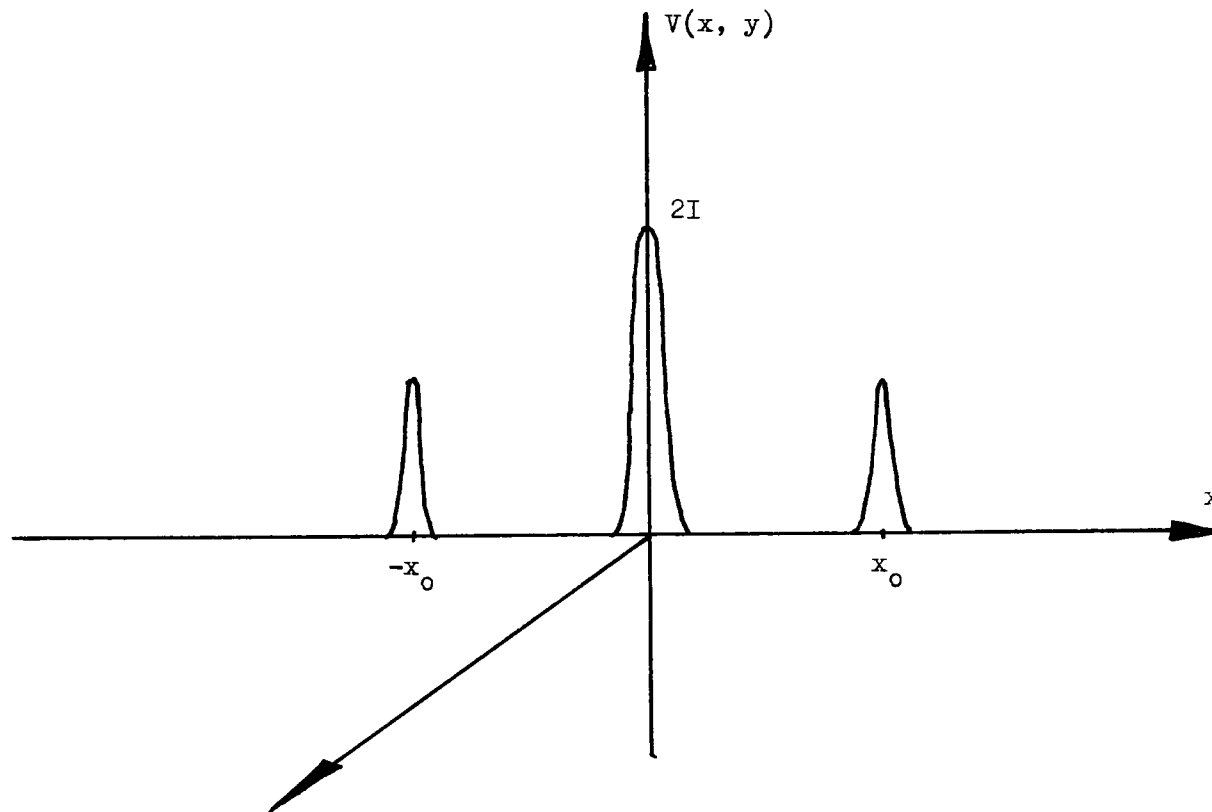


FIGURE 44
 PLOT OF THE CORRELATION FUNCTION
 OF $r(x, y)$ SHOWING THE CENTRAL PEAK
 AND TWO SMALLER PEAKS AT $(-x_0, 0)$
 AND $(x_0, 0)$

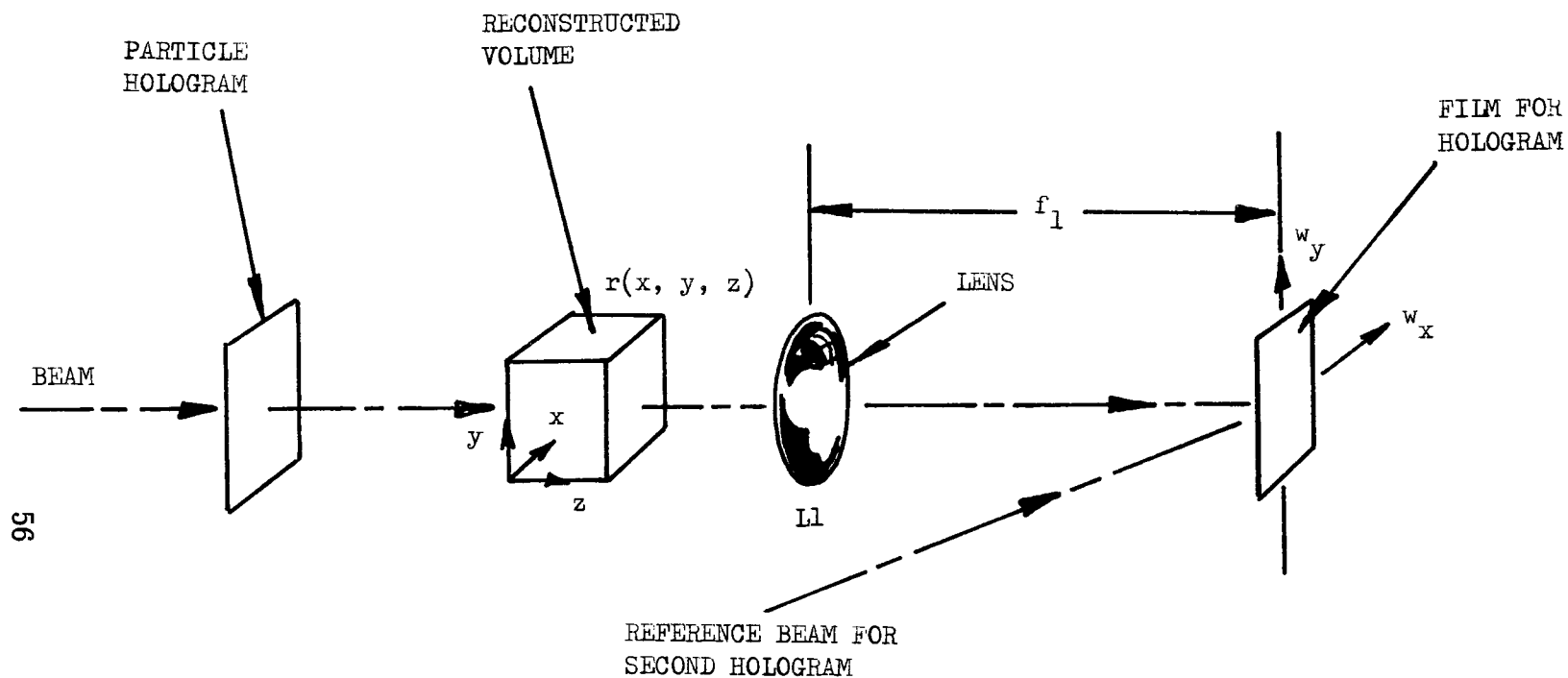


FIGURE 45
SCHEMATIC OF THE SYSTEM TO MAKE
A TWO-BEAM HOLOGRAM OF LIGHT
FROM THE RECONSTRUCTION IN THE
FOCAL PLANE OF A LENS

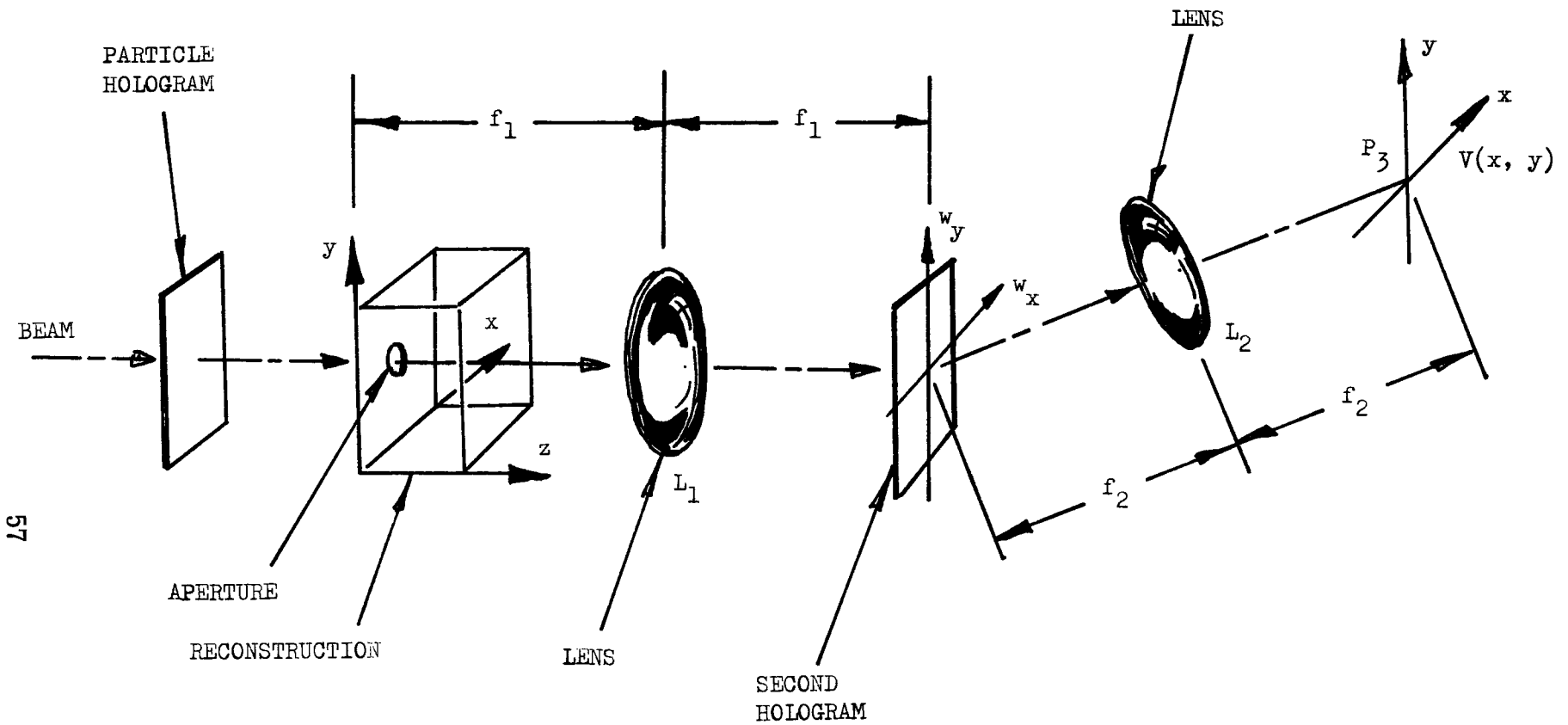


FIGURE 46
SCHEMATIC OF CORRELATION METHOD
FOR MEASURING THE VELOCITY
FROM PARTICLE HOLOGRAMS

hologram is given by

$$R(w_x, w_x, 0) \quad (8)$$

The wavefront leaving the hologram will be the product of the amplitude transmission of the hologram and the wavefront of Eq. (8) and is given by

$$R(w_x, w_y) R(w_x, w_y)$$

Lens L2 performs an Inverse Fourier transform of the wavefront and is given by

$$\begin{aligned} \mathcal{F}^{-1} [R(w_x, w_y) R(w_x, w_y)] \\ = \int_{-\infty}^{\infty} \int_{-\infty}^{\infty} r(x', y') r(x + x', y + y') dx' dy' \\ = v(x, y) \end{aligned}$$

Hence, in plane P3, the output light amplitude distribution is the correlation $v(x, y)$ of the light amplitude distribution in the plane of the aperture.

As for the optical data processing methods, both would require a considerable amount of developmental work to make them efficient and workable. The correlation method has perhaps more potential than the Fourier transform method since the cosine fringes of the Fourier transfer method might well be so close together, especially for wide separations of particles in a pair, that they would be difficult to count. Also, for large particles, the cosine fringes may become confused with the fringes produced by the Fraunhofer diffraction pattern of the particle.

The correlation method effectively reduces many particle pairs (so many in fact that they might be indistinguishable as pairs) into a single pair of bright spots whose separation is related to the velocity by Equation (4). The separation of the spots gives the magnitude of the velocity, and the direction of the line determined by the spots gives the direction of the velocity. This reduction of data from many particle pairs to a single pair of bright spots would greatly facilitate the problem of measuring particle velocities.

During the period of the effort when the dust and particulate dispenser had not yet been made, the above mentioned data reduction techniques were investigated. The correlation technique was experimentally demonstrated by using a simulated group of particle pairs on a transparency as

the reconstruction from a hologram. The transparency resembled Figure 42. From this transparency, a two-beam hologram was made as shown in Figure 45. The system in Figure 46 was shown to work quite well for particles on the transparency as small as 35 microns. The limiting factor seemed to be the intensity of the particle reconstruction rather than the particle size.

Since the emphasis on the contract was placed on making particle holograms of various duct flows, the optical data processing techniques were not pursued further. However, it is felt that if the particle velocimetry techniques are to become standard techniques, such optical data reduction techniques are desirable. The correlation technique has the promise of becoming an efficient means of deriving particle information from pulsed holograms.

II. E. 3 - Holographic Systems Selected for Experimental Programs

System Used for Making Holograms:

The system used to make the holograms in the potential and turbulent test sections was a single beam holographic system shown schematically in Figures 47 and 48. The laser used was a Korad Model K-1Q pulsed ruby laser with a pockels cell Q-switch and a temperature tuned sapphire etalon. This laser operated in the TEM₀₀ mode and had a coherence length of about 50 cm. Due to the excellent temporal and spatial coherence properties of this laser, holographic schemes which have been required to compensate for the poor coherence of older ruby lasers were not required. The pulsed ruby laser was aligned with a Spectra-Physics Model 130 helium-neon laser. The Ruby laser has the capability of being double pulsed with pulse intervals ranging from .2 to .9 milliseconds. Each pulse has a time duration of approximately 10 nanoseconds. Due to the excessive amount of flyash in the test facility room where the duct was located and due to the delicate optics of the ruby laser, the laser was placed in a separate room. The laser beam entered the test facility room through a hole in the wall. The room in which the laser was installed was kept clean and the air was continually filtered with electrostatic precipitators.

In order to monitor the energy of each pulse and time interval between the pulses, a pulse monitoring system was devised as shown in the schematic. The beam from the laser passed through a glass plate and about 5% of the beam was reflected to a photoelectric cell followed by an integrating circuit. The output of the integrator was displayed on a storage oscilloscope giving the relative output pulse energies and pulse spacing. Figure 49 is a photograph of the pulsed ruby laser and monitor showing the laser head, the laser cooling unit, the glass plate, photo electric cell, and storage oscilloscope.

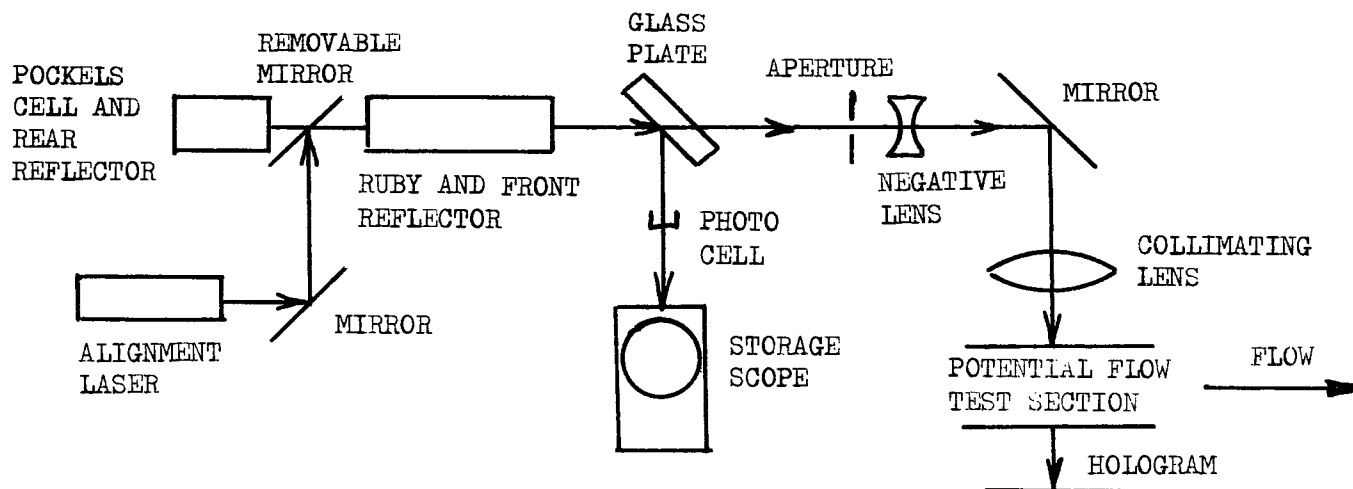


FIGURE 47 SCHEMATIC OF POTENTIAL FLOW TEST SECTION HOLOGRAPHIC SYSTEM

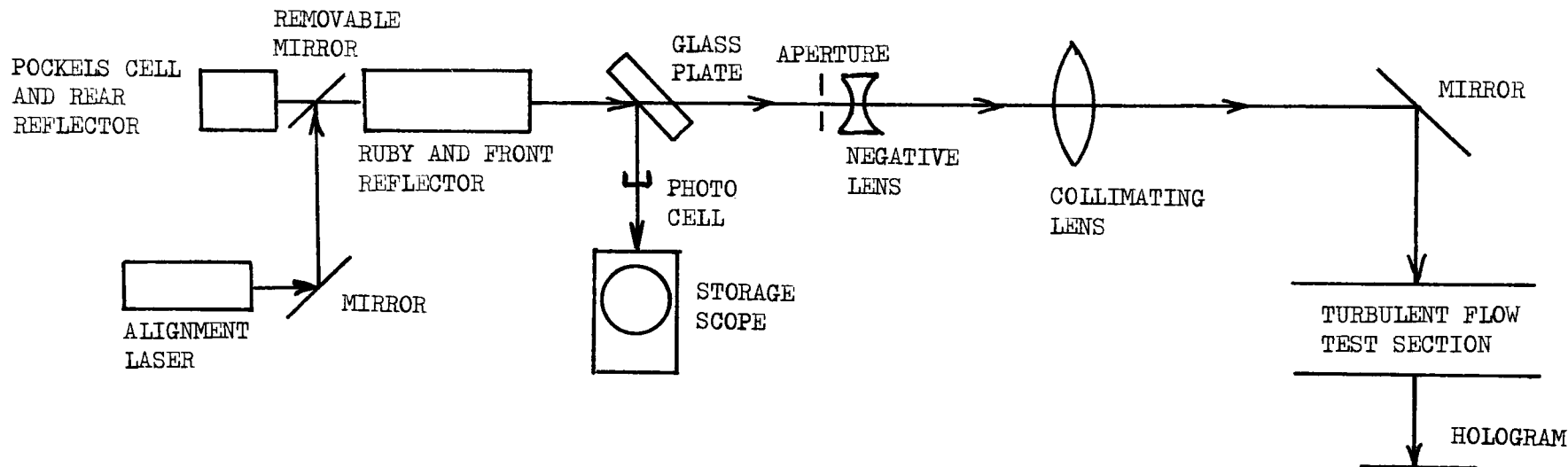


FIGURE 48 SCHEMATIC OF TURBULENT FLOW TEST SECTION HOLOGRAPHIC SYSTEM

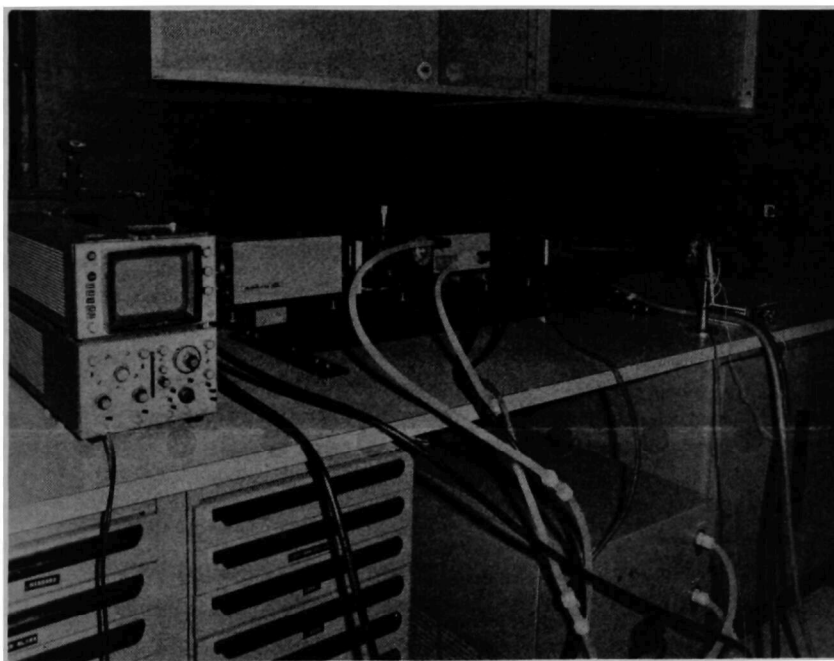


FIGURE 49
PULSED RUBY LASER USED IN THE EXPERIMENTAL WORK
AND THE PULSE MONITORING SYSTEM CONSISTING OF
A GLASS PLATE WHICH REFLECTS A SMALL PORTION OF
THE BEAM, A PHOTOELECTRIC CELL, AND A STORAGE
SCOPE

The stray incoherent white light from the flashlamp of the laser can expose the holographic film, and for this reason the white light had to be removed. Most of the stray light did not get through the hole in the wall to the room in which the hologram was made. The light which did get through was removed by a 5 mm aperture placed just before the expanding lens (negative lens) shown in the schematic. To insure that stray light was not a factor, the laser was fired with the system misaligned so that no laser beam was produced and only stray white light was present. A sheet of film in the film holder where the hologram was made was not exposed indicating that the stray white light was negligible.

The beam was either routed to the potential flow test section or the turbulent flow section depending on where the hologram was to be made. Considering the system for the potential flow section first, the beam was expanded by a negative lens (-13 mm focal length) and reflected by a mirror as shown in the schematic in Figure 47. The beam was then collimated by a lens which had a focal length of 24 inches and a diameter of 3 inches. Figure 50 is a photograph of the aperture to filter out the stray light, the negative lens, the mirror, and the collimating lens. The beam passed through the test section to the film holder. Figure 51 shows the potential flow test section and the film holder. The film was 4.16 inches away from the test section. The test section windows were 4 by 5 inch glass plates, 1/4 inch thick, flat to 1/4 wavelength and made from Kodak Type 649-F spectroscopic plates by removing the 649-F emulsion. The windows are shown in Figure 8.

The holographic system for the turbulent flow test section was essentially the same as the potential flow section. As shown in the schematic of Figure 48, and the photograph of Figure 52, the beam was expanded by the negative lens and collimated by the 24-inch focal length positive lens. The beam then travelled parallel to the tunnel and was then reflected to the turbulent flow test section by a mirror. The beam from the mirror passed through the test section and exposed the film which, as in the potential flow section, was placed in a holder three inches from the duct.

System Used for Reconstructing the Holograms:

The system used to reconstruct the holograms is shown schematically in Figure 53. The laser used for reconstruction was a Spectra-Physics Model 140 argon laser. The high power argon laser, usually operated at 400 milliwatts, was required to make the small particle reconstructions visible. The beam was expanded and spatially filtered by a lens pinhole combination and then collimated. The collimated beam illuminated the hologram producing a real image of the particles in front of the hologram.

Since the particle reconstructions were too small to be easily seen, the reconstructions were magnified by a factor of 22 by a 2-1/2 power microscope objective. The reconstructions were projected onto a ground glass viewing screen allowing the observer to see magnified

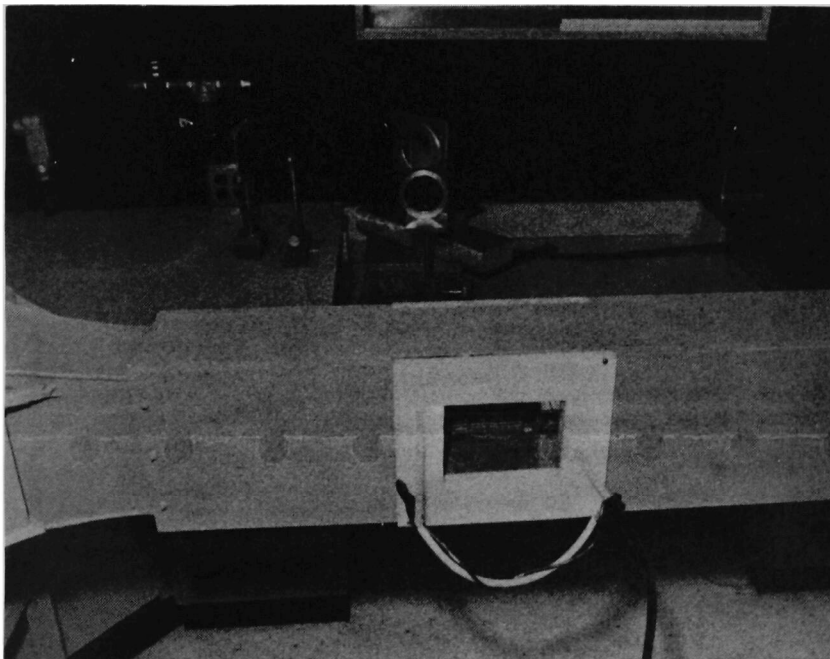


FIGURE 50
HOLOGRAPHIC SYSTEM FOR THE POTENTIAL FLOW TEST
SECTION SHOWING APERTURE, NEGATIVE LENS, MIRROR,
AND COLLIMATING LENS, AND THE TEST SECTION

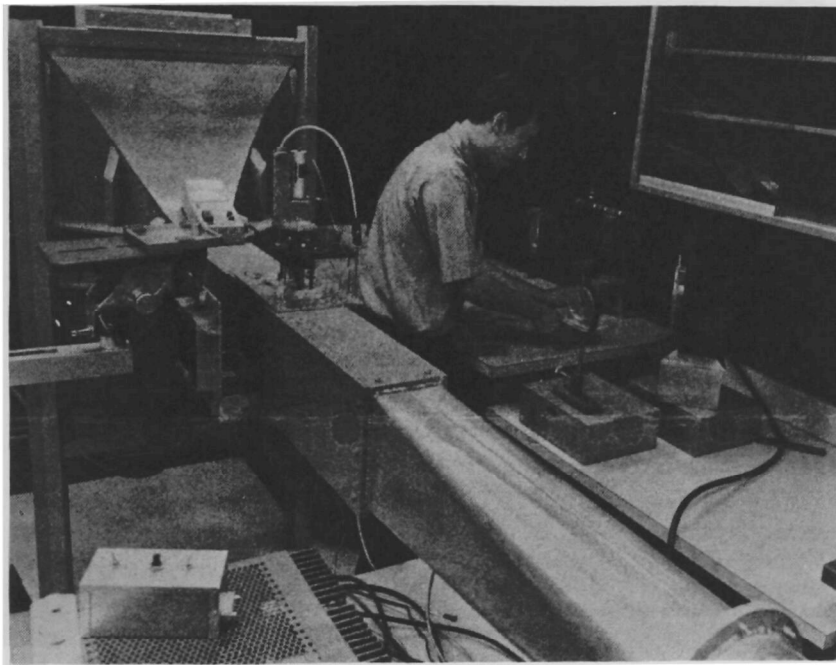


FIGURE 51
THE HOLOGRAPHIC SYSTEM AROUND THE POTENTIAL
FLOW TEST SECTION SHOWING THE OPTICAL SYSTEM,
TEST SECTION, AND FILM HOLDER

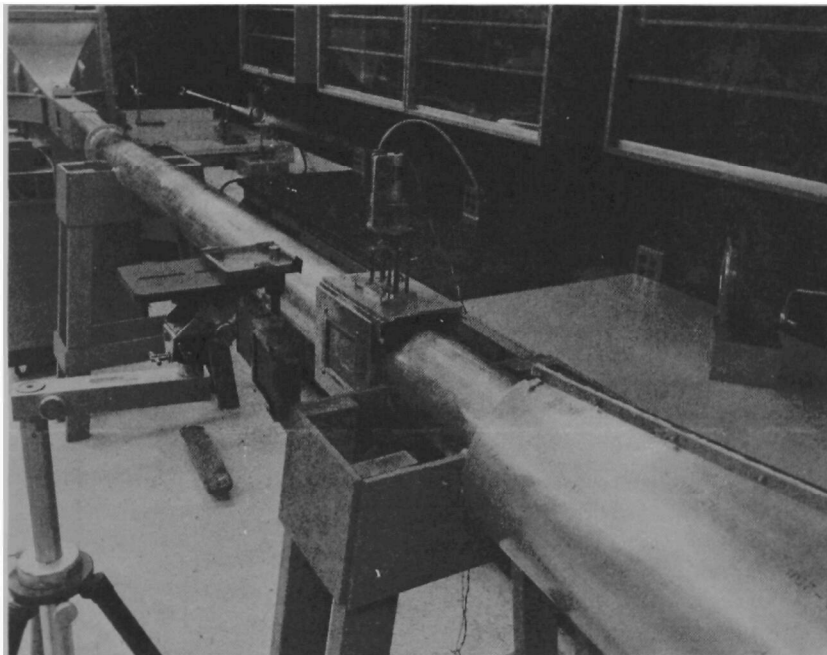


FIGURE 52
THE HOLOGRAPHIC SYSTEM FOR THE TURBULENT FLOW
TEST SECTION SHOWING THE LASER BEAM, NEGATIVE
LENS, COLLIMATING LENS, MIRROR, TEST SECTION
AND FILM HOLDER

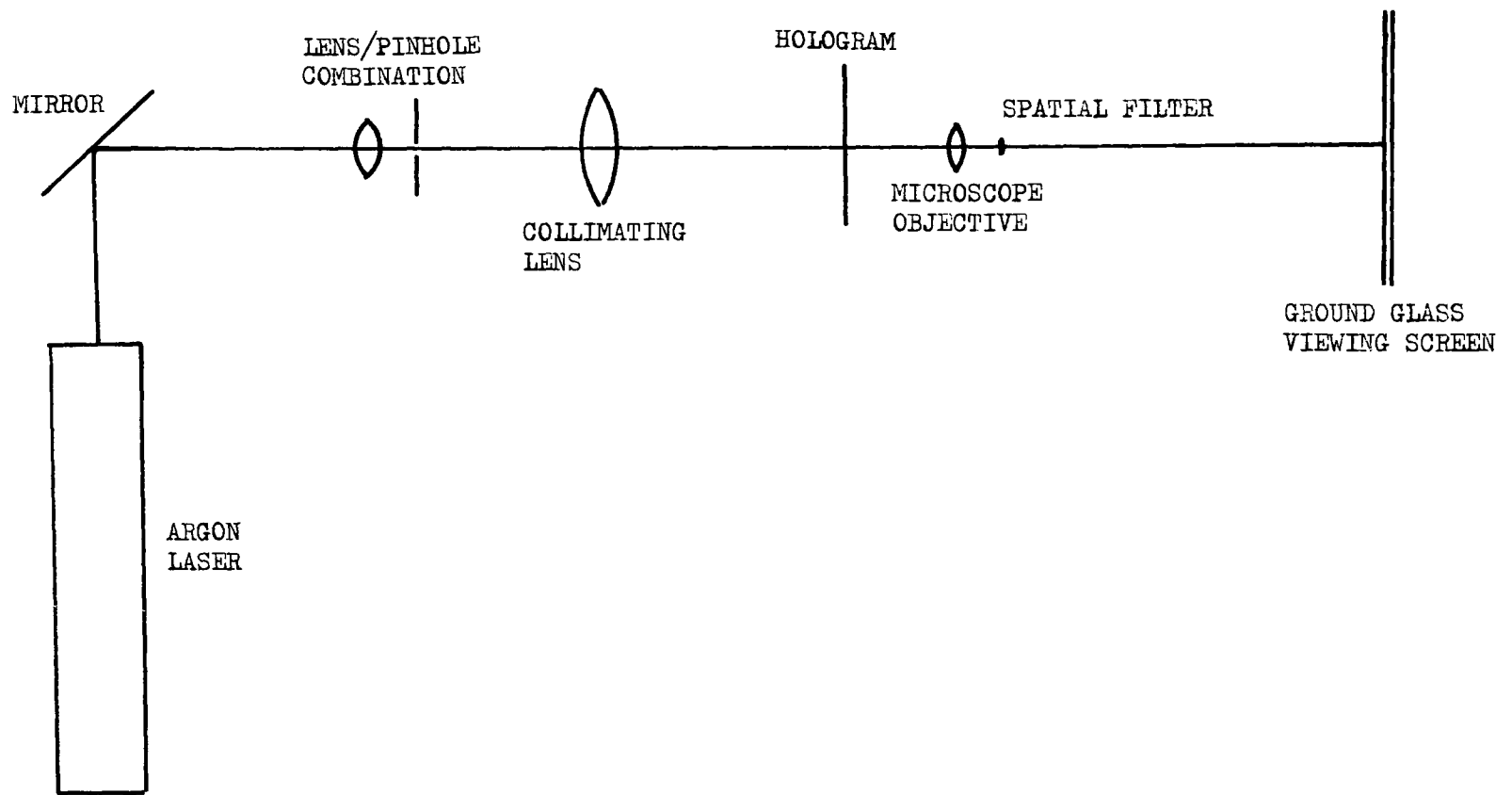


FIGURE 53
SCHEMATIC OF THE SYSTEM TO VIEW
AND MAKE MEASUREMENTS OF THE
PARTICLE HOLOGRAMS

particle images. A small wire filament was placed at the focal point of the microscope objective to remove the light not scattered by the particles and thereby making the magnified particle reconstructions easier to see. Figures 54 and 55 are photographs showing the argon laser, lens/pinhole combination, collimating lens, hologram, microscope objective, spatial filter and the ground glass viewing screen.

Resolution:

The hologram recorded a cylindrical volume of the test section 3 inches in diameter and 4 inches long as shown in Figure 56. The resolution R of the hologram is determined by the diameter D of the reference beam, the distance L that the hologram is from the particle, and the wavelength λ of the laser and is given by

$$\begin{aligned} R &= \frac{1.22 \lambda L}{D} \\ &= \frac{(1.22) (.6942 \times 10^{-6}) (6.16)}{3} \\ &= 1.74 \text{ microns.} \end{aligned}$$

Where $D = 3$ inches

$\lambda = .6942$ microns

$L = 6.16$ (distance to a particle in the middle of the test section).

In reality the resolution is somewhat less than the value of R computed above for several reasons. The optics are not perfect and aberrations in the optics degrade the resolution. Also, the intensity of the light scattered to the holograms is much less for small particles than for larger particles. Hence, only the more intense portions of the wavefront scattered by the smaller particles is recorded and the lower intensity portions of the light beam may well be lost in the noise of the hologram or not recorded at all. Because less light from the smaller particles is actually recorded, the resolution of the system may be less than the predicted value of 1.74 microns.

The resolution of the system was measured with the aid of a USAF 1951 Resolving Power Test Target. This target consists of sets of lines spaced progressively closer together, the sets becoming progressively smaller. By observing the last set of lines that an optical system can resolve, the resolution of the system can be determined. The test chart was placed in the middle of the test section and a hologram was made of the test chart. Upon placing the hologram into the viewing

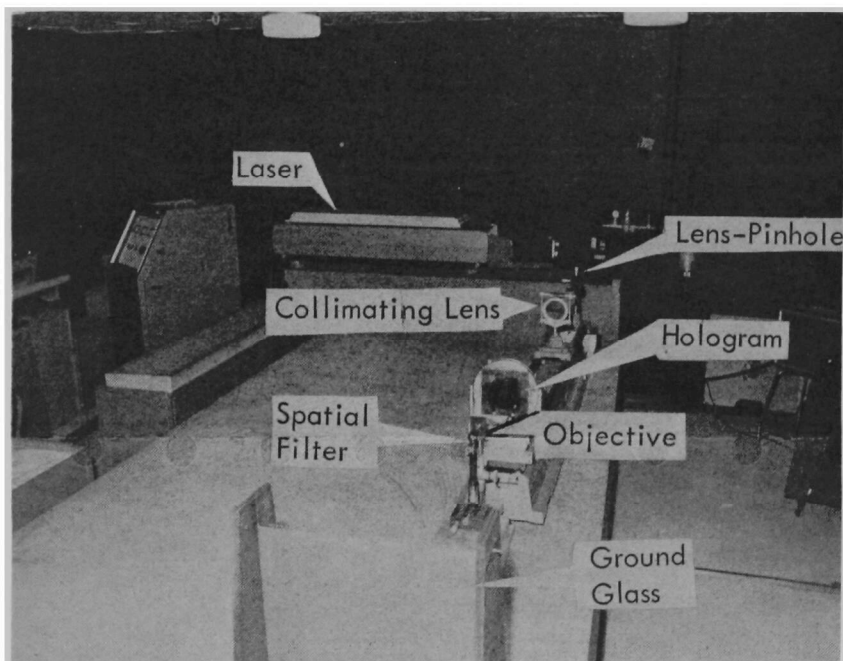


FIGURE 54
THE SYSTEM USED TO RECONSTRUCT THE PARTICLE HOLOGRAMS SHOWING THE ONE-WATT ARGON LASER, LENS PINHOLE COMBINATION, COLLIMATING LENS, HOLOGRAM, MICROSCOPE OBJECTIVE, SPATIAL FILTER, AND GROUND GLASS VIEWING SCREEN

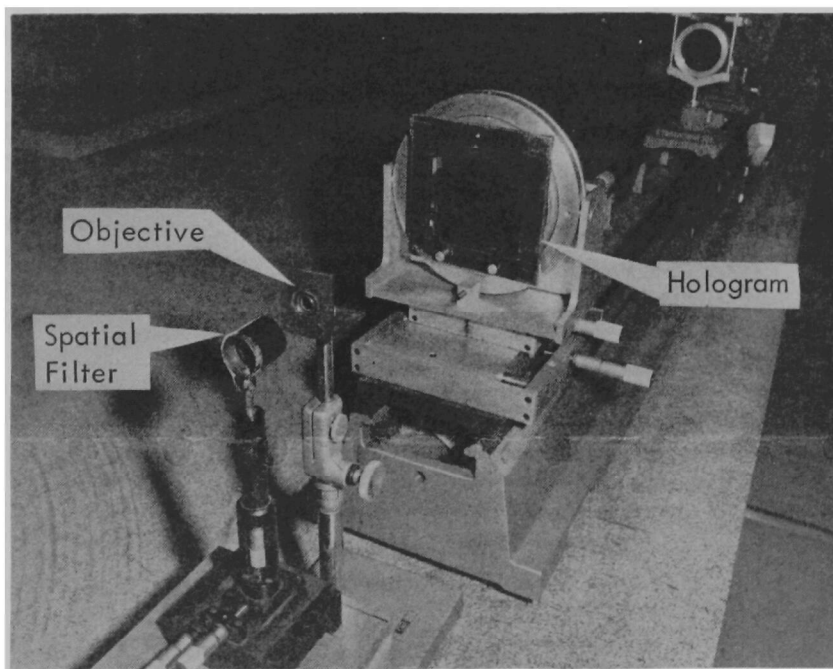


FIGURE 55
CLOSE-UP OF THE RECONSTRUCTION SYSTEM SHOWING
THE HOLOGRAM, MICROSCOPE OBJECTIVE, AND SPATIAL
FILTER

section, the smallest set of lines which could be resolved was set 6.4 which corresponds to 90.5 lines/mm or a minimum particle size of 5.5 microns.

Obtaining Data from the Holograms:

It was required for this effort to locate the position of each particle pair in the test section, to measure the size and shape of the particle, and to measure the magnitude and direction of the velocity of the particle. The coordinate systems used to record particle location differed from one experiment to the next and were chosen primarily for convenience. The coordinate system for the potential flow holograms is illustrated in Figure 56. Here, the origin is located on the bottom of the test section as indicated and the positive x - direction is in the direction of the free stream flow, the positive z-direction is in the direction opposite to that of the laser beam and the positive y-direction is in the vertical direction of the test section. For other experiments, the origin was shifted to other points in the test section.

In order to obtain data from the holograms, the hologram was placed in the holder shown in Figure 55 and 57. When the hologram is illuminated a real image of the test section is formed in the front of the hologram. Since both the beams used to make and reconstruct the hologram were collimated, there is no magnification in the x and y directions due to the difference in wavelengths between the laser used to make and reconstruct the hologram. However, there is a magnification M_z in the z-direction given by the ratio of the two wavelengths which is

$$\begin{aligned} M_z &= \frac{\lambda_r}{\lambda_a} \\ &= \frac{.6943}{.4880} \\ &= 1.42 \end{aligned}$$

Where λ_r = the wavelength of the ruber laser given by .6943 μ

λ_a = the wavelength of the argon laser given by .4880 μ

Hence, the width of the test section in the reconstruction was not 4 inches which was the actual width, but 5.68 inches.

The microscope objective images various portions of the real image onto a ground glass viewing screen as described earlier. Since the objective aperture is only .3 inches, only a very small portion of the

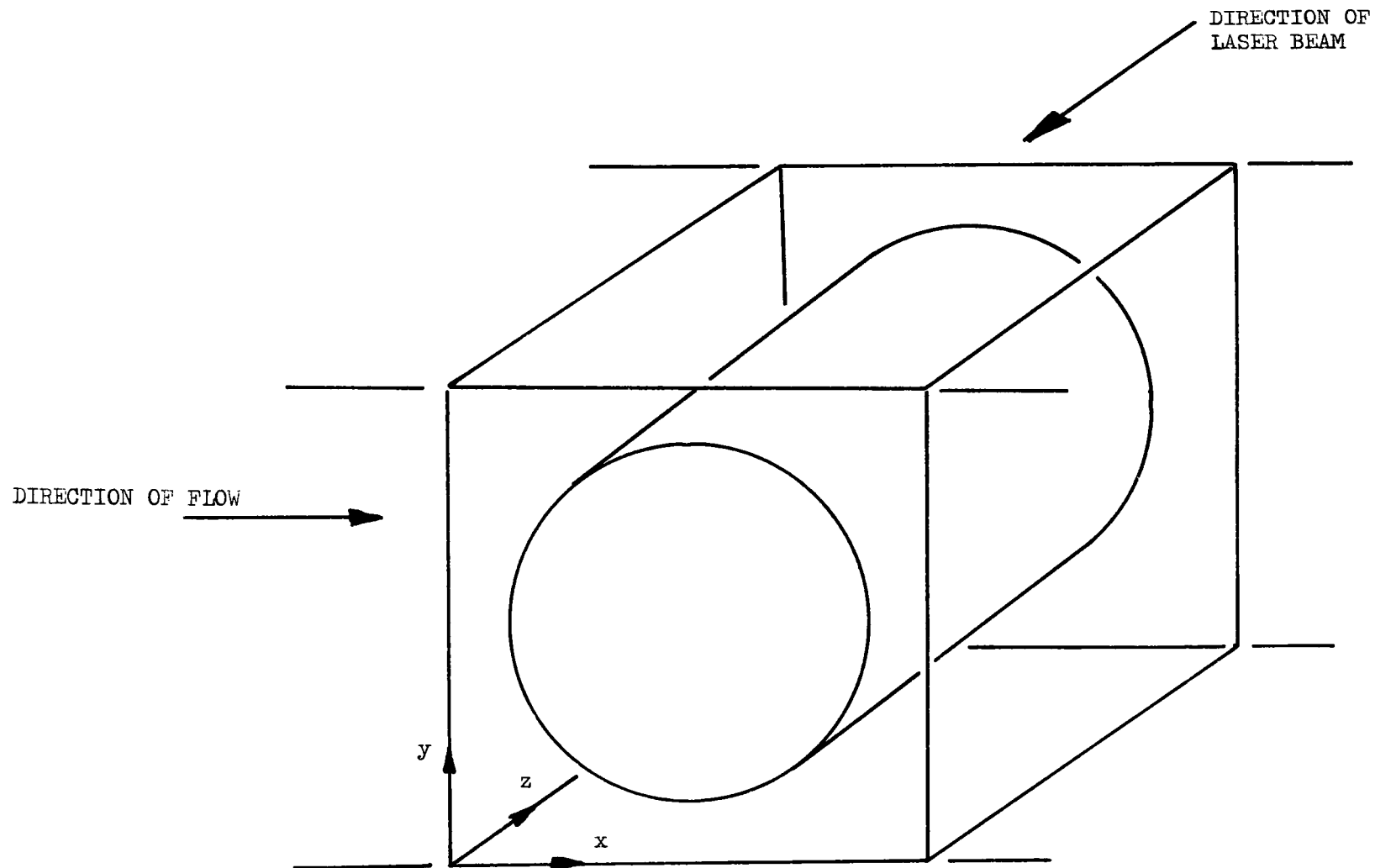


FIGURE 56
SKETCH OF THE POTENTIAL FLOW
SECTION SHOWING THE CYLINDRICAL
PORTION OF THE TEST SECTION
WHICH IS HOLOGRAPHED

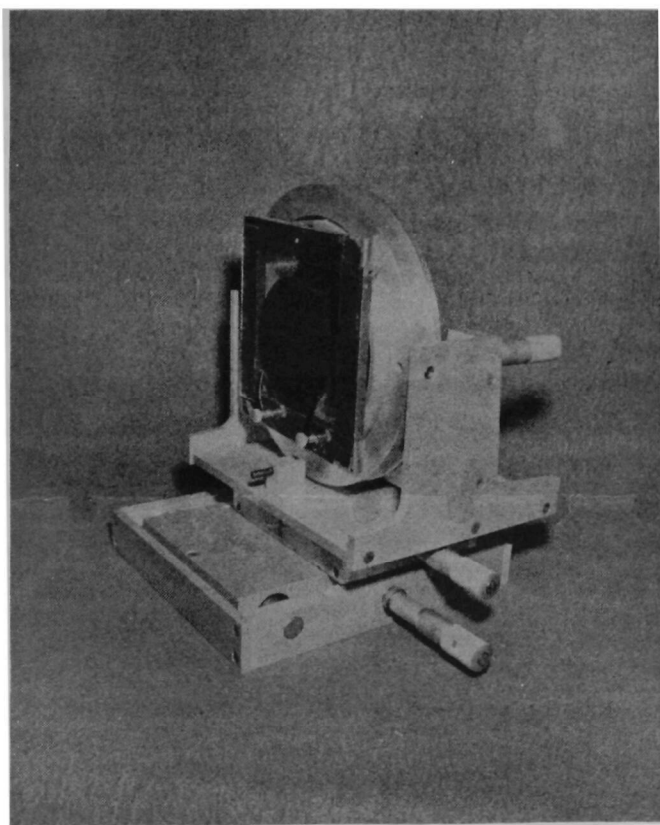


FIGURE 57
MICROMETER POSITIONED HOLOGRAM HOLDER USED
IN PARTICLE RECONSTRUCTION EXPERIMENTS

real image can be viewed at once. In order to view other portions of the image, the objective is mounted on a drive which can be moved up and down in the y-direction as shown in Figure 55. In order to scan the reconstruction in the x-direction, the hologram itself is translated in the x-direction by means of the two translation stages shown in Figure 57. The real image of the test section is moved in the x-direction by an amount equal to the distance the hologram is moved in that direction. The test section was scanned in the z-direction by sliding the hologram holder to different positions along the optical bench. The edge of the bench was marked with a millimeter scale so that the location in the z-direction of the portion of the tunnel being viewed could be measured. The z reading had to be corrected by a factor of 1.42 to take into account the magnification in the z-direction. By noting the height of the microscope objective, the readings of the verniers in the translation stages, and the reading of the scale mounted to the optical bench, the x, y, z coordinates of the particle pair can be measured. Since the typical spacing between two reconstructions of a single particle was about .07 inches, each particle pair was assigned one (x, y, z) location corresponding to the center of the particle pair. It is felt that each particle pair was located by this technique to an accuracy of about 0.05 inches.

Having located the particle in the test section, the next task was to measure the magnitude and direction of the velocity of the particle and the shape of the particle. The particles in the particle pairs were generally separated by about 1 inch on the ground glass viewing screen. The separation was measured by placing a scale which was graduated in units of .02 inches on the screen and measuring the separation as accurately as the scale could be read. The scale was viewed by the observer with a comparator so that it could be accurately read. The particle was then viewed by the observer with the comparator (using a .1 mm reticle) so that the shape and size of the particle could be determined. By correcting for the magnification of the viewing system, the true size and particle separation were determined. By knowing the particle pair separation, and the time interval between the pulses, the particle velocity was computed.

The angle of the velocity vector was measured with a protractor included on a reticle mounted in the comparator. The reference for the angle measurement was a plumb line which was dropped in front of the test section and recorded on the hologram. The reconstruction of the plumb line provided a vertical reference for the measurement of the velocity angle.

Only velocity components in the x and y directions, directions which were transverse to the laser beam, were measured. It would have been difficult to obtain the z component of velocity for several reasons. The primary reason was that the depth of focus of a particle was in the z direction, and it was difficult to determine the precise value of z where the particle was in focus. In contrast, the shape of the particle is clearly delineated in the x and y directions allowing its position with respect to these coordinates to be clearly determined. Also, the magnitude of the z component of velocity was likely of the same order

as the y component, since both components were transverse to the free stream velocity. If this was the case, the displacement of the particle in the z direction during the interval between the two pulses was about 400 microns for the potential flow holograms. For the holographic system used, the depth of field of a 50 micron particle would be about 200 microns which was about the same as the displacement in the z direction. The depth of focus being on the same order as the displacement further complicated the measurement of the z component. For these reasons, only the x and y components were measured.

General Comments on the Performance of the Holographic System:

In general, all of the holographic systems for the experiments performed quite well. Before the holograms were made, it was necessary to make sure that the pulsed ruby laser beam uniformly illuminated the hologram. A slight misalignment would result in parts of the film being overexposed and parts being underexposed. The alignment laser did not always trace out the path of the ruby laser beam precisely enough to ensure uniform illumination so a few test shots had to be fired with polaroid film in place of holographic film to check for uniform illumination.

Flyash was deposited on the test section windows while the duct was running to the extent that high quality holograms could not be made after one minute of operation. Generally, however, one minute of operation was enough time to make three holograms. After each run, the windows were cleaned in an ultrasonic cleaner and then reused. The windows usually became so "sand blasted" after ten runs, or so, that they had to be replaced with new windows. The flyash particles on the windows had the effect of reducing the amount of unscattered light and thereby destroying the reference beam for the single beam holograms. Also, the particles on the windows were out of focus in other parts of the test section and thereby contributed noise to the particle reconstructions inside the test section. Although the flyash deposits on the windows were a nuisance, they did not significantly degrade the quality of the holograms because the holograms were made as soon as possible after the duct was turned on. However, the flow was so turbulent in the experiment with the precipitator plates, that the windows became covered with flyash after only 10 seconds of operation. For these experiments, the windows were removed.

The laser at times did not produce two pulses or did not produce two equal intensity pulses. For this reason, the pulses were monitored by the monitoring system described above each time the laser fired to make sure that the hologram was exposed by two equal intensity pulses.

Obtaining the location, size, and velocity data from the hologram by the techniques described above worked satisfactorily. However, it was a tedious operation. The problem of finding matching particles in a pair was made difficult by the fact that most flyash particles were spherical

and hence a great many of the particles look alike. Also, the particles in a pair were separated by a distance equal to 40 diameters, on the average. The particles in a pair could be made closer together and, consequently, more easily identified if the pulse separation of the laser could be reduced. If the particles had a distinctive shape, it was considerably easier to locate the pairs. However, distinctly shaped particles occurred very rarely. Figures 58 and 59 are photographs of reconstructions of distinctively shaped particles. Note that there is little doubt that these are double pulsed pairs due to their shapes. If the flow is reasonably parallel, double pulsed pairs can be identified even if the shapes of all the particles in the region are about the same. Figure 60 shows two pairs of particles. Figure 61 is a photograph of the reconstruction from a parallel flow. Note that at least four double pulsed pairs are visible.

If the flow were turbulent, particles in the same vicinity of the flow would have different velocities both in magnitude and direction. Also, distinctively shaped particles (non-spherically) might rotate from one position to the second changing the particular view recorded by the hologram. Hence, the first reconstruction of a given particle may differ from the second because of the change in particle orientation between the two reconstructions. The .5 and 1.5 isokinetic holograms of the APCO train were so turbulent that double pulsed pairs could not be found in the vicinity of the probe. Figure 62 is a photograph of the reconstruction from a .5 isokinetic double pulsed hologram of the APCO train. Note that although plenty of particles are visible, it is difficult with certainty to find the double pulsed pairs. Again, the difficulty in matching reconstructions could be eliminated if the pulse interval were smaller, making the resulting double pulsed reconstructions closer together.

All holograms were made using Agfa-Gevaert 10E75, 4 by 5 inches, AH backed, photographic plates and were developed using Kodak D-19 developer. The development time varied between 2 minutes 15 seconds to 4 minutes depending on the exposure of the holograms and age of the developer. Typical development time was 2 minutes 45 seconds.

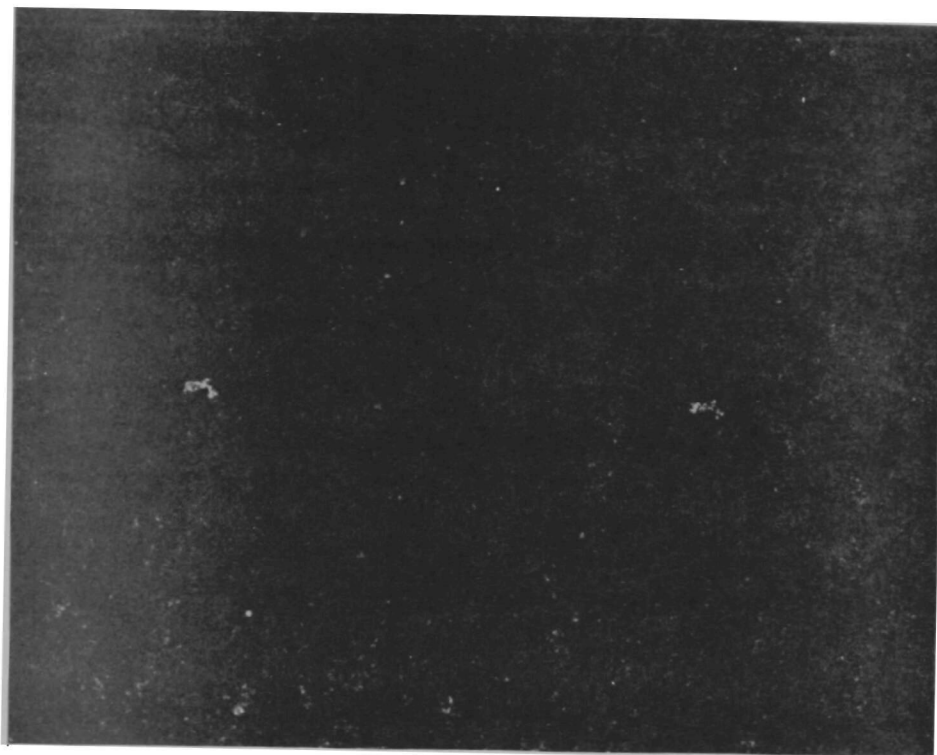


FIGURE 58
EXAMPLE # 1 - DISTINCTIVELY SHAPED PARTICLE PAIR

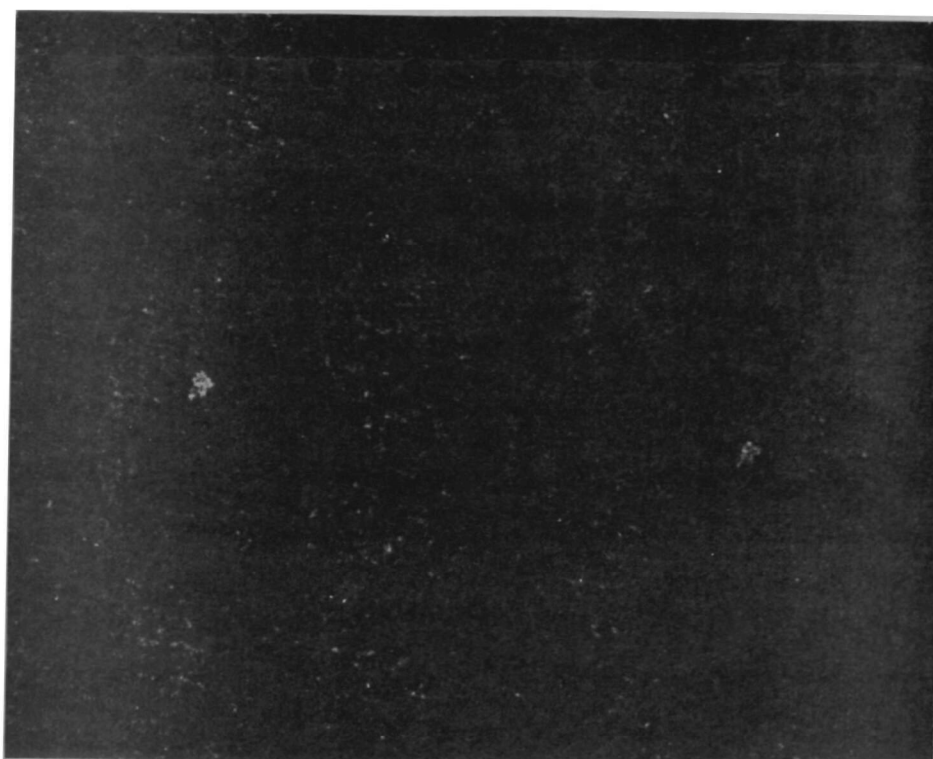


FIGURE 59
EXAMPLE #2 - DISTINCTIVELY SHAPED PARTICLE PAIR

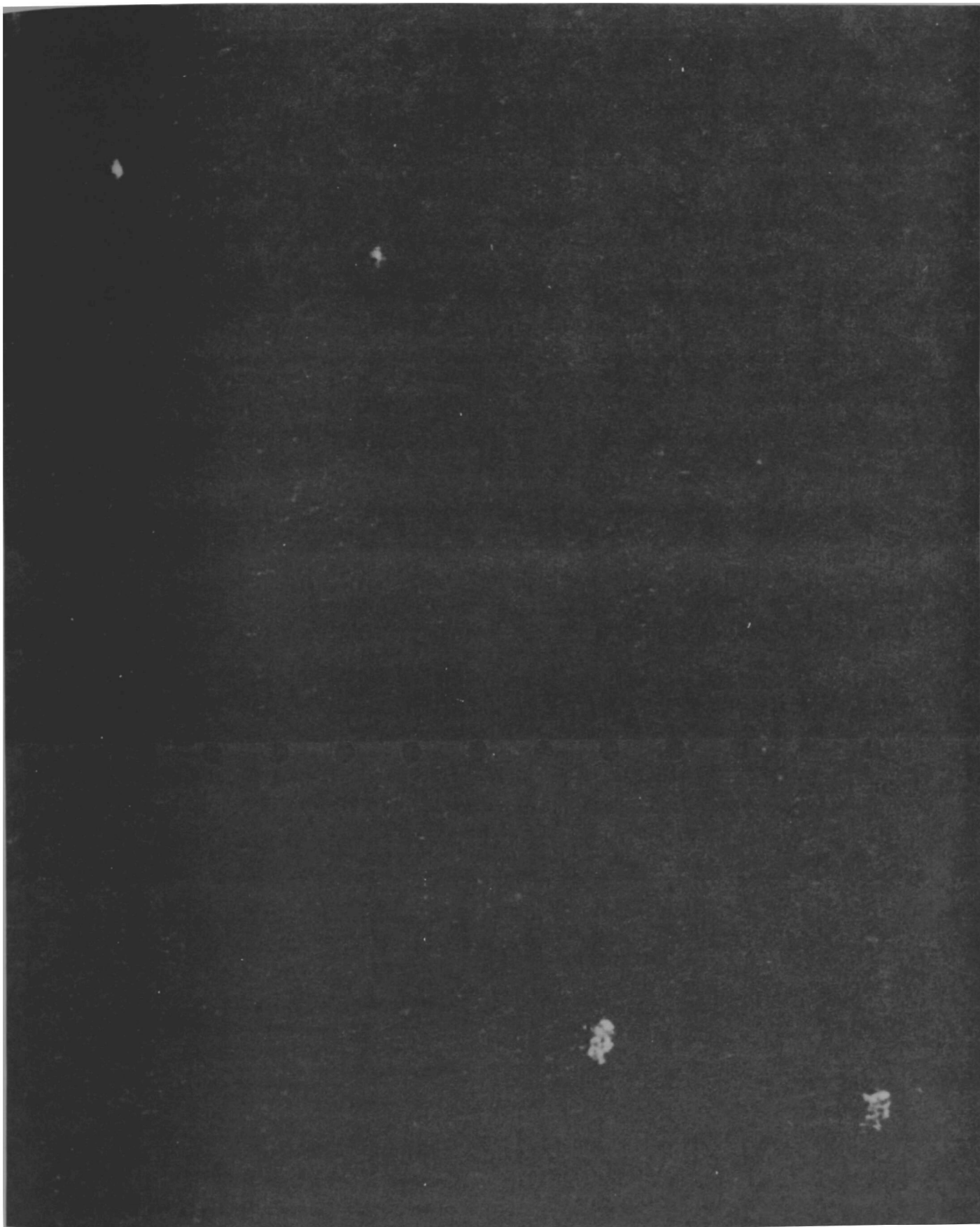


FIGURE 60
TWO PARTICLE PAIR RECONSTRUCTION

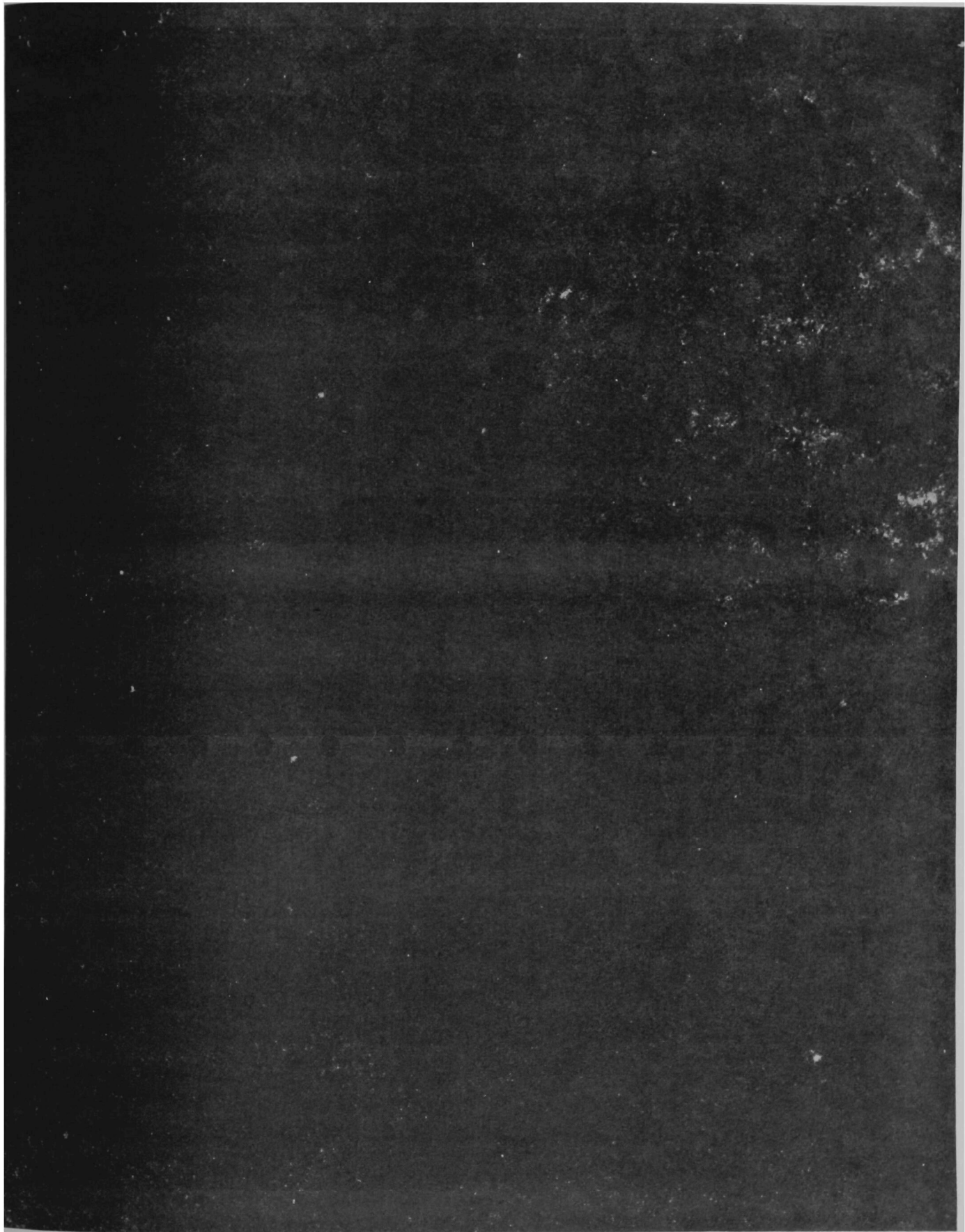


FIGURE 61
FOUR DOUBLE PULSED PARTICLE PAIRS
IN POTENTIAL FLOW
78

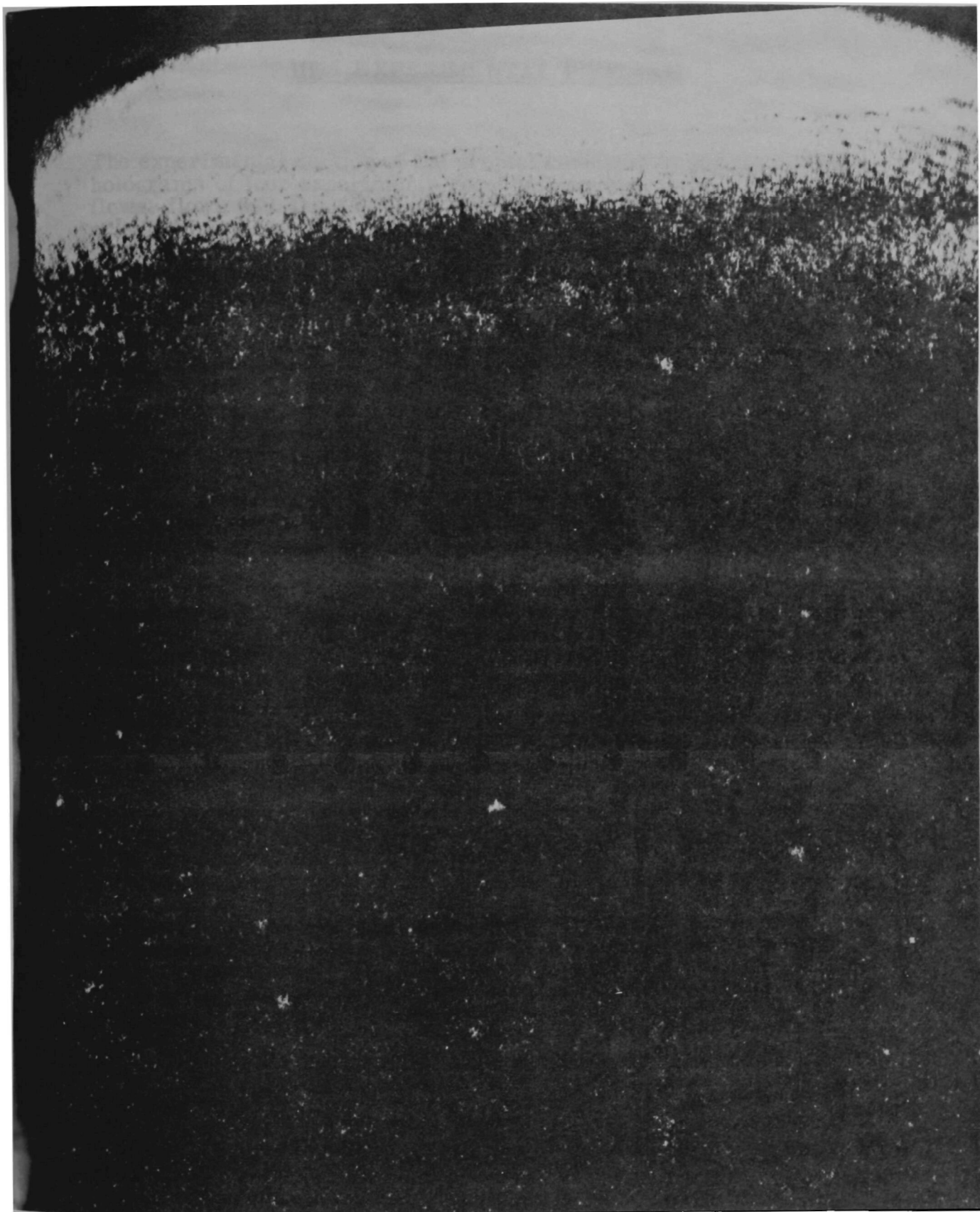


FIGURE 62
PARTICLE RECONSTRUCTION OF FLOW ABOUT THE
APCO TRAIN PROBE (.5 ISOKINETIC)

III. EXPERIMENTAL PROGRAM

The experimental section of the project consisted of making pulsed holograms of four experiments, namely, potential flows, turbulent flows, flows with the APCO train probe, and flows with charged precipitator plates. Several pulsed holograms were made of each flow with the single beam system described in the previous section with the duct seeded with flyash. The size, shape, two velocity components, and location of each particle was then measured with the reconstruction system also described in the previous section. The particle data from each hologram is presented in charts on the following pages.

To conduct an experiment usually required three people: One to manipulate instrumentation associated with the duct facility and to record data; one to operate the particulate dispenser, change hologram plates and fire the pulsed laser; and one to recharge the laser and monitor pulse quality. A typical run would last approximately three minutes with three holograms being recorded. Figure 63 illustrates a test being prepared for a run at the potential flow test section.

The material used in the four major experiments was flyash obtained from the Office of Air Programs and the Georgia Power Company. Figure 64 is an electron scanning microscope picture of the flyash showing the spherical nature of the material. The larger particles in the photograph are approximately 20 microns. The magnification ratio for the picture is approximately 1,250.

III. A. - POTENTIAL FLOW HOLOGRAMS

Several holograms were made in the potential flow test section at mean velocities of 25 feet/second and 33 feet/second at loadings ranging from .5 to 3.5 grains/scf. Table I lists the holograms made and gives general comments about them. Hologram No. 110 was analyzed in detail with many particles located, measured, and velocities computed. The data from the hologram is presented on the following pages. The particles in three planes parallel to the x - z plane were located and velocities measured. The planes were located at $y = 3.53''$, $y = 4.53''$, and $y = 5.03''$ as indicated in the sketch of Figure 65. There were so many double pulsed pairs visible that they could not all be counted in this hologram. Tables I-a, I-b, and I-c are tabulations for Hologram No. 110 of particle shape, size, x-y location, x component of velocity, y component of velocity, absolute value of velocity, and angular direction of the particle velocity in relation to the axis of the duct facility. The velocity profiles measured at 25 feet/second by the pitot tube are presented in Figures 16 and 23 for comparison with the particle velocities.



FIGURE 63
PERSONNEL PROGRAMMING FACILITY FOR TESTS

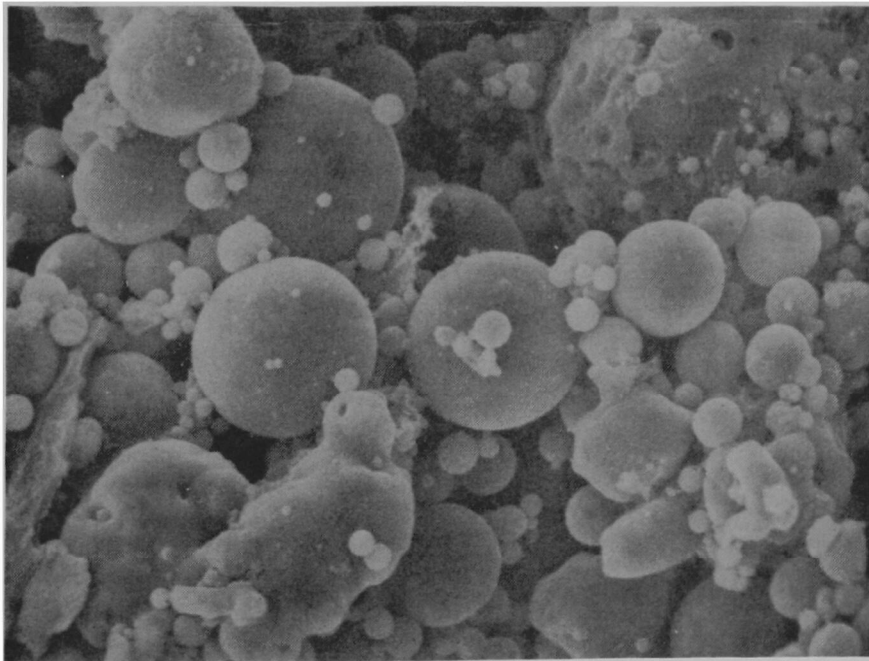


FIGURE 64
SCANNING ELECTRON MICROSCOPE PHOTOGRAPH
OF FLYASH 1250 X

TABLE I - POTENTIAL FLOW HOLOGRAMS

<u>Hologram Number</u>	<u>Mean Velocity Ft/Sec</u>	<u>Loading (Grains/Scf)</u>	<u>Comments</u>
110	25	1. 5	Excellent hologram, lots of double pulsed pairs visible
112	25	. 5	Few particles, double pulsed pairs visible
113	25	. 5	Effectively same as 112
115	33	3. 5	Double pulse pairs visible
116	33	3. 5	Effectively same as 112
117	33	3. 5	Effectively same as 112
119	33	3. 5	Effectively same as 112
122	33	1. 5	Double pulsed pairs visible
123	33	1. 5	Slightly overexposed, some double pulsed pairs visible
124	33	. 5	Double pulsed pairs visible but few particles
125	33	. 5	Effectively same as 124
129	33	3. 5	Excellent in all respects

Loading - 1.5 grains/scf
Pulse Separation - .2 milliseconds
Mean Velocity - 25 ft./sec.

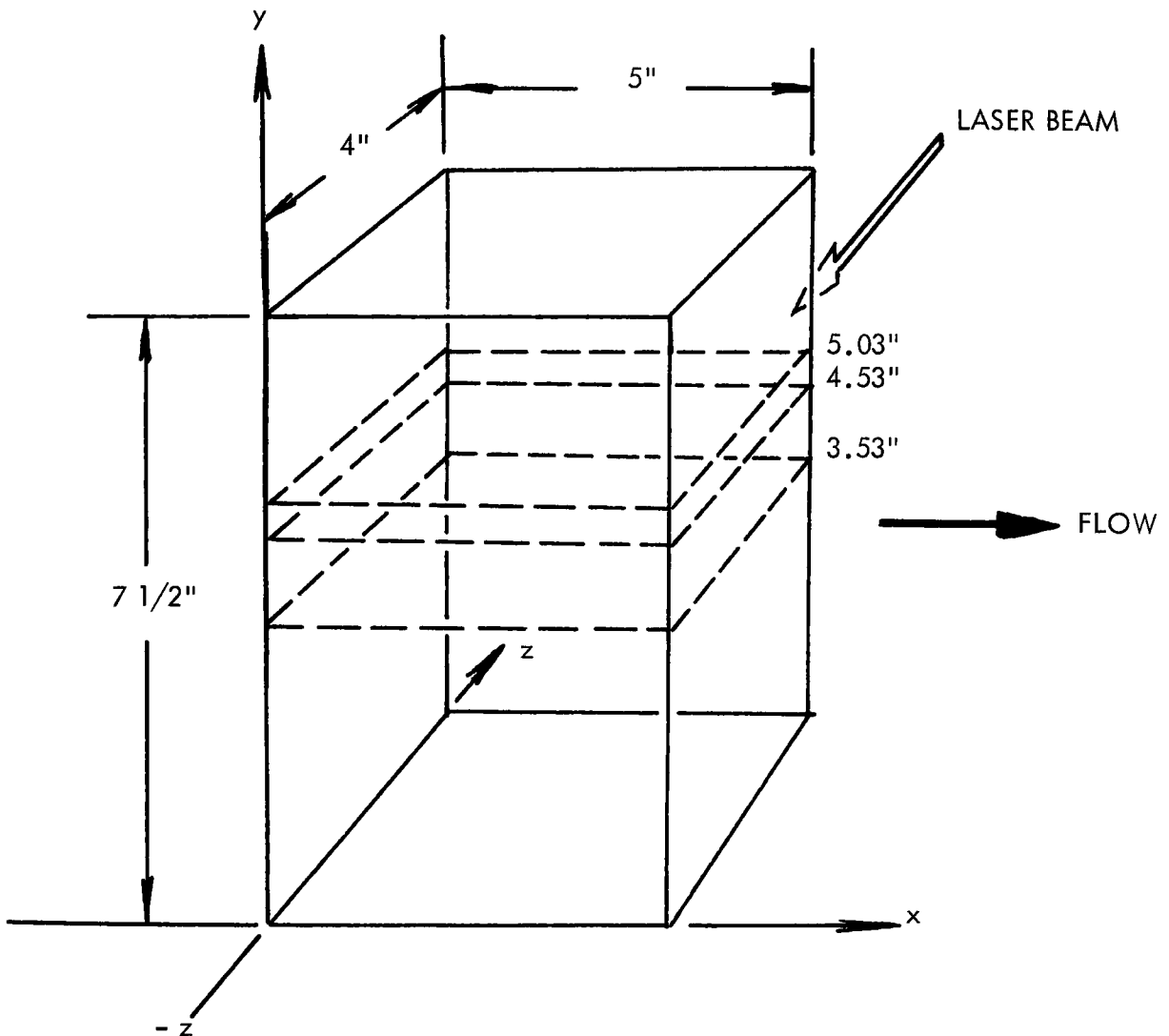


FIGURE 65
POTENTIAL FLOW HOLOGRAM #110

Particle No. and Location (x, z)		V_x	V_y (ft./sec.)	IVI	V°	Size/Shape D = Diameter in Microns
1.	(2.90 , 3.38)	27.60	-1.445	27.65	$3^\circ \downarrow$	Sphere D = 18
2.	(2.90 , 3.50)	27.25	0.00	27.25	0°	Sphere D = 27
3.	(1.80 , 3.50)	26.85	-1.405	26.90	$3^\circ \downarrow$	Sphere D = 18
4.	(1.80 , 3.66)	27.20	-1.905	27.25	$4^\circ \downarrow$	Sphere D = 27
5.	(2.70 , 2.14)	27.60	-1.94	27.65	$4^\circ \downarrow$	Irreg. \triangle 54 36
6.	(2.70 , 2.14)	27.95	-1.96	28.00	$4^\circ \downarrow$	Sphere D = 27
7.	(2.70 , 2.14)	28.35	-1.49	28.40	$3^\circ \downarrow$	Sphere D = 18

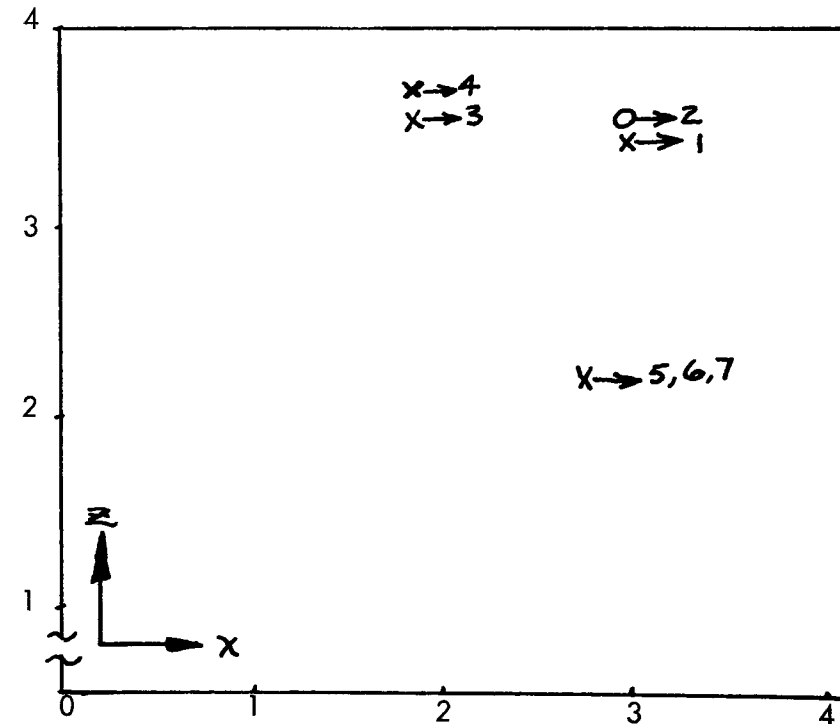
Loading: 1.5 grains/scf

Pulse Separation - .2 milliseconds

Cut at $y = 5.03''$

- Positive y Component
- × Negative y Component
- Zero y Component

TABLE Ia
POTENTIAL FLOW HOLOGRAM #110



Particle No. and Location (x, z)		V_x	V_y (ft./sec.)	IVI	V°	Size/Shape D = Diameter in Microns
1.	(2.70 , 1.30)	26.85	-1.88	26.90	4° ↓	Sphere D = 130
2.	(2.70 , 1.35)	27.25	-0.95	27.25	2° ↓	Sphere D = 44
3.	(2.70 , 1.44)	27.20	-1.43	27.25	3° ↓	⊙ D _o = 54
4.	(1.80 , 1.89)	27.53	-2.41	27.65	5° ↓	Sphere D = 44
5.	(1.80 , 1.89)	27.53	-2.41	27.65	5° ↓	Sphere D = 36
6.	(1.70 , 1.89)	27.90	-2.44	28.00	5° ↓	Sphere D = 54
7.	(1.50 , 1.89)	27.55	-2.41	27.65	5° ↓	Sphere D = 27
8.	(1.35 , 1.89)	27.30	-2.39	27.40	5° ↓	Sphere D = 44
9.	(1.10 , 1.95)	27.15	-2.38	27.25	5° ↓	Sphere D = 36
10.	(1.05 , 1.95)	27.35	-1.92	27.40	4° ↓	⊙ D ₃₆
11.	(2.75 , 2.56)	28.40	0.00	28.40	0°	Sphere D = 67
12.	(2.80 , 2.65)	28.40	0.00	28.40	0°	Irreg. ⊙ D ₄₄
13.	(1.55 , 2.90)	26.90	0.00	26.90	0°	Sphere D = 44

Loading: 1.5 grains/scf

Pulse Separation - .2 milliseconds

Cut at $y = 4.53$

● Positive y Component

X Negative y Component

○ Zero y Component

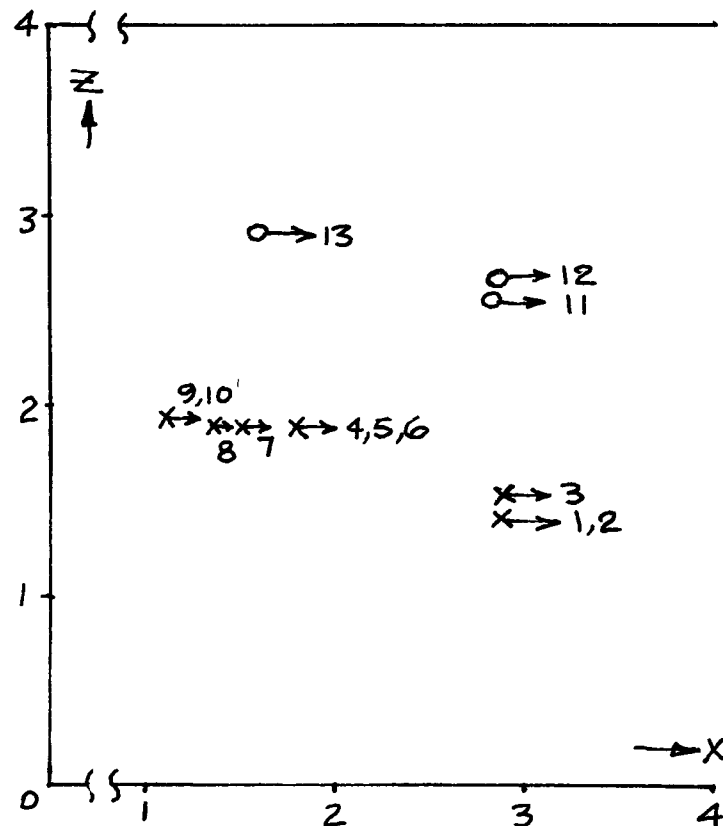


TABLE 1b
POTENTIAL FLOW HOLOGRAM #110

TABLE Ic
POTENTIAL FLOW HOLOGRAM #110

Loading: 1.5 grains/scf


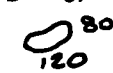
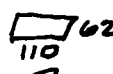

Pulse Separation - .2 milliseconds

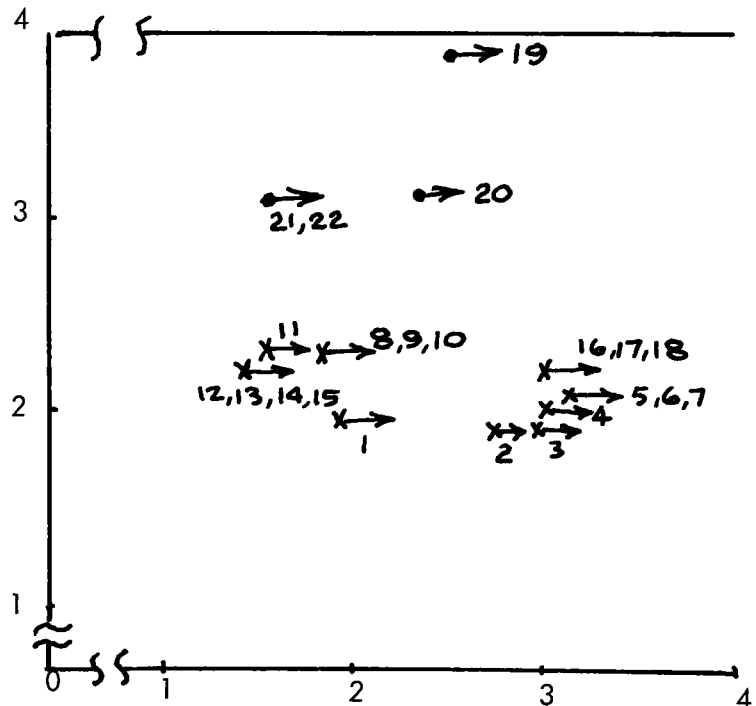
Cut at $y = 3.53$

● Positive y Component

✕ Negative y Component

○ Zero y Component

Particle No. and Location (x, z)		V_x	V_y (ft./sec.)	V	V°	Size/Shape D = Diameter in Microns
1.	(1.85 , 2.00)	27.15	-2.38	27.25	5° ↓	Irreg. 
2.	(2.65 , 1.95)	27.30	-2.39	27.40	5° ↓	Sphere D = 36
3.	(2.80 , 1.95)	27.85	-2.93	28.00	6° ↓	Sphere D = 27
4.	(2.90 , 2.05)	27.55	-2.41	27.65	5° ↓	Sphere D = 44
5.	(3.00 , 2.08)	27.95	-1.96	28.00	4° ↓	Sphere D = 27
6.	(3.00 , 2.14)	27.65	-2.415	27.75	5° ↓	Sphere D = 44
7.	(3.00 , 2.14)	27.65	-2.41	27.75	5° ↓	Sphere D = 62
8.	(1.75 , 2.36)	27.40	-1.435	27.35	3° ↓	Sphere D = 54
9.	(1.75 , 2.36)	27.35	-1.435	27.40	3° ↓	Sphere D = 18
10.	(1.75 , 2.36)	27.35	-1.435	27.40	3° ↓	Sphere D = 36
11.	(1.45 , 2.36)	26.80	-3.30	27.80	7° ↓	Sphere D = 54
12.	(1.35 , 2.31)	28.00	-2.45	28.10	5° ↓	Sphere D = 22
13.	(1.35 , 2.31)	27.85	-2.93	28.00	6° ↓	Sphere D = 36
14.	(1.35 , 2.31)	27.90	-2.44	28.00	5° ↓	Sphere D = 40
15.	(1.35 , 2.31)	27.25	-2.95	28.40	6° ↓	Sphere D = 40
16.	(2.90 , 2.23)	27.65	-2.415	27.75	5° ↓	Sphere D = 44
17.	(2.90 , 2.23)	27.95	-1.96	28.00	4° ↓	Sphere D = 71
18.	(2.90 , 2.23)	27.35	-1.91	27.40	4° ↓	Sphere D = 67
19.	(2.40 , 3.90)	26.55	0.928	26.55	2° ↑	Irreg. 
20.	(2.25 , 3.18)	26.65	1.16	26.65	2.5° ↑	Irreg. 
21.	(1.55 , 3.16)	26.90	0.941	26.90	2° ↑	Irreg. 
22.	(1.45 , 3.16)	26.85	1.88	26.90	4° ↑	D = 44



III. B. - TURBULENT FLOW HOLOGRAMS

Holograms of the turbulent flow section were made at mean velocities of 24 feet/second and 33 feet/second at loadings ranging from .5 to 3.5 grains/scf. Table II lists the holograms with comments about them. Hologram No. 175 was analyzed in detail, and the plots of particle velocity are shown in Tables IIa - IIc. The velocity of particles in four parallel planes located at $y = 0.446''$, $0.396''$, 0 , $-.891''$ was measured. The location of these planes and the coordinate systems used are shown in Figure 66. The velocity profiles measured with the pitot tube are those flow velocities as shown in Figures 24 and 25.

From Table IIb, it would appear that a minor swirl exists in the turbulent section since most particles at the top of the diagram have an "up" component of velocity whereas all particles at the bottom of the diagram have a "down" component. Apparently, gravitational effects were very small in both the potential and turbulent sections since the deviation from the horizontal was at most only a few degrees.

III. C. - HOLOGRAMS OF APCO TRAIN PROBE

Holograms were made of the APCO train probe with the probe operated at .5 isokinetic, 1.0 isokinetic, and 1.5 isokinetic at a mean flow velocity of 25 feet/second. Table III lists the holograms made, and hologram No. 142 (1.0 isokinetic) was selected for detailed analysis. The flow around the probe in the 0.5 and 1.5 isokinetic cases was so turbulent that double pulsed pairs could not easily be determined. Figure 67 shows the coordinate system used and the plane ($z=0$) selected for measuring particle characteristics. This plane is a vertical plane located at the center of the probe. The location of the particles in this plane are shown in Figure 68. Table IIIa is a listing of particle characteristics.

The experimental set-up used to obtain the particulate samples is shown in Figure 69. Figure 70 shows the sampling probe located in the potential flow section. The probe was a 1/2" O. D. copper tube with the inside opening beveled to form a sharp entrance such that the area of the opening was equivalent to that determined at the outside diameter of the probe. The bend radius of the tube was approximately 4 inches, and the distance from the mouth of the tube to the bend was also 4 inches.

The sampling system was calibrated using the set-up shown in Figure 71. A basic assumption made was that the flow in the probe inlet would be potential; that is, the flow would be of constant velocity with no areas of separation. By making this assumption, the velocity in the inlet can be assumed to be a function of the quantity of air removed from the tunnel. More specifically, $V_{\text{probe}} = Q/A$ where Q is the quantity of air removed in cubic feet per second and A is the probe inlet area in square feet.

TABLE II - TURBULENT FLOW HOLOGRAMS

<u>Hologram Number</u>	<u>Mean Velocity Ft/Sec</u>	<u>Loading (Grains/Scf)</u>	<u>Comments</u>
172	24	0.5	Very few particles
174	24	0.5	Very few particles
175	24	0.5	Appears to be more particles than 172 or 174
177	24	0.5	Same as 172, 174
178	24	3.5	Lots of particles, some difficulty in identifying double pulsed pairs
179	24	3.5	Same comments as 178
180	24	3.5	Same comments as 179
182	33	1.5	Double pulsed pairs visible
183	33	1.5	Not as many pairs as 182
184	33	3.5	Double pulsed pairs visible
185	33	3.5	Same comments as 184
187	33	1.5	Double pulsed pairs visible
188	33	1.5	Same comments as 187
189	33	1.5	Same comments as 189

68

Particle No. and Location (x, z)		V_x	V_y (ft./sec.)	V	V°	Size/Shape D = Diameter in Microns
1.	(-0.050 , +2.246)	23.29	0	23.29	0°	Sphere D = 36
2.	(-0.175 , +0.970)	21.78	0	21.78	0°	\square^{82}
3.	(-0.500 , +0.166)	23.48	0	23.48	0°	Sphere D = 90
4.	(-0.500 , -1.608)	25.93	- .91	25.95	$2^\circ \downarrow$	$\text{II} \begin{matrix} 8 \\ 45 \end{matrix}$
5.	(-0.750 , -0.721)	24.98	- .87	25.00	$2^\circ \downarrow$	Sphere D = 23
6.	(-0.700 , -0.527)	24.98	- .87	25.00	$2^\circ \downarrow$	\triangle^{72}
7.	(-0.675 , +1.026)	24.43	2.13	24.43	$5^\circ \uparrow$	Sphere D = 45
8.	(-0.675 , +1.830)	22.64	1.98	22.73	$5^\circ \uparrow$	Sphere D = 73
9.	(-0.850 , +1.636)	21.18	1.11	21.21	$3^\circ \uparrow$	Sphere D = 45
10.	(-0.800 , +1.747)	23.27	1.22	23.30	$3^\circ \uparrow$	Sphere D = 54
11.	(-0.900 , -1.830)	25.51	-1.78	25.57	$4^\circ \downarrow$	Sphere D = 27
12.	(+0.575 , +0.887)	19.44	-1.67	19.51	$5^\circ \downarrow$	Sphere D = 23

Loading: 1.5 grains/scf

Pulse Separation - .2 milliseconds

Cut at $y = 0$

- Positive y Component
- X Negative y Component
- Zero y Component

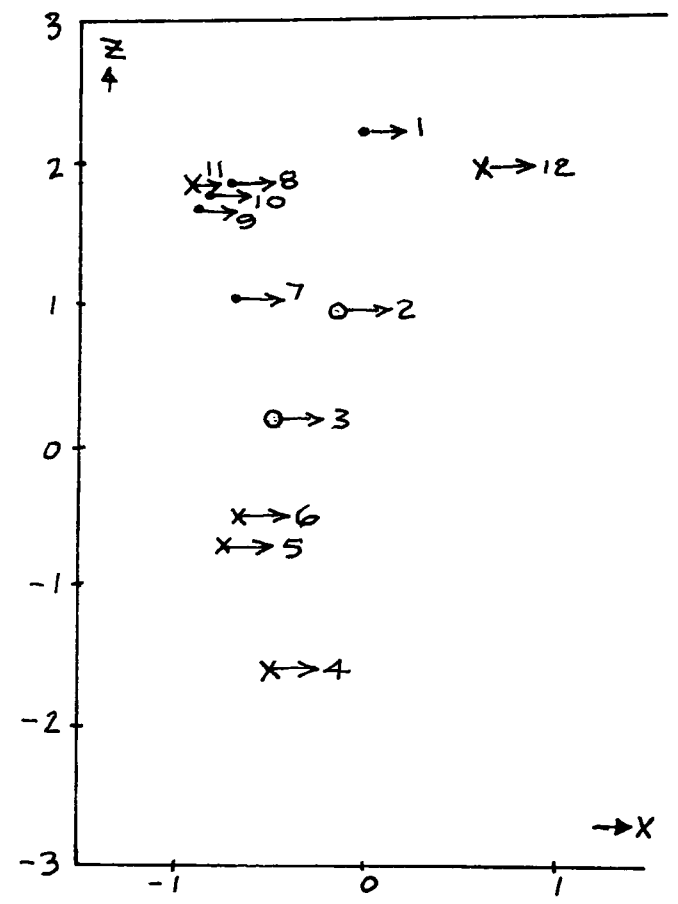


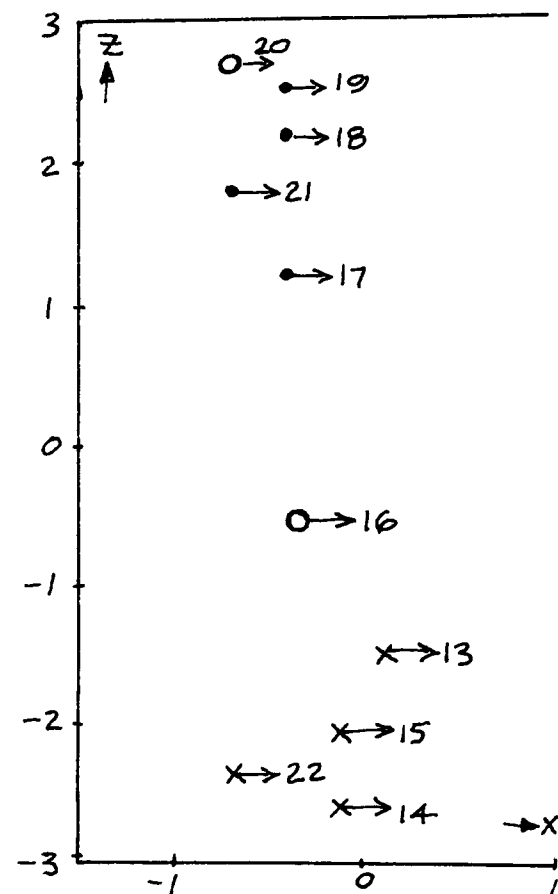
TABLE IIa
TURBULENT FLOW HOLOGRAM #175

	Particle No. and Location (x, z)	V_x	V_y (ft./sec.)	IVI	V°	Size/Shape D = Diameter in Microns
13.	(+0.075 , -1.580)	26.51	- .46	26.52	$1^\circ \downarrow$	Δ_{27}^{73}
14.	(-0.150 , -2.634)	21.75	-1.14	21.78	$3^\circ \downarrow$	Sphere D = 81
15.	(-0.150 , -2.107)	23.21	-2.03	23.30	$5^\circ \downarrow$	Sphere D = 100
16.	(-0.400 , -0.555)	24.43	0	24.43	0°	Sphere D = 45
17.	(-0.450 , +1.164)	24.98	.87	25.00	$2^\circ \uparrow$	Sphere D = 18
18.	(-0.450 , +2.190)	21.56	1.13	21.59	$3^\circ \uparrow$	Sphere D = 32
19.	(-0.450 , +2.523)	20.94	1.83	21.02	$5^\circ \uparrow$	Sphere D = 54
20.	(-0.725 , +2.689)	20.64	0	20.64	0°	Sphere D = 45
21.	(-0.725 , +1.747)	21.77	.76	21.78	$2^\circ \uparrow$	Δ_{45}^{45}
22.	(-0.725 , -2.468)	22.26	-1.95	22.35	$5^\circ \downarrow$	Sphere D = 27

TABLE IIb
TURBULENT FLOW HOLOGRAM #175

Loading: 1.5 grains/scf
Pulse Separation - .2 milliseconds
Cut at $y = -0.891$

- Positive y Component
- X Negative y Component
- Zero y Component



	Particle No. and Location (x, z)	V_x	V_y (ft./sec.)	V	V°	Size/Shape D = Diameter in Microns
	23. (-0.250 , +1.192)	24.04	- .42	24.05	$1^\circ \downarrow$	Sphere D = 73
	24. (-0.450 , -0.360)	25.89	-1.81	25.95	$4^\circ \downarrow$	Sphere D = 23
	25. (-0.450 , -0.210)	25.74	- .90	25.76	$2^\circ \downarrow$	Δ_{27}^{54}
	26. (-0.750 , -1.081)	24.34	-2.13	24.43	$5^\circ \downarrow$	Sphere D = 23
	27. (-0.800 , -0.444)	25.62	-2.69	25.76	$6^\circ \downarrow$	Sphere D = 23
	28. (-1.00 , -1.664)	24.62	- .43	24.62	$1^\circ \downarrow$	\bigcirc_{145}^{54}
	29. (-1.00 , -2.412)	25.95	0	25.95	0°	Sphere D = 45
	30. (+0.550 , +2.911)	17.99	0	17.99	0°	Sphere D = 36
10	31. (+0.550 , +0.083)	25.93	0	25.95	0°	Sphere D = 36
	32. (+0.800 , -0.776)	26.04	-2.28	26.14	$5^\circ \downarrow$	Sphere D = 82

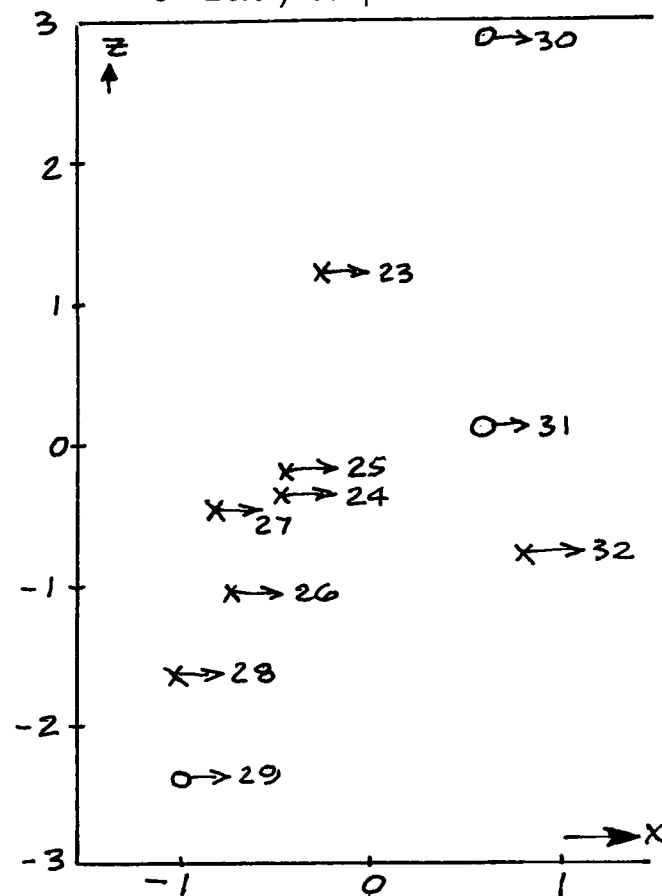
TABLE IIc
TURBULENT FLOW HOLOGRAM #175

Loading: 1.5 grains/scf

Pulse Separation - .2 milliseconds

Cut at $y = 0.446$

- Positive y Component
- x Negative y Component
- Zero y Component




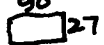
	Particle No. and Location (x, z)	V _x	V _y (ft./sec.)	V	V°	Size/Shape D = Diameter in Microns
	33. (+0.300 , -2.052)	24.96	1.31	25.00	3° ↑	Sphere D = 36
	34. (-0.025 , +1.081)	22.54	0	22.54	0°	Sphere D = 45
	35. (-0.525 , +0.222)	23.30	.41	23.30	1° ↑	Sphere D = 59
	36. (-0.500 , -0.832)	23.96	-2.10	24.05	5° ↓	82 
	37. (-0.500 , -0.222)	24.58	-1.29	24.62	3° ↓	Sphere D = 23
	38. (-0.900 , -0.832)	26.33	0	26.33	0°	Sphere D = 36
	39. (+0.200 , -1.220)	23.02	-2.01	23.11	5° ↓	90 
	40. (+0.200 , -1.192)	23.99	-1.68	24.05	4° ↓	Sphere D = 45
22	41. (+0.250 , -0.832)	23.10	- .40	23.11	1° ↓	Sphere D = 50
	42. (+0.500 , -1.275)	20.83	0	20.83	0°	Sphere D = 73
	43. (+0.450 , -1.192)	23.67	0	23.67	0°	Sphere D = 50
	44. (+0.400 , -1.164)	23.86	0	23.86	0°	Sphere D = 32

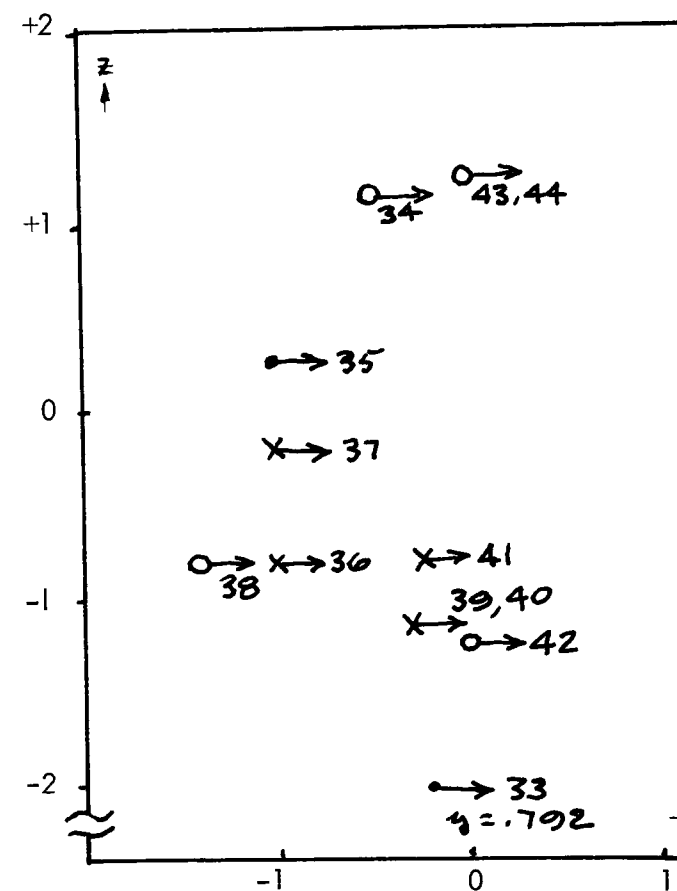
TABLE IIId
TURBULENT FLOW HOLOGRAM #175

Loading: 1.5 grains/scf

Pulse Separation - .2 milliseconds

Cut at y = 0.396

- Positive y Component
- X Negative y Component
- Zero y Component



Loading - .5 grains/scf
Pulse Separation - .2 milliseconds
Mean Velocity - 24 ft./sec.

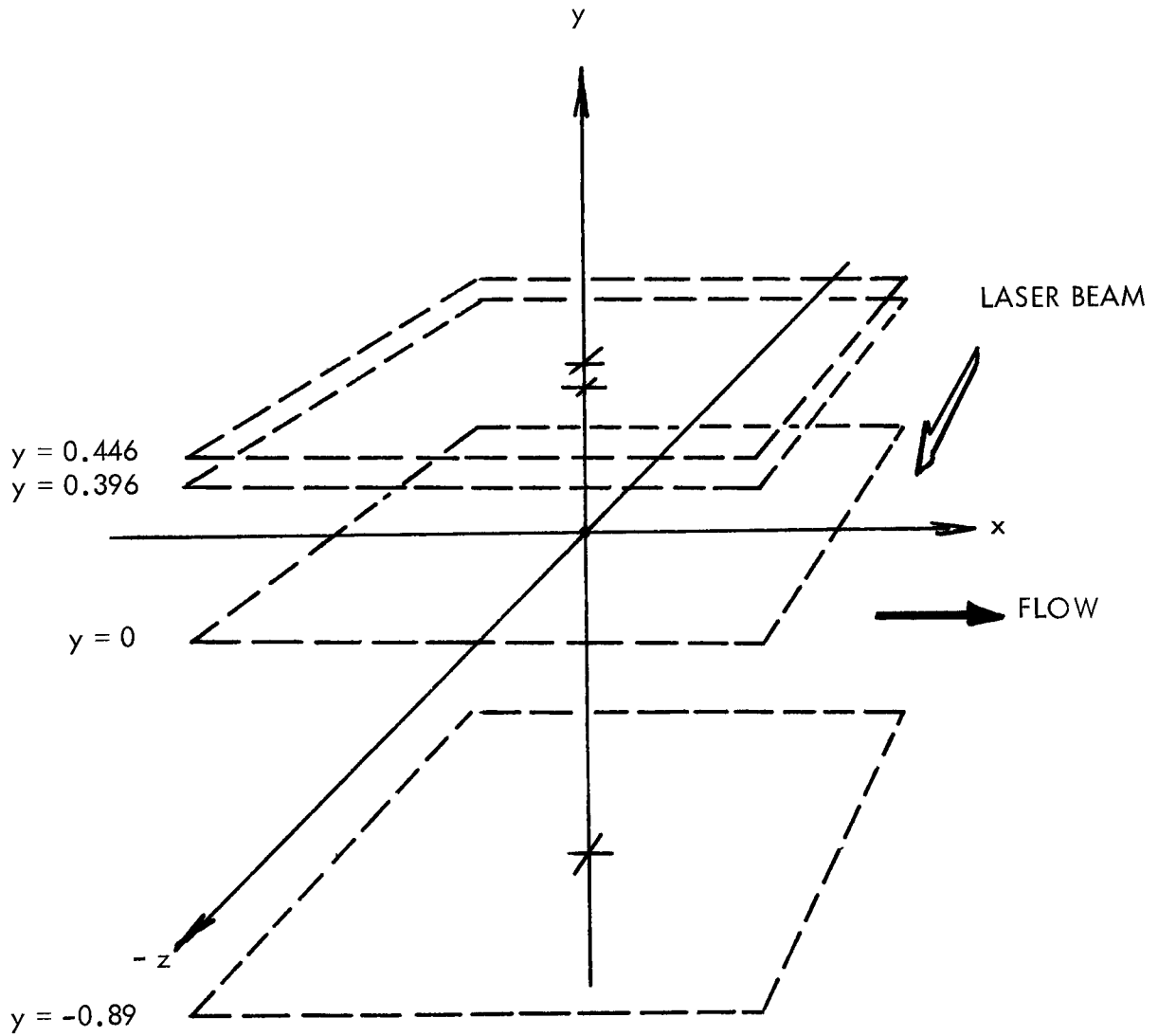


FIGURE 66
TURBULENT FLOW HOLOGRAM #175

TABLE III - APCO TRAIN

<u>Hologram Number</u>	<u>Mean Velocity Ft/Sec</u>	<u>Loading (Grains/Scf)*</u>	<u>Comments</u>
136	25	. 5	. 5 isokinetic, lots of particles
142	25	. 47	1. 0 isokinetic, lots of double pulsed pairs
143	25	. 47	Same as 142
149	25	5. 84	Maybe some double pulsed pairs 1. 0 isokinetic
151	25	3. 4	. 5 isokinetic, some particles
152	25	3. 4	Same as 152
153	25	3. 4	Best of all, . 5 isokinetic
154	25	1. 9	1. 5 isokinetic, high noise due to dirty windows
155	25	1. 9	Same as 154
156	25	1. 9	Same as 154
160	25	2. 93	1. 5 isokinetic some particles visible
161	25	2. 93	Same as 160
162	25	2. 93	Same as 160
165	25	3. 06	Same as 160
166	25	. 475	1. 5 isokinetic some particles
167	25	. 475	. 5 isokinetic best of all, lots of particles
169	25	4. 3	. 5 isokinetic lots of particles
171	25	4. 3	. 5 isokinetic same

* As calculated using sample obtained through probe.

1.0 Isokinetic
Loading - .47 grains/scf
Pulse Separation - .2 milliseconds
Mean Velocity - 25 ft./sec.
The x and y components of velocity of particles in the $z = 0$ plane were measured.
The origin is at the center of probe of the APCO Train as indicated.

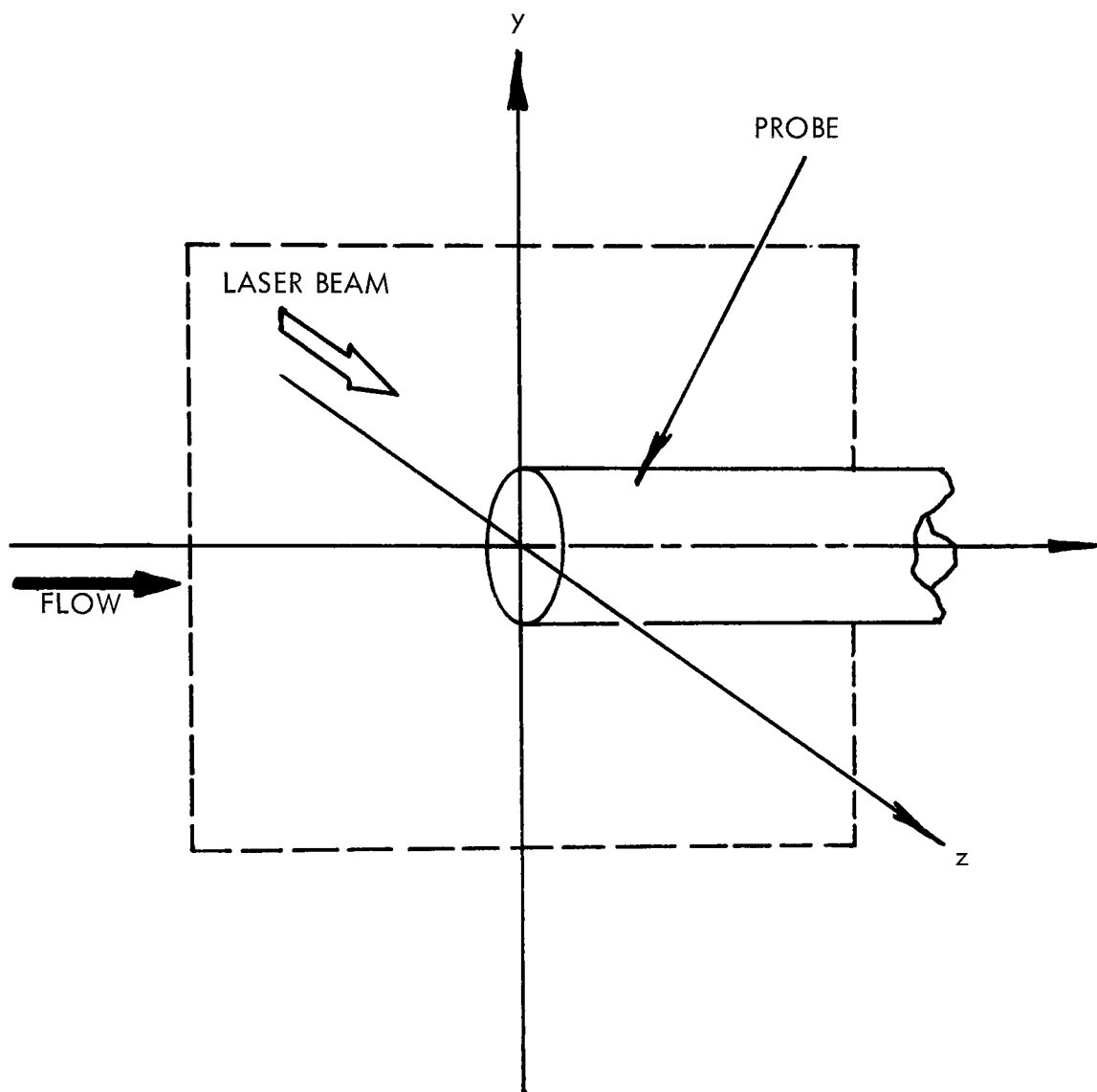


FIGURE 67
APCO TRAIN HOLOGRAM #142

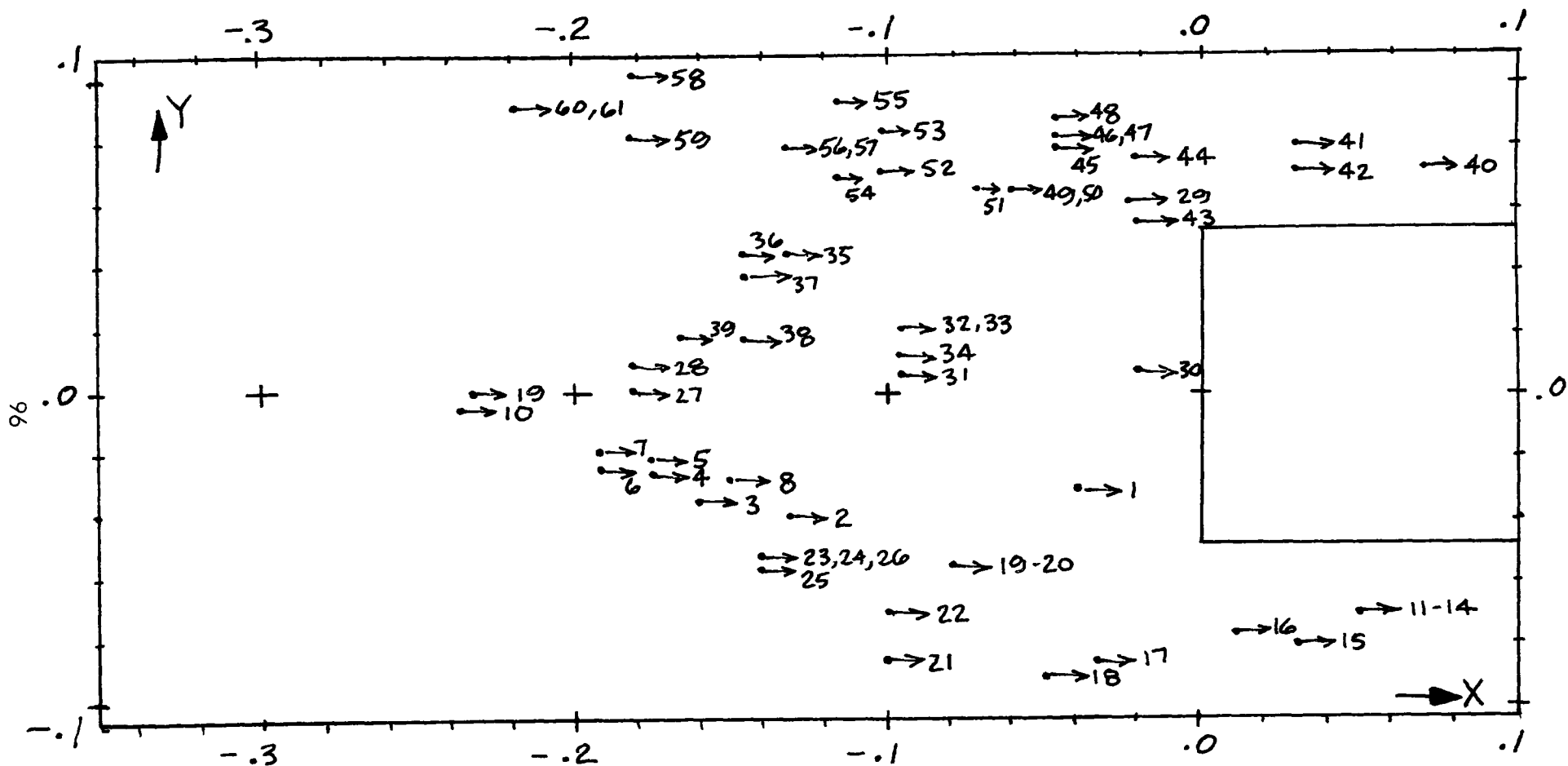


FIGURE 68
APCO HOLOGRAM #142

TABLE IIIa
APCO Train Hologram #142
1.0 Isokinetic, Loading 1.5 Grains/scf
Pulse Separation - .2 Milliseconds
Mean Velocity 25 ft./sec.



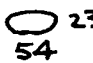
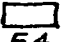
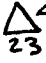



	Particle No. and Location (x, y, z)	V _x	V _y (ft./sec.)	IVI	V°	Size/Shape D = Diameter in Microns
1.	(-0.200 , -0.159 , +0.058)	22.91	- .800	22.92	2°↓	 82
2.	(-0.650 , -0.205 , +0.418)	22.72	- .793	22.73	2°↓	Sphere D = 45
3.	(-0.800 , -0.181 , +0.058)	22.54	- .393	22.54	1°↓	 90
4.	(-0.875 , -0.136 , +0.058)	22.34	- .780	22.35	2°↓	Sphere D = 45
5.	(-0.875 , -0.114 , +0.058)	22.34	- .780	22.35	2°↓	 23 54
6.	(-0.950 , -0.125 , +0.058)	22.53	-1.18	22.54	3°↓	Sphere D = 36
7.	(-0.950 , -0.090 , +0.058)	22.72	-1.19	22.73	3°↓	Sphere D = 14
8.	(-0.750 , -0.148 , +0.085)	22.73	- .397	22.73	1°↓	Sphere D = 36
9.	(-1.150 , -0.012 , +0.058)	22.53	-1.18	22.54	3°↓	Sphere D = 27
10.	(-1.175 , -0.034 , +0.058)	22.34	-1.17	22.35	3°↓	Sphere D = 9
11.	(+0.250 , -0.364 , 0.000)	23.11	0	23.11	0°	Sphere D = 36
12.	(+0.250 , -0.364 , 0.000)	22.34	.780	22.35	2°↑	Sphere D = 27
13.	(+0.250 , -0.364 , 0.000)	22.35	0	22.35	0°	Sphere D = 23
14.	(+0.250 , -0.364 , 0.000)	22.35	0	22.35	0°	Sphere D = 18
15.	(+0.150 , -0.409 , 0.000)	22.73	.397	22.73	1°↑	Sphere D = 32
16.	(+0.050 , -0.386 , -0.026)	22.35	0	22.35	0°	Sphere D = 9
17.	(-0.150 , -0.432 , -0.026)	22.73	0	22.73	0°	Sphere D = 9
18.	(-0.250 , -0.466 , -0.186)	22.35	0	22.35	0°	Sphere D = 54
19.	(-0.400 , -0.284 , 0.000)	22.73	0	22.73	0°	Sphere D = 36
20.	(-0.400 , -0.284 , +0.030)	22.35	0	22.35	0°	Sphere D = 54
21.	(-0.500 , -0.432 , +0.030)	22.54	0	22.54	0°	Sphere D = 27
22.	(-0.500 , -0.365 , +0.030)	22.73	0	22.73	0°	Sphere D = 7
23.	(-0.700 , -0.227 , +0.196)	22.54	0	22.54	0°	Sphere D = 14
24.	(-0.700 , -0.227 , +0.196)	21.97	0	21.97	0°	Sphere D = 18
25.	(-0.700 , -0.284 , +0.196)	22.35	0	22.35	0°	Sphere D = 36
26.	(-0.700 , -0.227 , +0.196)	22.35	0	22.35	0°	Sphere D = 18
27.	(-0.900 , 0.0 , +0.196)	22.73	0	22.73	0°	Sphere D = 23
28.	(-0.900 , +0.307 , +0.335)	22.54	- .393	22.54	1°↓	Sphere D = 41

TABLE IIIa (Continued)

Particle No. and Location (x, y, z)		V_x	V_y (ft./sec.)	V	V°	Size/Shape D = Diameter in Microns
29.	(-0.110 , +0.295 , +0.390)	22.73	0	22.73	0°	 32 54
30.	(-0.100 , +0.034 , +0.055)	22.83	-2.00	22.92	5° ↓	Sphere D = 23
31.	(-0.475 , +0.023 , -0.083)	22.68	-1.58	22.73	4° ↓	 45 23
32.	(-0.475 , +0.091 , -0.083)	22.86	-1.60	22.92	4° ↓	Sphere D = 9
33.	(-0.475 , +0.091 , -0.083)	22.86	-1.60	22.92	4° ↓	Sphere D = 7
34.	(-0.475 , +0.057 , -0.083)	22.86	-1.60	22.92	4° ↓	Sphere D = 7
35.	(-0.650 , +0.216 , -0.055)	22.86	-1.60	22.92	4° ↓	Sphere D = 27
36.	(-0.725 , +0.216 , -0.216)	22.68	-1.58	22.73	4° ↓	Sphere D = 9
37.	(-0.725 , +0.182 , -0.055)	22.48	-1.57	22.54	4° ↓	 32 5
38.	(-0.725 , +0.091 , -0.055)	22.86	-1.60	22.92	4° ↓	Sphere D = 27
39.	(-0.825 , +0.091 , -0.055)	22.86	-1.60	22.92	4° ↓	Sphere D = 18
40.	(+0.350 , +0.341 , 0.000)	22.54	0	22.54	0°	Sphere D = 45
41.	(+0.150 , +0.386 , 0.000)	22.54	0	22.54	0°	 36 59
42.	(+0.150 , +0.341 , +0.055)	22.16	- .387	22.16	0°	Sphere D = 45
43.	(-0.100 , +0.277 , 0.000)	22.72	- .793	22.73	2° ↓	Sphere D = 23
44.	(-0.100 , +0.368 , 0.000)	22.53	- .787	22.54	2° ↓	Sphere D = 27
45.	(-0.225 , +0.382 , 0.000)	22.15	- .773	22.16	2° ↓	Sphere D = 45
46.	(-0.225 , +0.391 , 0.000)	22.10	- .772	22.11	2° ↓	Sphere D = 36
47.	(-0.225 , +0.400 , 0.000)	22.72	-1.19	22.73	3° ↓	Sphere D = 54
48.	(-0.225 , +0.427 , 0.000)	22.72	- .793	22.73	2° ↓	Sphere D = 36
49.	(-0.300 , +0.318 , 0.000)	22.73	- .397	22.73	1° ↓	Sphere D = 32
50.	(-0.300 , +0.313 , 0.000)	22.73	- .397	22.73	1° ↓	Sphere D = 18
51.	(-0.350 , +0.313 , 0.000)	23.10	- .806	23.11	2° ↓	Sphere D = 36
52.	(-0.500 , +0.341 , 0.000)	22.73	- .397	22.73	1° ↓	Sphere D = 54
53.	(-0.500 , +0.409 , 0.000)	22.72	- .793	22.73	2° ↓	 45 30
54.	(-0.575 , +0.341 , 0.000)	23.11	.403	23.11	1° ↑	Sphere D = 45
55.	(-0.575 , +0.455 , 0.000)	22.73	.397	22.73	1° ↑	Sphere D = 45
56.	(-0.650 , +0.386 , 0.000)	22.72	.793	22.73	2° ↑	Sphere D = 18
57.	(-0.650 , +0.386 , 0.000)	22.72	.793	22.73	2° ↑	Sphere D = 27
58.	(-0.900 , +0.511 , 0.000)	22.16	.387	22.16	1° ↑	Sphere D = 90
59.	(-0.900 , +0.398 , 0.000)	22.92	.400	22.92	1° ↑	Sphere D = 27
60.	(-1.075 , +0.443 , 0.000)	22.72	.793	22.73	2° ↑	Sphere D = 64
61.	(-1.075 , +0.455 , 0.000)	22.72	.793	22.73	2° ↑	Sphere D = 45

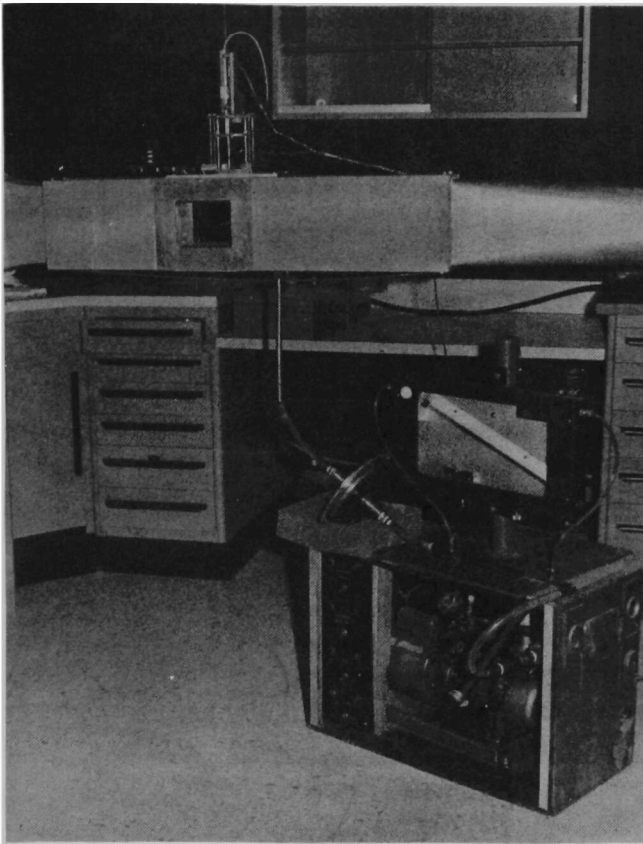


FIGURE 69
PARTICLE SAMPLING SYSTEM
USING THE APCO TRAIN

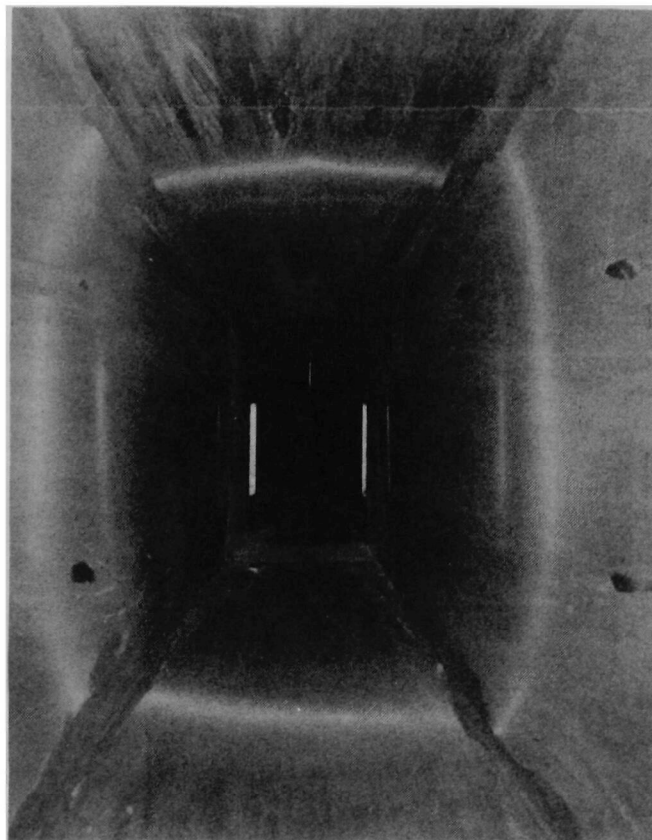


FIGURE 70
SAMPLING PROBE LOCATED IN
POTENTIAL FLOW SECTION

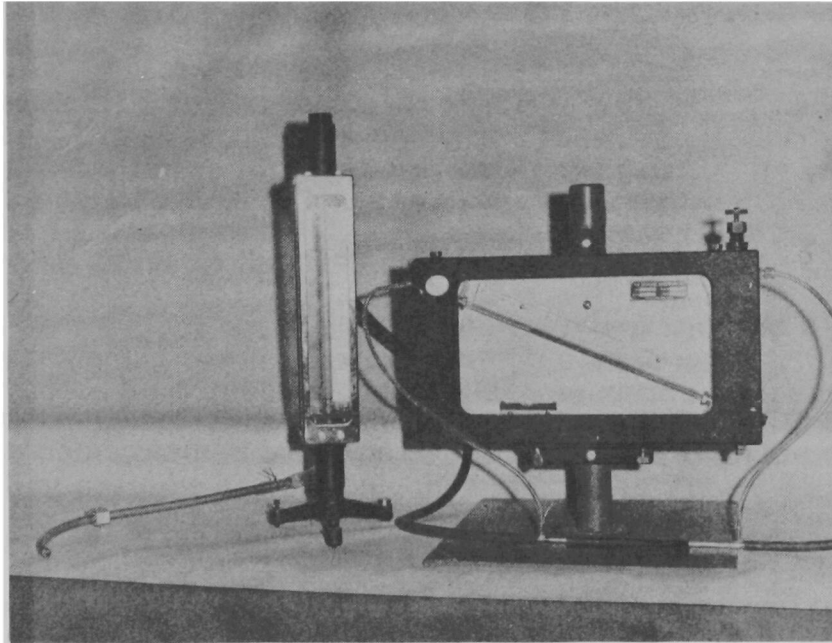


FIGURE 71
SYSTEM FOR CALIBRATING APCO TRAIN ASSEMBLY

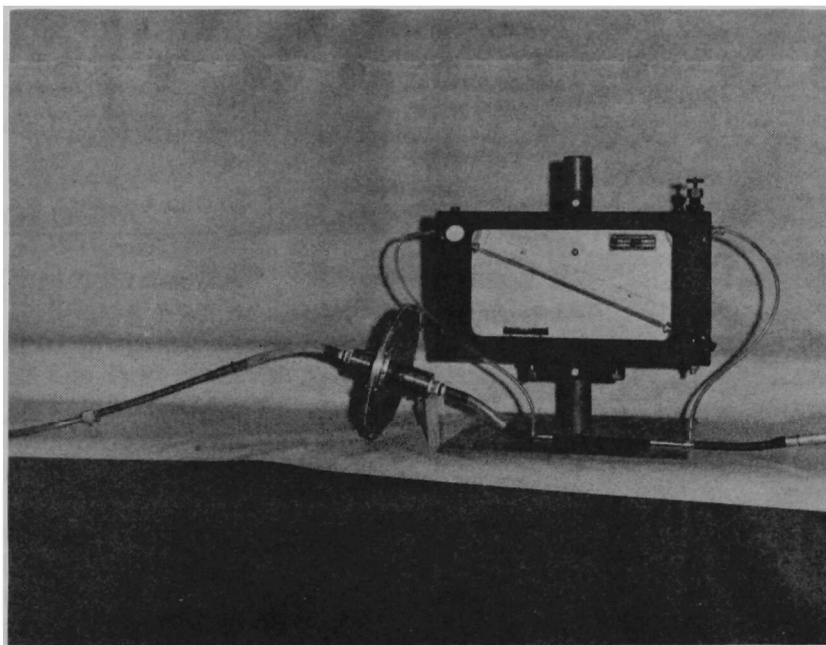


FIGURE 72
AIR SAMPLING SYSTEM

The sampling system was calibrated using a Brooks rotometer to correlate the flow rate to the pressure drops in a 10" length of 0.25 I. D. tubing.

The pressure drop across the calibrated tube was read by an inclined manometer. The flow rate was converted to probe inlet velocity and plotted against differential pressure on log-log paper. By calibrating a length of tubing, any additional resistance or change of resistance in front of the 10" length of tubing such as placing the filter in the line would have no effect on the system calibration.

Figure 72 shows a portion of the sampling system with the filter assembly and probe replacing the rotometer. Samples were taken with the system over a 2 minute time interval during which holograms were made of the flow about the probe. The grain loadings shown in Table III were calculated using data obtained from the probe samples. Both the calibration and sampling systems are shown schematically in Figure 73.

In the isokinetic case, there were few deviations of the particles from straight line paths as they approached the probe. The .5 isokinetic case produced results which were predictable since it was expected that there should be areas of separated flow due to flow stagnation ahead of the probe caused by the inlet velocity being lower than that of the free-stream. The theoretical expectations matched the actual situation as observed on the hologram.

However, the 1.5 isokinetic case was somewhat puzzling. The flow should have been a smoothly accelerating flow, starting at freestream conditions and converging toward the probe. However, a great deal of turbulence was noted in the holographic reconstructions, making the measurements of velocity almost impossible since particle pairs were not easily matched. No satisfying explanation was concluded.

III. D. - HOLOGRAMS OF CHARGED PLATES

A listing of holograms made of flow between the charged plates is shown in Table IV. There was some difficulty in making these holograms since the mechanical structure used to support the charged plates disturbed the flow of air in the test section and caused particulate to be deposited on the glass windows. However, three excellent holograms were made of the flow when the windows were removed. Hologram No. 196 was selected for analysis.

Figure 74 shows the planes selected for taking particle data from Hologram No. 196. Tables IVa through IVf are tabulations of particle characteristics and include diagrams showing the location of each recorded particle in the selected planes.

Figure 75 is a photograph of the device used in the charged plates experiment. The screen was centered between the plates (2 inches from each plate) and had a mesh of approximately 3/4 inch. The upright posts

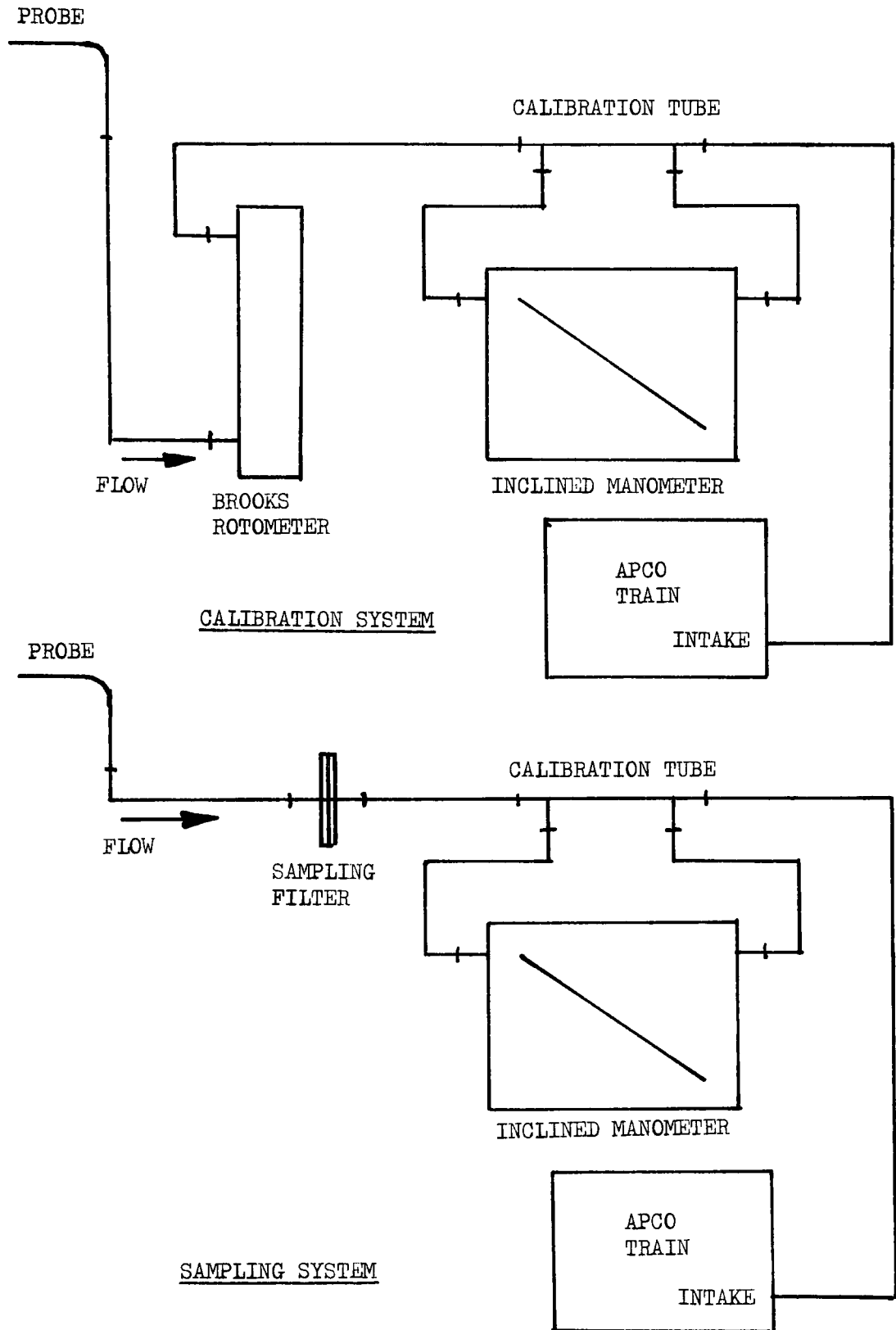


FIGURE 73
SCHEMATIC OF CALIBRATION SYSTEM
AND SAMPLING SYSTEM

TABLE IV - CHARGED PLATES

<u>Hologram</u>	<u>Mean Velocity</u>	<u>Loading (Grains/Scf)</u>	<u>Comments</u>
190	25 Ft/Sec	1.5	Windows so dirty that no reconstruction was visible
191	25 Ft/Sec	1.5	Same as 190
192	25 Ft/Sec	1.5	Same as 190
193	25 Ft/Sec	1.0	Windows so dirty that no reconstruction was visible
194	25 Ft/Sec	1.0	Same as 193
196	10 Ft/Sec	.5	No windows in test section, double pulsed particles visible
197	10 Ft/Sec	.5	Same as 196
198	10 Ft/Sec	.5	Same as 196

Loading - .5 grains/scf
Pulse Separation - .2 milliseconds

The precipitator plates were in the $y = 2$ " and $y = -2$ " planes and the screen was in the $y = 0$ plane. The x and y components of velocity were measured in the planes $y = -1.5$ ", -1.0 ", 0 ", 0.495 ", 0.792 ", 0.990 ".

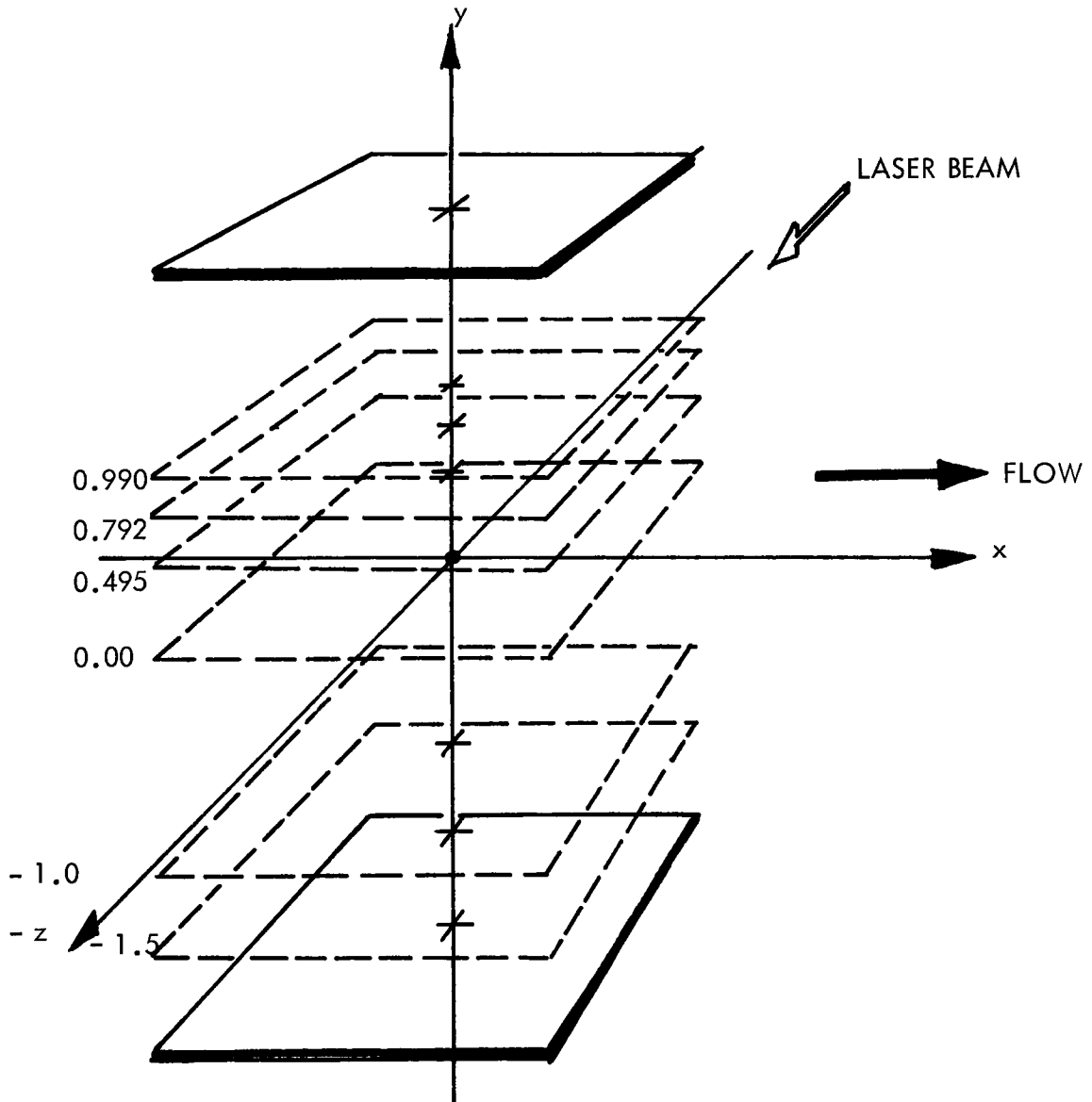



FIGURE 74
PRECIPITATOR PLATES HOLOGRAM #196

	Particle No. and Location (x, z)	V_x	V_y (ft./sec.)	V	V°	Size/Shape D = Diameter in Microns
1.	(-0.200 , +0.915)	8.58	-4.00	9.47	$25^\circ \downarrow$	
2.	(-0.350 , -1.109)	9.31	6.52	11.36	$35^\circ \uparrow$	Sphere D = 36
3.	(-0.350 , -1.109)	11.19	-1.97	11.36	$10^\circ \downarrow$	Sphere D = 23
4.	(-0.450 , +0.776)	10.64	-1.87	10.80	$10^\circ \downarrow$	Sphere D = 27
5.	(-0.500 , +0.970)	7.28	-1.28	7.39	$10^\circ \downarrow$	Sphere D = 23
6.	(-0.600 , +1.026)	7.33	- .90	7.39	$7^\circ \downarrow$	Sphere D = 45

Loading: 0.5 grains/scf

Pulse Separation - .2 milliseconds

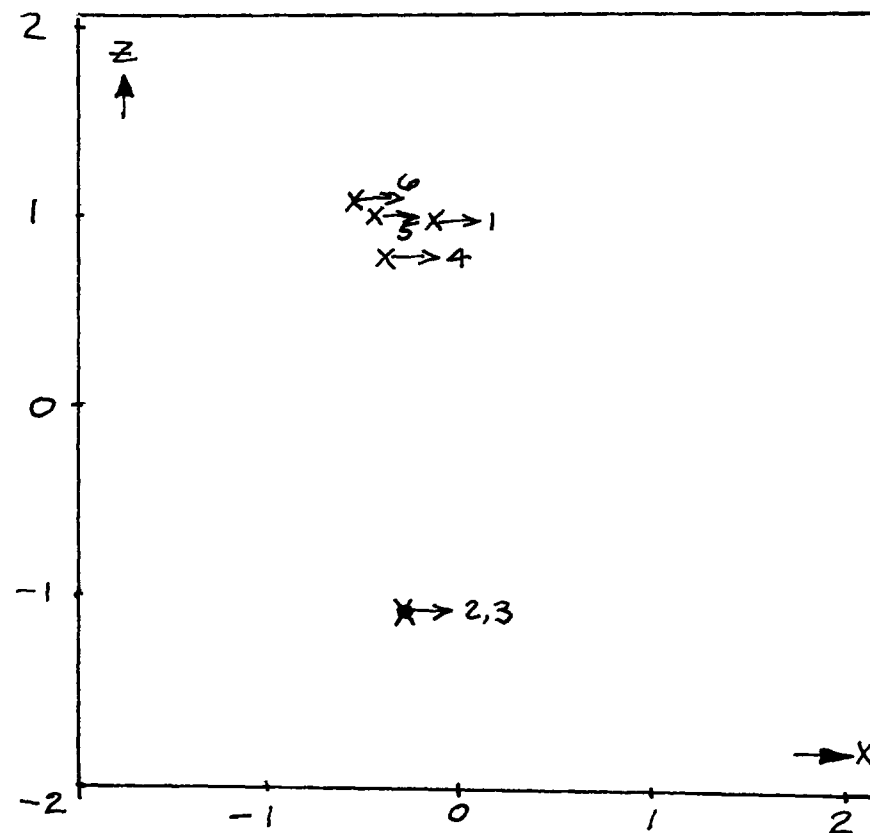
Cut at $y = 0.990$

● Positive y Component

✕ Negative y Component

○ Zero y Component

TABLE IVa
PRECIPITATOR PLATE HOLOGRAM #196



Particle No. and Location (x, z)	V_x	V_y (ft./sec.)	V	V°	Size/Shape D = Diameter in Microns
7. (-0.275 , -0.776)	11.97	-1.90	12.12	$9^\circ \downarrow$	Sphere D = 64
8. (-0.225 , +0.943)	8.58	-4.00	9.47	$25^\circ \downarrow$	Sphere D = 73
9. (-0.500 , +0.749)	8.58	-4.00	9.47	$25^\circ \downarrow$	Sphere D = 36
10. (+0.500 , -0.915)	14.63	-3.92	15.15	$15^\circ \downarrow$	Sphere D = 54

Loading: 0.5 grains/scf

Pulse Separation - .2 milliseconds

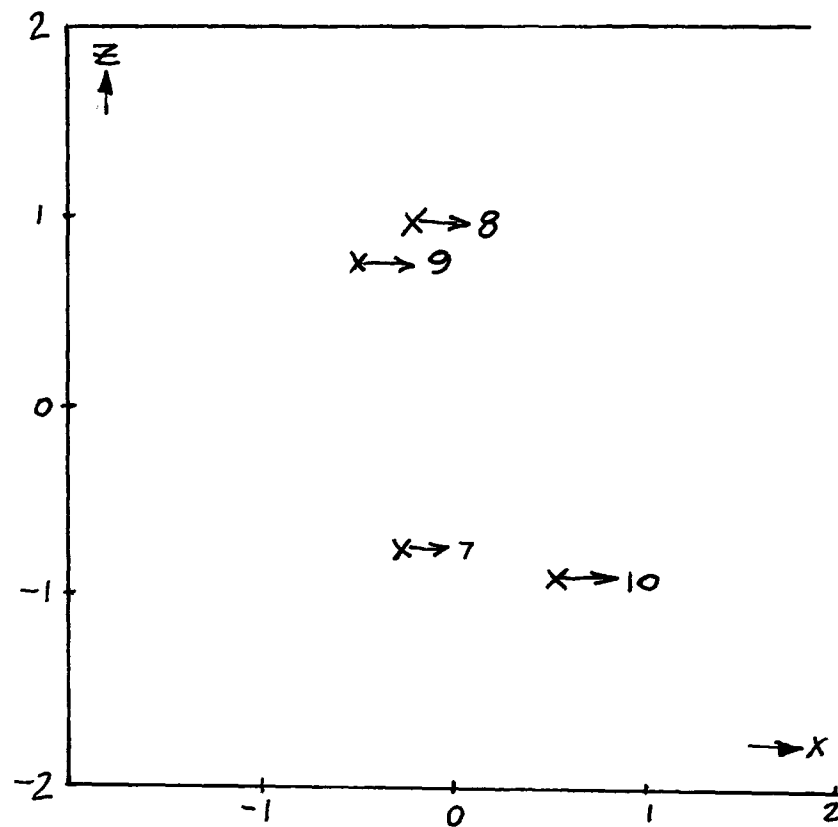
Cut at $y = 0.792$

● Positive y Component

X Negative y Component

○ Zero y Component

TABLE IVb
PRECIPITATOR PLATE HOLOGRAM #196



	Particle No. and Location (x, z)	V_x	V_y (ft./sec.)	V	V°	Size/Shape D = Diameter in Microns
11.	(+1.000 , +0.582)	12.02	5.60	13.26	$25^\circ \uparrow$	Sphere D = 73
12.	(+0.100 , +0.495)	10.79	2.89	11.17	$15^\circ \uparrow$	54 \triangle 63 68
13.	(-0.175 , +0.970)	8.41	-2.25	8.71	$15^\circ \downarrow$	Sphere D = 82
14.	(-0.175 , +0.970)	8.08	-3.26	8.71	$22^\circ \downarrow$	Sphere D = 36
15.	(-0.175 , +0.638)	9.77	-4.14	10.61	$23^\circ \downarrow$	Sphere D = 14
16.	(-0.175 , +0.305)	9.84	-3.97	10.61	$22^\circ \downarrow$	Sphere D = 64
17.	(-1.000 , +1.081)	11.48	-8.04	14.02	$35^\circ \downarrow$	118 \square 23

Loading: 0.5 grains/scf

Pulse Separation - .2 milliseconds

Cut at $y = 0.495$

- Positive y Component
- X Negative y Component
- Zero y Component

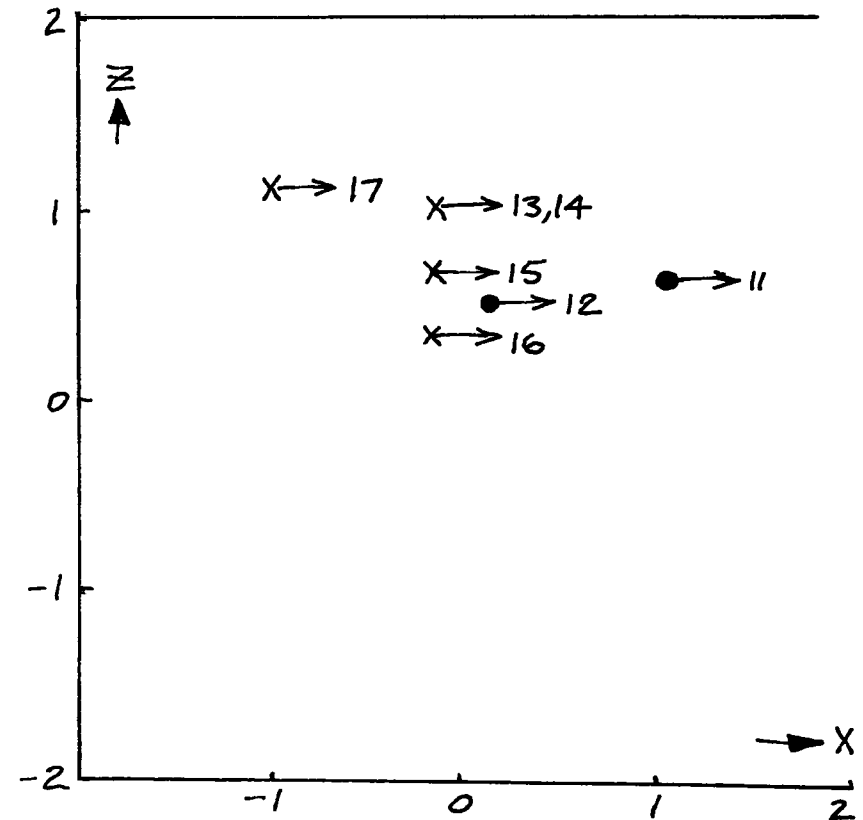


TABLE IVc
PRECIPITATOR PLATE HOLOGRAM #196

	Particle No. and Location (x, y, z)	V_x	V_y (ft./sec.)	V	V°	Size/Shape
						D = Diameter in Microns
18.	(-0.600 , +0.099 , +1.164)	6.70	-6.70	9.47	$45^\circ \downarrow$	Sphere D = 45
19.	(-0.075 , +0.099 , +0.832)	6.37	-5.94	8.71	$43^\circ \downarrow$	Sphere D = 27
20.	(+1.000 , -0.099 , -1.303)	6.96	6.96	9.85	$45^\circ \uparrow$	Sphere D = 36

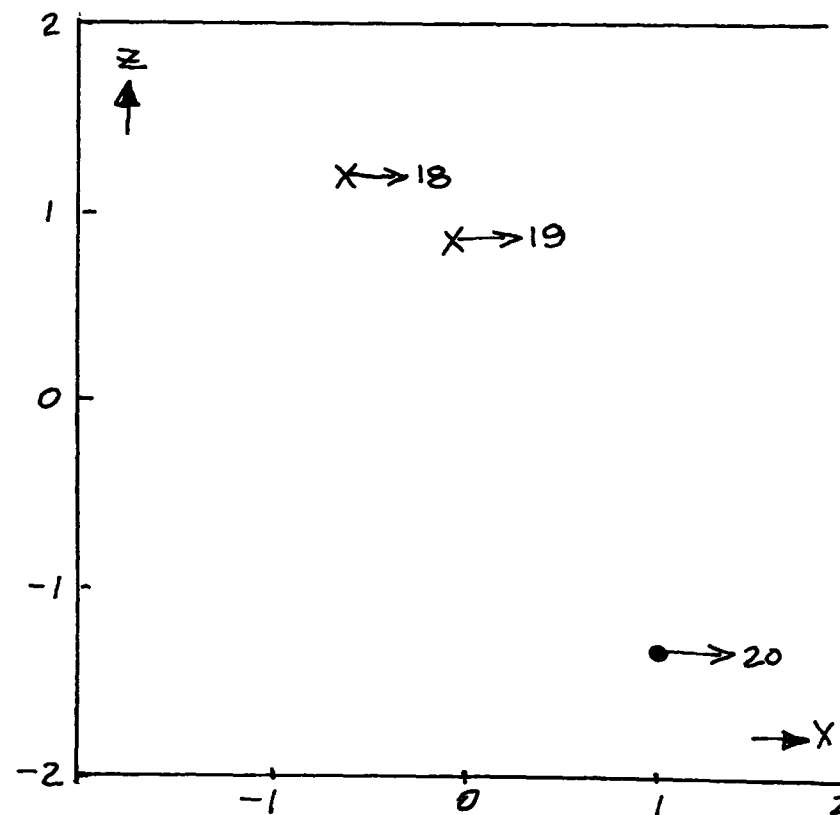
Loading: 0.5 grains/scf

Pulse Separation - .2 milliseconds

Cut at y = 0

- Positive y Component
- X Negative y Component
- Zero y Component

TABLE IVd
PRECIPITATOR PLATE HOLOGRAM #196



	Particle No. and Location (x, y, z)	V_x	V_y (ft./sec.)	V	V°	Size/Shape D = Diameter in Microns
21.	(-1.000, -0.891, +0.083)	8.32	.44	8.33	3°↑	Sphere D = 32
22.	(+0.550, -1.188, +0.499)	8.86	5.12	10.23	30°↑	Sphere D = 18
23.	(-0.450, -1.188, +1.359)	5.14	3.21	6.06	32°↑	Sphere D = 59
24.	(-0.900, -1.188, -1.580)	1.52	1.82	2.37	50°↑	Sphere D = 27
25.	(-1.000, -1.188, -1.188)	4.14	3.47	5.40	40°↑	Sphere D = 27

Loading: 0.5 grains/scf

Pulse Separation - .2 milliseconds

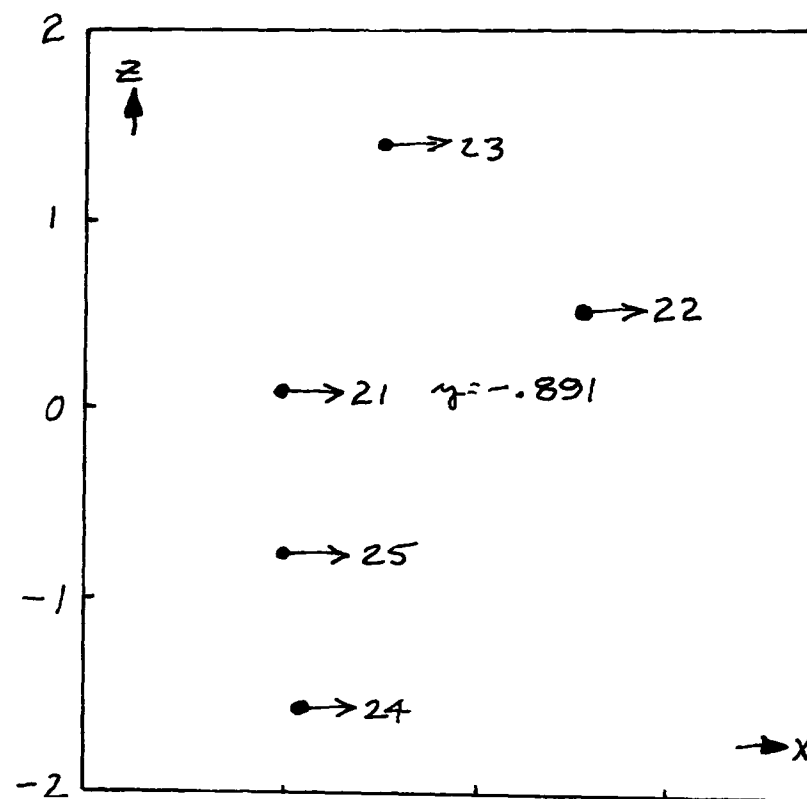
Cut at y = -1.0

● Positive y Component

X Negative y Component

○ Zero y Component

TABLE IVe
PRECIPITATOR PLATE HOLOGRAM #196



	Particle No. and Location (x, y, z)	V_x	V_y (ft./sec.)	IVI	V°	Size/Shape D = Diameter in Microns
26.	(-0.500 , -1.485 , +1.303)	5.19	3.64	6.34	$35^\circ \uparrow$	Sphere D = 32
27.	(-0.150 , -1.485 , -1.359)	6.01	-6.01	8.5	$45^\circ \downarrow$	Sphere D = 32
28.	(0.000 , -1.535 , +0.693)	4.88	3.42	5.96	$35^\circ \uparrow$	Sphere D = 41
29.	(-0.100 , -1.535 , -0.416)	10.80	0	10.80	0°	Sphere D = 27
30.	(-0.650 , -1.535 , +0.998)	4.40	2.86	5.25	$33^\circ \uparrow$	Sphere D = 23
31.	(-0.650 , -1.535 , +0.998)	4.13	4.43	6.06	$47^\circ \uparrow$	Sphere D = 27
32.	(-0.625 , -1.535 , +0.776)	3.21	3.21	4.54	$45^\circ \uparrow$	Sphere D = 23
33.	(-0.825 , -1.535 , -1.636)	.73	.87	1.14	$50^\circ \uparrow$	Sphere D = 27

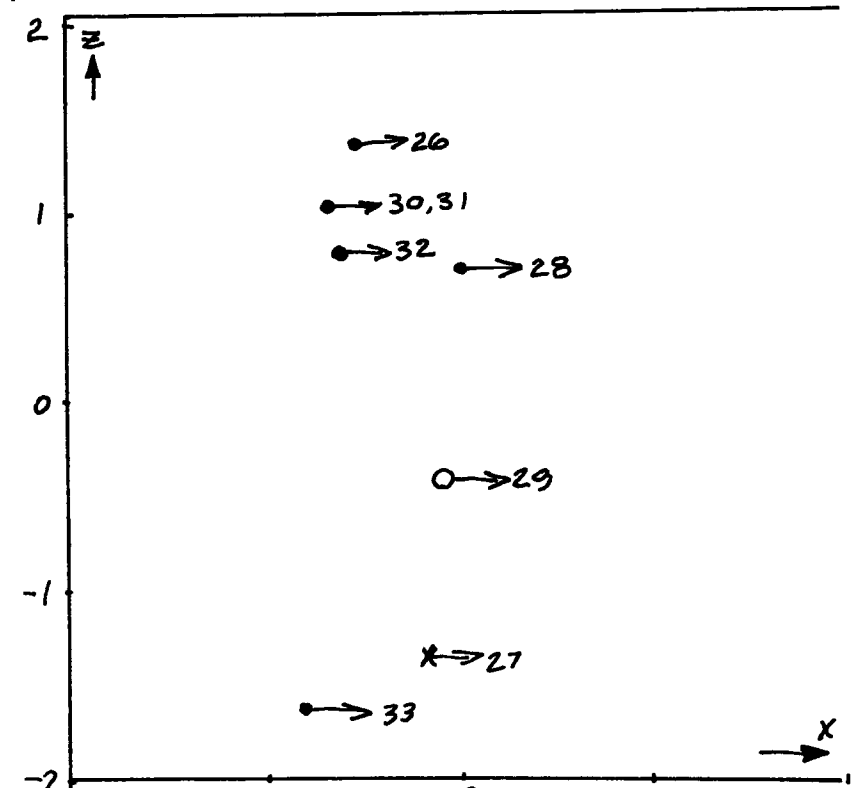
Loading: 0.5 grains/scf

Pulse Separation - .2 milliseconds

Cut at y = -1.5

- Positive y Component
- X Negative y Component
- Zero y Component

TABLE IVf
PRECIPITATOR PLATE HOLOGRAM #196



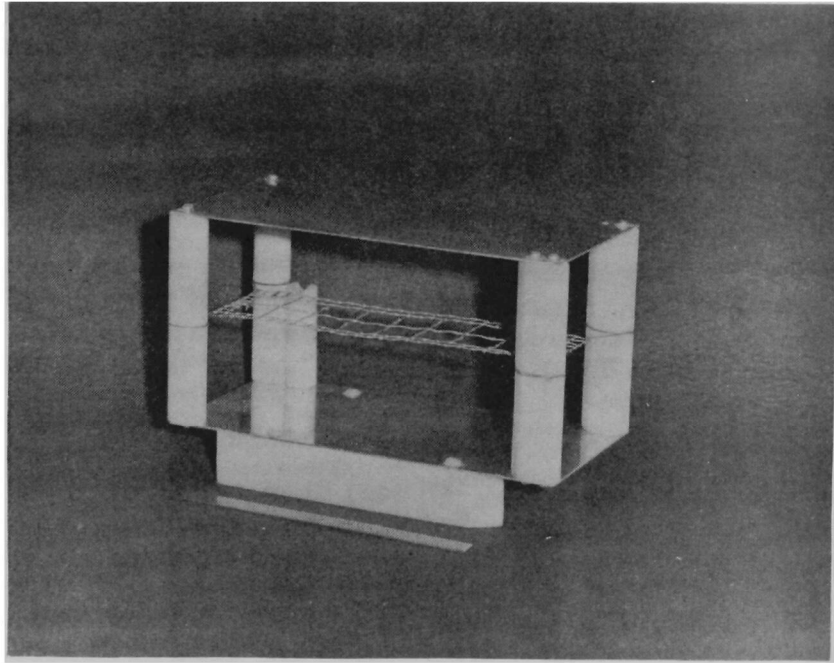


FIGURE 75
CHARGED PLATES DEVICE

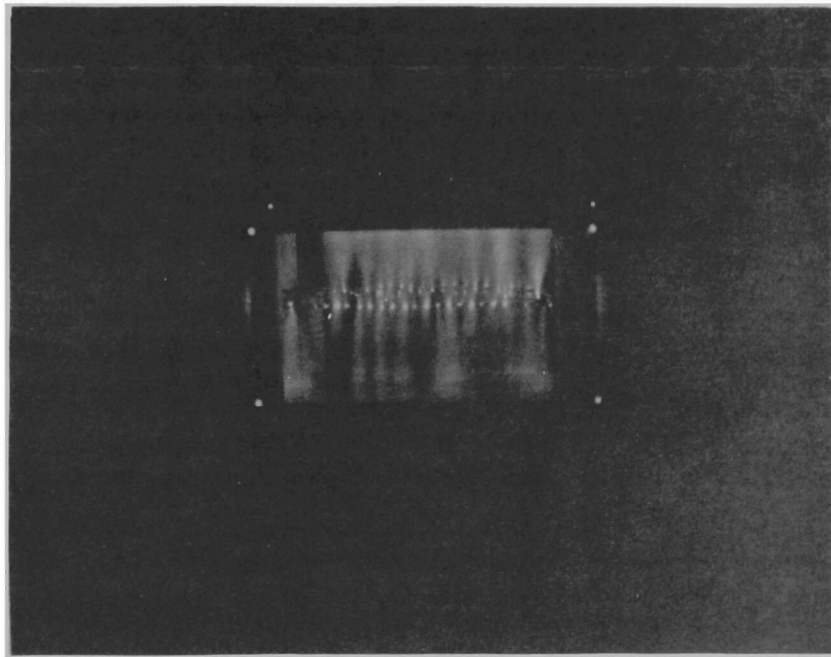


FIGURE 76
TIME EXPOSURE SHOWING CORONA DISCHARGE
PATTERNS BETWEEN PLATES AND SCREEN

at each corner were made of Teflon. The posts on the right were on the up-stream side and were shaped to reduce turbulence in the air-stream. The screen was supported from the Teflon posts by nylon cord. The short post located at the left rear of the device was used to support the negative electrode which was attached to the screen. The metal plates were made of aluminum and measured 8 inches by 4 inches. The wire screen was 7-1/4 inches long by 2 inches wide.

The potential between the plates and wire screen was 26,000 volts and was provided by a Litton Industries regulated high voltage power supply (Model 1014). The current drawn by the charged plate device varied from 50 microamps at 20 KV to 1 milliamp at 30 KV. At 26 KV (the setting used for Holograms 196, 197, and 198) the current drawn was approximately 300 microamps.

The design of the system was such that the power available would approximate the power requirements per cubic foot of processed air typical of commercial electrostatic precipitators. The literature indicated the range of energy requirements for precipitators to be on the order of 2 - 5 KW-hr./1,000,000 ft³ or 7.2 to 18 joules/ft³. For Hologram No. 196, mean velocity was 10 ft/sec. At this velocity, the power requirement was calculated to be between 4 and 10 watts (corresponding to 7.2 and 18 joules/ft³). The input power to the system was actually 7.8 watts, indicating a reasonable match of power input per unit volume to that required by commercial precipitators.

Figure 76 is a time exposure (approximately 1 minute) of the corona discharge patterns between the wire grid and plates.

Particles in the electric field were normally accelerated toward the grid. However, under column "V⁰" in Table IVa - IVf, it is noted that some particles were observed traveling in the opposite direction, indicating that either particles of opposite polarities were in the flow or that re-entrainment occurred of particles which had previously reached the grid and lost their charge.

IV - CONCLUSIONS AND RECOMMENDATIONS

IV. A. - CONCLUSIONS

From the experimental work conducted during this program, the following conclusions have been reached:

- o Double-pulsed holography is a feasible method of determining the velocity and behavior of particulate matter suspended in both potential and turbulent flow.
- o The Gabor hologram provides an excellent means to record the size and shape of particulate. Experimental results showed that a minimum particulate size of 5.5 microns could be resolved.
- o The Gabor hologram is usable over a wide range of particulate loadings. Although the best holograms were made at a low grain loading (.5 grains/scf or less), particles were quite visible at grain loadings as high as 4-5 grains/scf.
- o The velocities of particulate (flyash) in a given portion of a test section appeared to be independent of particle size and shape.
- o The type of duct facility designed and used in the program provides an excellent facility for investigating the behavior of particulate material in both potential and turbulent flow.
- o The "blender" type particulate dispenser proved to be a reliable and easy-to-use method for dispensing free-flowing powders, such as flyash, over a wide range of loadings.
- o No practical utility can be made of the Stokes-Cunningham equation based on the holographic experimental data. The Stokes-Cunningham factor becomes significant only for particles smaller than 1 micron (at atmospheric pressure) whereas the theoretical resolution limit of the holographic system used was no better than 1.74 microns (the actual resolution was approximately 5.5 microns). Consequently, the effects to which the Stokes-Cunningham factor relates would not be observed with the experimental system.
- o The accuracy of double-pulsed holography in determining velocity of a particle is a function of the care taken in measuring the spacing of the particles, the known accuracy of the time interval between light pulses, the magnification ratios in the reconstruction system, etc. The accuracy of the system used in the program was approximately ± 0.05 feet/second.

IV. B. - RECOMMENDATIONS

There are four areas where, in the opinion of the authors, additional studies should be conducted: (1) determination of methods for achieving small particle (.01 to 5 microns) sizing and velocity characteristics, (2) development of rapid data gathering and data reduction techniques for determining statistical characteristics of particles in air flow, (3) determination of the maximum deviation from isokinetic conditions where data obtained from sampling probes will produce valid information, and (4) studies and experiments of simulated electrostatic precipitators to determine the extent and conditions under which re-entrainment of particles occurs.

The resolution of holographic systems is limited in a practical sense by the distance that the holograms must be away from the particle being recorded. Since it is probably desirable to maintain test facilities such that the test sections are at least several inches wide and high (to minimize wall effects and to allow conditions in smoke stacks, etc. to be simulated), the resolution of holographic systems under these restrictions would, most likely, continue to be inadequate for studying particle behavior in the sub-micron region. However, the behavior of particles in this region should be of special interest since their behavior could vary significantly from that of larger particles due to phenomena such as the molecular slip flow effect. Consequently, it should be desirable to develop techniques to extend the ability to measure particle characteristics down to the sub-micron levels.

Double pulsed holography is an excellent means to gather data on individual particle characteristics. However, where the interest is on the aggregate behavior of large numbers of particles, the data reduction problem becomes significant. As pointed out in the report, there are several methods which could be applied directly to the hologram itself. These techniques are suitable in areas where the particle pair patterns are repeatable such as in potential flow regions. However, where the flow is highly turbulent, these techniques may have serious shortcomings. Other electro-optical techniques should be investigated to achieve the capability of measuring particle size and velocity for large numbers of particles in unstructured flow fields.

The double-pulsed holograms of flow about the sampling probe raised several questions. From the tests conducted, it appeared that particle behavior at 1.5 isokinetic varied considerably from anticipated results. It is not clear why the discrepancy between theory and experiment arose, and it is felt that additional studies would be worthwhile to determine the cause of the noted particle behavior. Additionally, the experiments were conducted only for conditions of .5 and 1.5 isokinetic. At these points considerable turbulence was noted, indicating that a valid sample of particulate in the airstream did not occur. It would seem to be desirable to conduct tests to determine deviations allowable from the 1.0 isokinetic condition for purposes of setting tolerances in sampling procedures. A

set of double-pulsed holograms varying by increments of $\pm .05$ from the 1.0 isokinetic condition would probably provide sufficient data.

The small number of particles found to be traveling in a direction opposite to the majority of particles in the charged plate experiment also raised a number of questions. First of all, this experiment was not controlled aerodynamically in the same sense as the rest of the experiments. The charged plate assembly introduced turbulence in the test section and it was necessary to remove the windows to counter this effect. The removal of the windows also introduced unknown effects which would possibly account for the few particles which were found to move counter to the majority. However, the fact that some of these particles were very close to particles traveling in the direction of the majority seems to indicate that other effects were present.

A suggested experiment to resolve these questions (i. e. , whether the effects were aerodynamic, re-entrainment, or initial charging of the particles) would be to devise a larger test section and to redesign the charged plate assembly in order to assure potential flow. Also, the ability to measure the velocity profiles between the plates with pitot probes would be an important feature. If desirable, the charged plate assembly could be designed to closely approximate the characteristics of commercial precipitators.

The existing facility could be used for the above suggestions since the air flow capacity of the system is sufficient to allow an enlargement of a test section and still maintain required velocities.